EPA-600/3-76-080
July 1976

Ecological Research Series

SMOG CHAMBER STUDIES ON PHOTOCHEMICAL AEROSOL-PRECURSOR RELATIONSHIPS

Environmental Sciences Research Laboratory
Office of Research and Development
U.S. Environmental Protection Agency
Research Triangle Park, North Carolina 27711

RESEARCH REPORTING SERIES

Research reports of the Office of Research and Development, U.S. Environmental Protection Agency, have been grouped into five series. These five broad categories were established to facilitate further development and application of environmental technology. Elimination of traditional grouping was consciously planned to foster technology transfer and a maximum interface in related fields. The five series are:

1. Environmental Health Effects Research
2. Environmental Protection Technology
3. Ecological Research
4. Environmental Monitoring
5. Socioeconomic Environmental Studies

This report has been assigned to the ECOLOGICAL RESEARCH series. This series describes research on the effects of pollution on humans, plant and animal species, and materials. Problems are assessed for their long- and short-term influences. Investigations include formation, transport, and pathway studies to determine the fate of pollutants and their effects. This work provides the technical basis for setting standards to minimize undesirable changes in living organisms in the aquatic, terrestrial, and atmospheric environments.

This document is available to the public through the National Technical Information Service, Springfield, Virginia 22161.

SMOG-CHAMBER STUDIES ON PHOTOCHEMICAL AEROSOL PRECURSOR RELATIONSHIPS

by

David F. Miller and Darrell W. Joseph
BATTELLE - Columbus Laboratories
Columbus, Ohio 43201

Contract No. 68-02-1718

Marijon Bufalini
Technical Planning and Review Office
Environmental Sciences Research Laboratory
Research Triangle Park, North Carolina 27711

U.S. ENVIRONMENTAL PROTECTION AGENCY
OFFICE OF RESEARCH AND DEVELOPMENT
ENVIRONMENTAL SCIENCES RESEARCH LABORATORY
RESEARCH TRIANGLE PARK, NORTH CAROLINA 27711

DISCLAIMER

This report has been reviewed by the Environmental Sciences Research Laboratory, U.S. Environmental Protection Agency, and approved for publication. Approval does not signify that the contents necessarily reflect the views and policies of the U.S. Environmental Protection Agency, nor does mention of trade names or commercial products constitute endorsement or recommendation for use.

ABSTRACT

An experimental program was conducted in which controlled atmospheres containing water vapor, CO, NO_x (NO + NO_2), and a constant distribution of 17 hydrocarbons (NMHC) were irradiated in a smog chamber. The principal experimental variables were the initial concentrations of NMHC and NO_x. Complete smog profiles were developed for NO and hydrocarbon photooxidation and aerosol and ozone formation over 10-hour irradiation periods. The dependence of photochemical aerosol formation goes through a maximum with respect to the initial NO_x concentrations, and it is an ever-increasing function of the initial NMHC concentrations. The precursor relationships vary with irradiation time. As the irradiation period increases from 2 to 6 to 10 hours, peak aerosol concentrations relate to initial NMHC/NO_x ratios of 15/1, 13/1, and 10/1, respectively. At NMHC/NO_x ratios <10/1 there are maxima in the relationships between photochemical aerosol concentration and the initial pollutant concentrations. These maxima generally occur for initial NMHC concentrations in the 2-3 ppmC range. The relationships between aerosol formation and their precursors (NMHC and NO_x) were found to be qualitatively similar to those for ozone formation, and thus NMHC and NO_x control strategies for limiting ozone are mutually beneficial in reducing photochemical aerosols.

CONTENTS

Abstract iii
Figures v
Tables viii
Acknowledgments ix

1. Introduction. 1
2. Summary 3
3. Review of Aerosol Formation in Smog Chambers. 7
   - Reactivity Studies 7
   - Aerosol Studies With SO_2 7
   - Aerosol Studies Without SO_2. 8
4. Current Interpretation of Organic Aerosol Formation 20
   - Precursor Characteristics of Organic Aerosol Formation . . 20
   - Interlaboratory Comparisons. 26
5. Experimental Approach 32
6. Experimental Methods. 38
   - Smog-Chamber Description and Operation 38
   - Analytical 39
7. Results 43
8. Discussion. 47
   - Overall Reactivity 47
   - Hydrocarbon Oxidation. 49
   - Aerosol Precursor Relationships. 55
   - Ozone Precursor Relationships. 65
   - Aerosol and Ozone--Mutual Benefits From Precursor Controls 75

References 81
Appendices

A. Smog Profiles 86
B. Summary of Hydrocarbon Data Determined by Gas Chromatography. . 96

FIGURES

Number		Page
1a-c	Surface Projections Representing Instantaneous Aerosol Volume Concentrations as Functions of the Initial Concentrations of NMHC and NO_x At Irradiation Times of 2, 6, and 10 Hours.	4
2	Relative Reactivity of Exhaust Hydrocarbons in Forming Light-Scattering Aerosols in Simulated Smog.	10
3	Regression Relationship of Aerosol Formation (Light Scattering) With Hydrocarbon Reactivity For Auto Exhaust Derived From a Linear Summation of Individual Reactivities.	12
4	Profile of Aerosol Formation During Irradiation of Filtered and Diluted Auto Exhaust (16 ppmC Hydrocarbons)	16
5	Reproduction of Smog Profile From the Photooxidation of 1-Hexene and NO in the Calspan Chamber.	18
6	Photochemical Aerosol Formation During a Smog-Chamber Irradiation of a Toluene-NO_x-Air Mixture	21
7	Photochemical Aerosol Formation During a Smog-Chamber Irradiation of a 1-Heptene-NO_x-Air Mixture	22
8	Photochemical Aerosol Formation During a Smog-Chamber Irradiation of a Surrogate Hydrocarbon Mixture and NO_x.	25
9	Effect of NO_2/NO_x Ratio on Photooxidation Rate Parameters in the 1-Butene-NO_x-System.	28
10	The Effect of Primary Auto Exhaust Aerosol on Photochemical Aerosol Growth and Light Scattering. . .	33
11	Evidence of Preferential Homogeneous Nucleation of Photochemically Derived Aerosol in Air Containing Primary Nuclei	34
12	Initial Hydrocarbon and Nitrogen Oxide Concentration Coordinates in the Experimental Program. . . .	37

FIGURES (Continued)

Number		Page
13	Representative Chromatogram Showing Resolution of the Surrogate Hydrocarbon Mixture Obtained With Two Gas Chromatographs.	40
14	Computer-Generated Graphs of the Changes in the Aerosol Surface-Area and Volume-Size Distribution that Occur as a Function of Irradiation Time	42
15	Fractional Hydrocarbon Decay Rates at 9.1/1 NMHC/NO_x Ratio, Run No. 1	50
16	Effect of NMHC/NO_x Ratio on the Rate of Aromatic Hydrocarbon Decay.	53
17	Isopleths of Maximum Rates of Aerosol Formation as a Function of the Initial Concentrations of NMHC and NO_x (Isopleths correspond to intervals of volume production rates of 2 $\mu m^3/cm^3/hr.$)	57
18	A Surface Projection Representing Maximum Rates of Aerosol Formation as Functions of the Initial Concentrations of NMHC and NO_x	57
19a-c	Surface Projections Representing Aerosol Volume Concentrations as Functions of the Initial Concentrations of NMHC and NO_x at Irradiation Times of 2, 6, and 10 Hours.	59
20a-c	Isopleths of Aerosol Volume Concentration as Functions of Initial Concentrations of NMHC and NO_x at Irradiation Times of 2, 6, and 10 Hours (Isopleths correspond to volume concentration intervals of 2 $\mu m^3/cm^3/hr.$).	60
21a-c	Surface Projections Representing Aerosol Volume Concentrations as Functions of Initial Pollutant Concentrations at a Constant NMHC/NO_x Ratio of 10/1 and Irradiation Times of 2,6, and 10 Hours. . . .	63
22a-c	Surface Projections Representing Aerosol Volume Concentrations as Functions of Initial Pollutant Concentrations at a Constant NMHC/NO_x Ratio of 5/1 and Irradiation Times of 2, 6, and 10 Hours. . . .	64

FIGURES (Continued)

Number		Page
23	Isopleths of Constant Ozone Concentration (ppm) Developed From Peak Ozone Concentrations in an Earlier Smog-Chamber Study	66
24	Isopleths of Constant Ozone Concentration (ppm) Based on 5-Hr Data Predicted by a Kinetic Smog Model.	66
25	Isopleths of Constant Ozone Concentrations (ppm) Derived From the LACAPCD Smog-Chamber Studies.	67
26	Isopleths of Constant Ozone Concentrations (ppm) Derived From Instantaneous Ozone Concentrations at 6-Hr of Irradiation	67
27a-c	Surface Projections Representing Ozone Concentrations as Functions of Initial Concentrations of NMHC and NO_x at Irradiation Times of 2, 6, and 10 Hours	70
28a-c	Isopleths of Ozone Concentrations as Functions of Initial Concentrations of NMHC and NO_x at Irradiation Times of 2, 6, and 10 Hours (Isopleths correspond to concentration intervals of 0.05 ppm O_3.)	71
29a-c	Surface Projections Representing Ozone Concentrations as Functions of Initial Pollutant Concentrations at a Constant NMHC/NO_x Ratio of 10/1 and Irradiation Times of 2, 6, and 10 Hours . . .	73
30a-c	Surface Projections Representing Ozone Concentrations as Functions of Initial Pollutant Concentrations at a Constant NMHC/NO_x Ratio of 5/1 and Irradiation Times of 2, 6, and 10 Hours . .	74
31a-f	Comparisons of the Concentration Dependence of Aerosol (a,c,e) and Ozone (b,d,f) Volume on the Initial Concentrations of NMHC and NO_x at Irradiation Times of 2, 6, and 10 Hours.	76
32a-f	Comparisons of the Concentration Dependence of Aerosol (a,c,e) and Ozone (b,d,f) Volume on the Initial Concentrations of Pollutants at a Constant NMHC/NO_x Ratio of 10/1 and Irradiation Times of 2, 6, and 10 Hours	78
33a-f	Comparisons of the Concentration Dependence of Aerosol (a,c,e) and Ozone (b,d,f) Volume on the Initial Concentrations of Pollutants at a Constant NMHC/NO_x Ratio of 5/1 and Irradiation Times of 2, 6, and 10 Hours	79

TABLES

Number		Page
1	Aerosol Formation From Selected Hydrocarbons.	11
2	Comparisons of Aerosol Formation and Reactivity for Smog Chambers at Calspan and the University of Minnesota	17
3	Estimated Aerosol Conversion Efficiencies for a Few Familiar Hydrocarbons	23
4	Comparisons of Smog-Chamber Conditions at Calspan and Battelle and Some Reactivity Results of Olefin Photo-Oxidation	27
5	Reference Atmosphere.	36
6	Initial Pollutant Concentrations.	44
7	Summary of Experimental Results	46
8	Correlation Coefficients Among Measured Reactivities. . . .	47
9	Correlation Coefficients Between Aerosol Concentration and the Time Integrals of Hydrocarbon Decay	49
10	Hydrocarbon Oxidation Rates in Polluted Air and in Smog-Chamber Simulations.	52
11	Average Hydrocarbon Loss Rates Under Natural and Simulated Irradiation Conditions.	54
12	Selected Data on the NMHC and NO_x Distribution in Urban Areas.	61
13	Worst-Case Ozone Episodes in Pasadena (1969-1970) and the Precursor Hydrocarbon and NO_x Concentrations	69

ACKNOWLEDGMENTS

The generation, compilation, and presentation of data on which this report rests required the expertise of many coworkers. The authors are especially grateful to the contributions made by Fred Blakeslee, James Hoyland, George Keigley, Barbara Levine, Joseph Miller, Philip Schumacher, and Gerald Ward.

SECTION 1

INTRODUCTION

The photochemical conversion of gases to aerosols in the atmosphere results primarily in the formation of sulfate, nitrate, and oxygenated organic compounds. In submicron-size aerosol samples collected at the fringes of some eastern and midwestern cities, the mass concentrations (24-hour avg.) of these compounds fall into the following ranges[1]:

Sulfates (2-25 $\mu g/m^3$)
Nitrates (0.2-4 $\mu g/m^3$)
Oxygenated organics (2-40 $\mu g/m^3$).

Stationary and mobile combustion sources also make contributions to these aerosol compounds, and from chemical analyses of the samples alone it is not possible to specify the respective sources. In the Los Angeles basin where photochemical smog prevails, a recent study reports maximum concentrations of these compounds ranging 2-5 times as great as the maxima indicated above[2]. Such high concentrations illustrate the tremendous potential of our polluted atmosphere to produce aerosols via photochemical reactions.

Reduction of the photochemically derived aerosols can best be achieved by control of the gaseous precursors. Therefore, to develop an effective emission control strategy, it is necessary to quantitate the dependence of photochemically derived aerosols on the controllable gaseous precursors. In this program, a smog-chamber approach is taken in seeking these relationships. Emphasis is placed on measuring aerosol formation in complex but controllable experimental atmospheres whose composition closely resembles that of our polluted urban air. The principal experimental variables studied thus far are the concentrations of total nonmethane hydrocarbons and nitrogen oxides.

The major findings of the experimental study and some thoughts on control strategies are presented in the *Summary* section of the report. The scope of the study and the experimental details are presented in the sections entitled *Experimental Approach*, *Experimental Methods*, *Results*, and *Discussion*.

In addition to the laboratory investigation, we have been requested to provide some overall interpretations of photochemical aerosol formation in light of other smog-chamber research in this area. Those discussions are contained in the sections entitled *Review of Aerosol Formation in Smog Chambers* and *Current Interpretations of Organic Aerosol Formation*.

SECTION 2

SUMMARY

An experimental program was conducted in which controlled atmospheres containing water vapor, CO, NO_x (NO + NO_2), and a constant distribution of 17 hydrocarbons (NMHC) were irradiated in a smog chamber. Complete smog profiles were developed for NO and hydrocarbon photooxidation and aerosol and ozone formation over 10-hour irradiation periods. Comparisons of the smog-chamber results with data on hydrocarbon oxidation rates observed in the Los Angeles area and with worst-case ozone episodes in that area suggest that the models (precursor relationships) developed here for photochemical aerosol formation are highly relevant to the smog problems in polluted atmospheres.

The simultaneous dependence of aerosol formation on the initial NMHC and NO_x concentrations is summarized in Figure 1. In these graphs, aerosol formation is represented by a response surface in perspective while NMHC and NO_x are the abscissa and ordinate, respectively. In all regions of the graphs dependence of aerosol formation on NMHC is always positive, but the dependence with respect to NO_x is both positive and negative, i.e., the latter dependence goes through a maximum. In effect the initial NO_x concentration controls the extent to which hydrocarbon vapor is converted to organic aerosol, and the aerosol response surface can be thought of as a gas-to-aerosol conversion efficiency. The crest in the response surface thus corresponds to conditions for maximum conversion.

One of the most important features of aerosol precursor relationships is the time dependency. At 2 hours (Figure 1a) aerosol formation is strongly suppressed by high NO_x concentrations, and the crest corresponding to maximum conversion efficiency follows a NMHC/NO_x ratio of 15/1 in the region of lower pollutant concentrations. The ridge bends and follows a course of higher NMHC/NO_x ratios in the region of higher pollutant concentrations. By 6 hours (Figure 1b) the response surface has swelled up in the NO_x region of the graph--a result indicative of the diminishing suppression of NO_x as the irradiation time increases. This trend is further

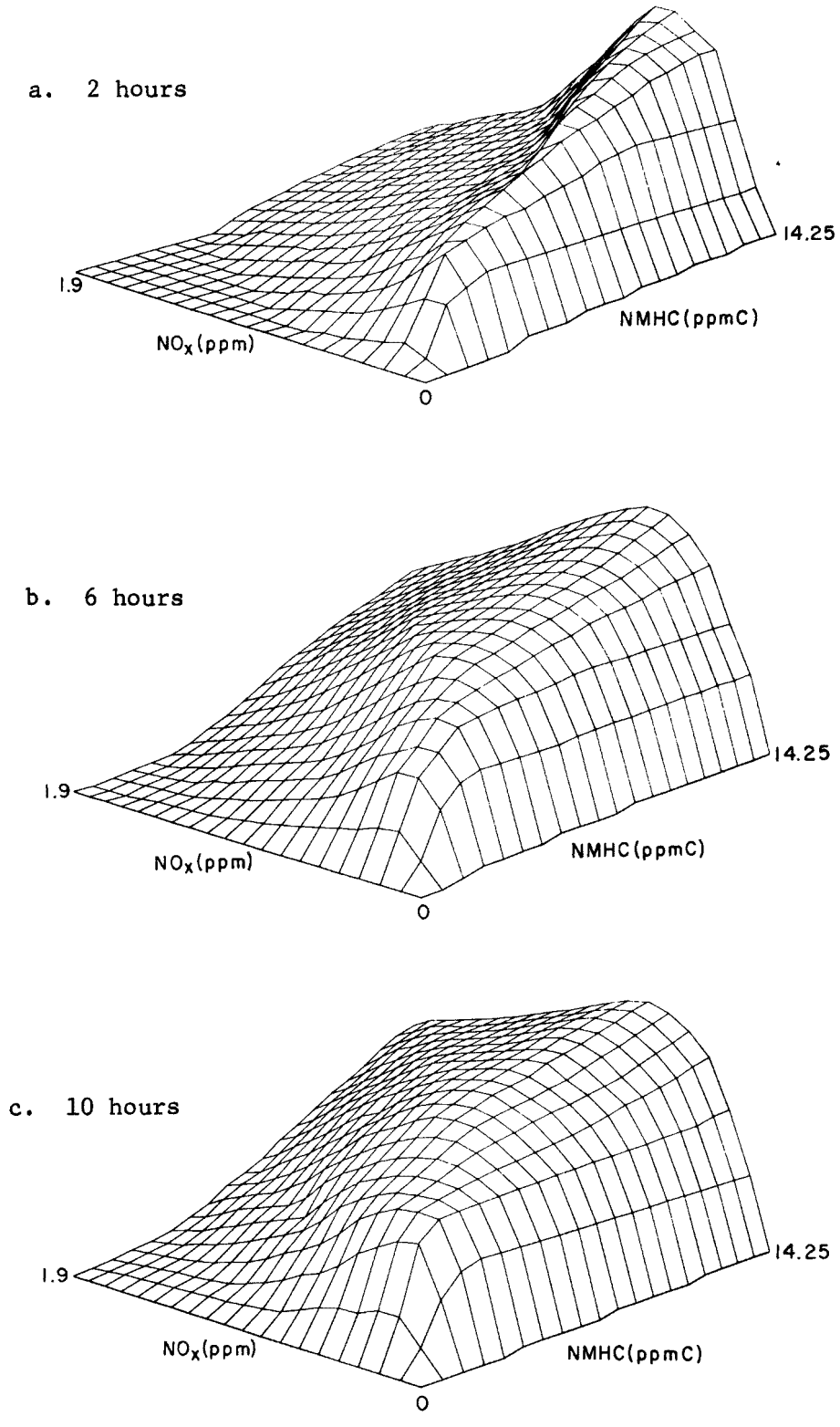

FIGURE 1. SURFACE PROJECTIONS REPRESENTING INSTANTANEOUS AEROSOL VOLUME CONCENTRATIONS AS FUNCTIONS OF THE INITIAL CONCENTRATIONS OF NMHC AND NO_x AT IRRADIATION TIMES OF 2, 6, AND 10 HOURS

illustrated by the response surface at 10 hours (Figure 1c). By this time the maximum aerosol concentrations correspond to a NMHC/NO_x ratio of 10/1 in the region of common atmospheric pollutant concentrations.

Another interesting feature of the data pertains to the dependency of aerosol formation on the initial pollutant concentrations, i.e., for varying NMHC and NO_x concentrations but constant NMHC/NO_x ratios (e.g., see Figures 21 and 22). For all irradiation periods there appears to be a region of initial pollutant concentrations where the aerosol concentration becomes constant; pollutant concentrations above the region do not increase the aerosol concentration. This phenomenon is interpreted to mean that, at limiting pollutant levels, gas-to-aerosol conversion efficiency diminishes, and the atmosphere is overburdened in its effort to oxidize primary pollutants. In general the point of limiting pollutant concentrations increases with increasing NMHC/NO_x ratios.

If the models developed can be trusted quantitatively, it appears that for NMHC/NO_x ratios of 10/1 and 5/1 the peak efficiency in aerosol production occurs near pollutant concentrations of 2 ppmC NMHC and 0.2 and 0.4 ppm NO_x, respectively. With this knowledge, there are two plausible approaches for reducing the concentrations of photochemically derived aerosols: (1) lower the overall primary pollutant (NMHC and NO_x) concentrations in the region of maximum conversion efficiency, or (2) cause a shift in the distribution of NMHC and NO_x in a direction which lowers the efficiency. The former approach is more asthetically appealing in that it permits the hydrocarbon degradation to proceed most efficiently while still maintaining acceptable concentrations of secondary pollutants. If we assume a starting point of 3.5 ppmC NMHC and 0.35 ppm NO_x and apply the 6-hour-irradiation model to obtain an 80 percent reduction in aerosol via the former strategy, a concomitant reduction in NMHC and NO_x concentrations of 74 percent would be required (NMHC = 0.9 ppmC and NO_x = 0.09 ppm). If the latter strategy of unilateral NMHC control was invoked at the same starting point, an 80 percent reduction in aerosol could be obtained by reducing the NMHC level about 83 percent (NMHC = 0.6 ppmC). From a practical standpoint the latter approach is more attractive. A drawback of this approach, however, is the pitfall of "hydrocarbon ruts" which

occurs when limitations of hydrocarbon emissions are reached before a standard is met. At this point of the hypothetical condition, large reductions in NO_x would be required before any further improvement in the level of photochemical aerosols would be realized.

Comparisons between precursor relationships for aerosol formation and ozone formation are brought out in the text of the report. Although there are some substantial differences in their relationships to NMHC and NO_x, it was quite satisfying to find that NMHC and NO_x control strategies follow mutually beneficial paths. However, in following a course of unilateral NMHC control, the benefit with respect to aerosol formation is predicted to be less than that for ozone.

SECTION 3

REVIEW OF AEROSOL FORMATION IN SMOG CHAMBERS

REACTIVITY STUDIES

Numerous smog-chamber studies have been conducted to assess the functions of hydrocarbons and nitrogen oxides in photochemical smog. Most of the studies have focussed on the reactivity of individual hydrocarbons or organics based on smog-chamber manifestations other than aerosol formation; i.e., the reactivities have been based on NO photooxidation rates, ozone formation, hydrocarbon depletion rates, aldehyde and PAN production, and eye irritation[3-17]. Insofar as this is an aerosol study, we have not attempted to review those reports with the objective of comparing our data on those reactivity bases. However, since aerosol formation, at least under the conditions investigated, is strongly linked to hydrocarbon oxidation some pertinent comparisons of this parameter are made here and in the text of the report. Other general comparisons of reactivity data are also interspersed in the report.

AEROSOL STUDIES WITH SO_2

Most of the smog-chamber studies on aerosol formation have involved irradiations of individual hydrocarbons with NO_x; often with SO_2 added[18-33]. Results of studies conducted with SO_2 generally concur with the following summary. When SO_2 is added to either aromatic-NO_x-air or alkane-NO_x-air mixtures, the total aerosol produced is approximately that predicted by an additive model; i.e., the sum of the organic aerosol produced when the respective hydrocarbon is irradiated with NO_x, and the sulfate aerosol produced when SO_2 is irradiated in the absence of the reactive hydrocarbon. With the more reactive aromatic and alkane hydrocarbons and SO_2 there may be some enhancement of total aerosol formation over the linear combination of the individual systems. With the olefins, the levels of aerosol obtained with added SO_2 show a definite synergistic effect. The enhancement of total aerosol production is greatest for the C_2-C_4 olefins which make little organic aerosol.

Data are also available showing the enhancement of photochemical aerosol formation when SO_2 is added to auto exhaust[29,34-36]. As expected, this effect is greatest for exhaust compositions highest in olefinic content. While these generalities on the involvement of SO_2 in aerosol formation may hold true, many quantitative and mechanistic aspects of SO_2 oxidation are not understood and are the subject of other investigations. In this study SO_2 was deliberately excluded from the experiments, and it will not therefore be considered further in our discussions.

AEROSOL STUDIES WITHOUT SO_2

In reviewing the aerosol studies conducted without SO_2, there appears to be some controversy over the relative importance of two hydrocarbon types, aromatics and olefins, in their roles as organic aerosol precursors. There is unanimous agreement that common alkanes and aldehydes play little part as precursors in photochemical aerosol production.

Several studies[20,25,29,32,37,38] have pointed out the tremendous propensity of some diolefins, cyclic olefins, and terpenes to form organic aerosols. In addition to being highly reactive with ozone, these hydrocarbons appear to be unusually prolific aerosol precursors by providing two sites for oxidation and thereby readily acquiring the low vapor pressures needed for condensation. A few examples of the oxidized compounds of aerosol produced in Battelle's smog chamber from cyclohexene and α-pinene are shown below. Identification was made by gas chromatography/chemical ionization mass spectrometry[38].

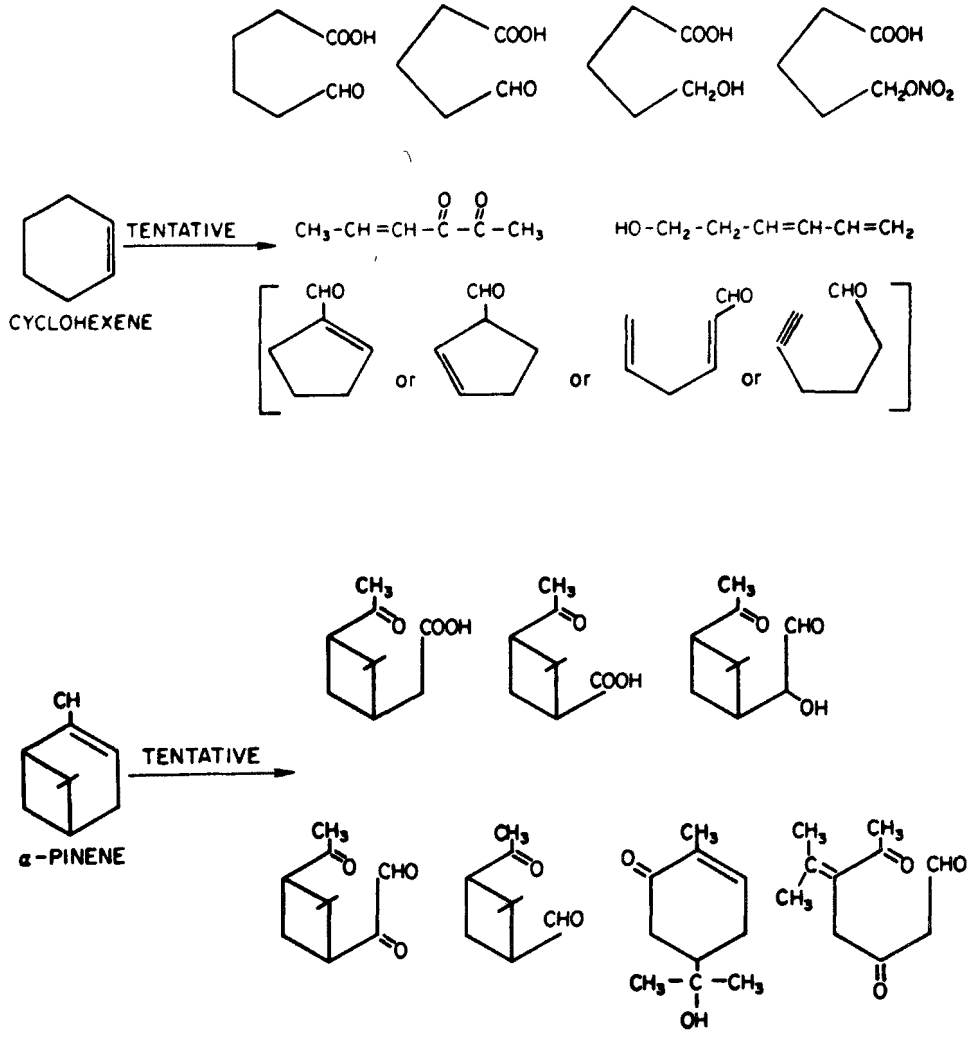

Apart from forested areas where terpenes are prevalent, the rather exotic olefins mentioned above are rarely found. Thus in polluted urban atmospheres we need be concerned about the more familiar olefins and the aromatic hydrocarbons typical of combustion and evaporative emissions. Here the distinction between the importance of olefins and aromatics in aerosol formation is not so clear.

In the early work of Stevenson, et al.[20], photochemical aerosol formation (measured by light scattering) was observed upon irradiation of 1,3,5-trimethylbenzene-NO_x-air mixtures as well as NO_x-air mixtures with

1-hexene, 1-heptene, 3-heptene, and cyclohexene. With trans-2-butene only smaller particles were produced as evidenced by condensation nuclei counts.

The results of our more detailed study of aerosol formation from hydrocarbon-NO_x mixtures showed that aromatic hydrocarbons were more reactive in aerosol production than the olefins and alkanes typical of urban pollution[29]. The relative reactivities of these classes are summarized in Figure 2.

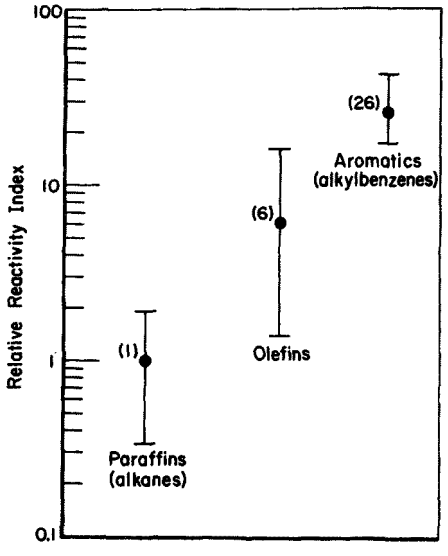

FIGURE 2. RELATIVE REACTIVITY OF EXHAUST HYDROCARBONS IN FORMING LIGHT-SCATTERING AEROSOLS IN SIMULTATED SMOG

The vertical bars in Figure 2 indicate the reactivity range within each structural class. Based on the average light scattering in each class, the relative reactivity ranking of the three classes was aromatic > olefins > alkanes in the ratio 26/6/1.

Results of a more recent study of organic aerosol formation by O'Brien, et al.[33] are shown in Table 1. With the exception of o-xylene, these data indicate that aromatic compounds and monoolefins with carbon

TABLE 1. AEROSOL FORMATION FROM SELECTED HYDROCARBONS O'Brien(33).

Hydrocarbon(a)	Maximum Light Scattering $b_{scat} \times 10^4$ m^{-1}
Glutaraldehyde	0
Ethylbenzene	1
Mesitylene	1
2,6-Octadiene	1
1-Octene	1
trans-4-Octene	1
5-Methyl-1-hexene	1
2,6-Dimethylheptane	1
1-Heptene	1
o-Xylene	8
1,5-Hexadiene	40
Cyclohexene	90
2-Methyl-1,5-hexadiene	110
1,6-Heptadiene	160
1,7-Octadiene	180
α-Pinene	180

(a) Each hydrocarbon (2.0 ppm) irradiated with 1.0 ppm nitric oxide and 70% RH measured at 22 C.

chains $\geq C_4$ produce aerosols corresponding to similar light-scattering levels. A rather reactive alkane, 2,6-dimethylheptane, was also found to be in this category. Olefins of carbon length <5 were found to produce no light scattering in accord with the other studies.

Even more relevant to the atmospheric situation, we want to know the reactivity of these hydrocarbons behaving in complex mixtures. Studies of secondary aerosol formation from auto exhaust have helped in this respect.

In some of the early work, Schuck, et al.[35] observed that the higher olefinic exhausts produced the most aerosol (measured by light scattering), but the sulfur content of the fuels employed was quite high (up to 0.22 weight percent). Data from a study by Hamming, et al.[36], where fuel sulfur levels were only 0.01-0.04 weight percent, indicated that fuels high in aromatic content produced more aerosol than other compositions.

Selected results of several years' work at Battelle on auto exhaust are summarized in Figure 3[39]. The smog-chamber experiments (replicate experiments shown as averages) were conducted with 8 ppmC exhaust hydrocarbons generated from low-sulfur (<0.02 weight percent) nonleaded fuels. Figure 3 depicts an implied linear relationship between

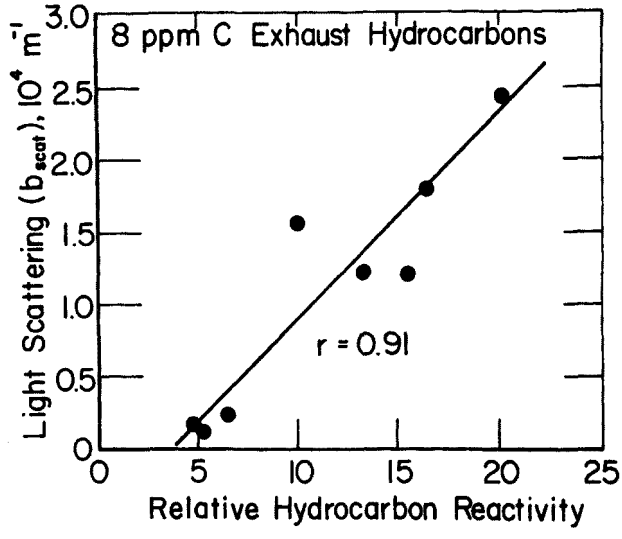

FIGURE 3. REGRESSION RELATIONSHIP OF AEROSOL FORMATION (LIGHT SCATTERING) WITH A HYDROCARBON REACTIVITY FOR AUTO EXHAUST DERIVED FROM A LINEAR SUMMATION OF INDIVIDUAL REACTIVITIES

peak light scattering and a normalized hydrocarbon reactivity parameter computed for the exhaust composition on the basis of linear summation using a 26/6/1 weighting for aromatic/olefin/alkane hydrocarbons. While there is considerable scatter

in the mid-region of the reactivity scale the correlation is reasonably good (0.91) especially realizing that innumerable factors (slight variations in HC/NO_x ratios, light intensity, CO concentration, etc.) are not taken into account. Actually, an improvement in the correlation coefficient for this type regression was obtained if the aromatic/olefin/paraffin weighting factors were changed from 26/6/1 to 10/6/1. This analysis would suggest that, for exhaust mixtures, aromatic hydrocarbons (on the average) are only 2 rather than 4 times as reactive as olefins in promoting photochemical aerosol formation. A reduction in the relative reactivity for aromatic hydrocarbons in extrapolating reactivity data from experiments with single hydrocarbons to those with mixtures of hydrocarbons is also consistent with the results obtained when binary hydrocarbon mixtures containing aromatics are irradiated. That is, the peak light scattering observed with a binary hydrocarbon mixture (including one or two aromatics) of different reactivity is consistently less than (and often half) that predicted by a linear summation of peak light scattering derived from experiments with the individual hydrocarbons[39].

Results from two other laboratories conducting similar research with auto exhaust seem to support, at least qualitatively, our findings regarding the relationship between exhaust aromatic content and peak light scattering from secondary aerosol formation[40,41].

One final point should be made here about the relevance of aromatics. Several investigators have dismissed aromatics as major participants in aerosol formation on the basis that there is little aromatic character associated with the organic extracts of atmospheric aerosols. Indeed, we found that the ratio of aliphatic to aromatic protons was >10/1 for most samples[1]. The explanation, we feel, is that the oxygenated compounds emanating from aromatic degradation loose their aromatic character via ring cleavage. Evidence of this is demonstrated by the structures shown below. These compounds were identified as major aerosol products when toluene and NO_x were irradiated in a smog chamber[38]. Note that with the exception of the nitrated compound, all products have lost their ring structure.

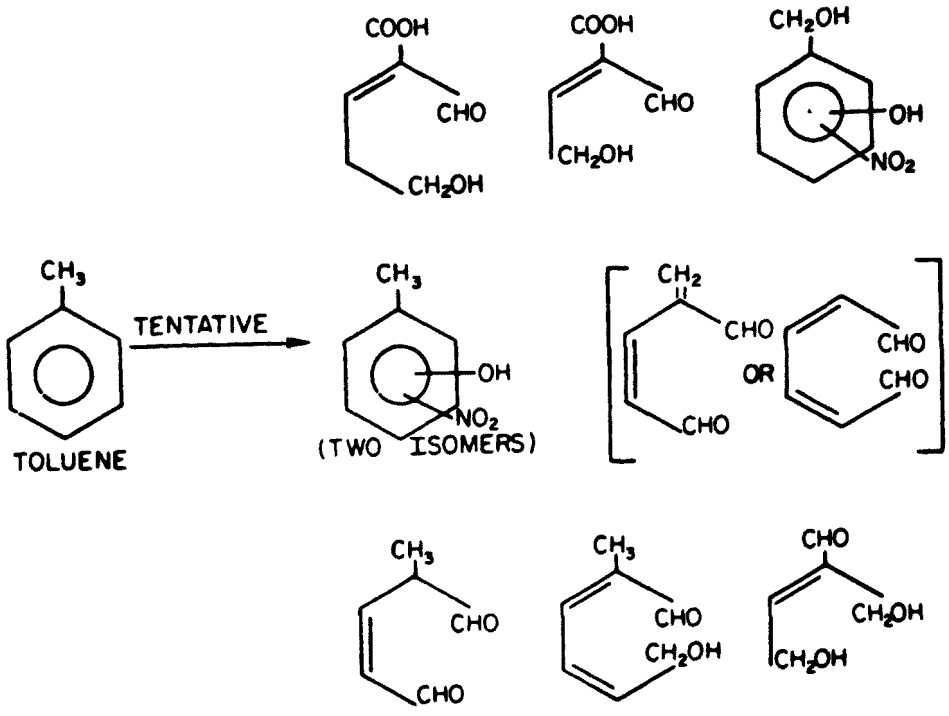

In nearly all the aforementioned studies, aerosol formation has been determined by light-scattering principles[42] or condensation nuclei counters[43]. For reasons that we will not attempt to detail here, neither the light-scattering methods nor the nuclei counters is completely satisfactory for quantitating the concentration of aerosol produced in units of volume or mass. The volume (or mass) of aerosol formed is the most important quantity to determine in this work because it is the only quantity conserved during the experiments*: Since aerosol volume is conserved, the rate of its formation is directly proportional to the rate of gas-to-aerosol conversion (whether via nucleation or condensation). How the photochemical aerosols manifest in the real atmosphere (i.e., how the aerosol mass is eventually distributed with respect to aerosol size) will depend in large part on the nature of the aerosol environment in which they are generated.

*Other quantities, such as the number concentration (CNC), the total surface area concentration or the surface cross section in a particular size range (light scattering) cannot be interpreted in terms of volume or mass without additional information.

The most serious limitations of the light-scattering instruments are the strong dependence of light scattering on particle size in the diameter range 0.1 to 0.5 μm and their insensitivity to aerosols <0.1 μm. Since most smog-chamber experiments are conducted without primary aerosols in the light-scattering range, secondary aerosol growth begins from nucleation, and the subsequent growth via condensation (and, in some cases, continued nucleation) requires a substantial degree of gas-to-aerosol conversion before many of the aerosols approach the light-scattering size range[39].

With the development[44], refinement[45], and calibration[46] of the Electrical Aerosol Analyzer over the past several years, it is now possible to monitor, in real time, the size distribution of secondary aerosol growth over a considerable size range (0.005 to 0.3 μm)* and thereby infer by integration the aerosol volume concentration.

An example of the information obtained by this new monitoring technique is shown in Figure 4 where filtered auto exhaust (16 ppmC hydrocarbons) was irradiated for 6 hours. The aerosol number, surface and volume concentrations were derived from the electrical aerosol analyzer. The light-scattering curve was determined by an integrating nephelometer.

For the last few years electrical aerosol analyzers have been utilized in smog-chamber research at the University of Minnesota (U of M) and Calspan, as well as at Battelle. Currently, these instruments are operating at several other laboratories including EPA-RTP, University of North Carolina, California Institute of Technology, Science Center at Rockwell International, and General Motors Research.

In spite of the vast improvements in aerosol monitoring, there remain major differences in the rates of aerosol production for seemingly similar experiments conducted in different smog chambers. Table 2 summarizes results from a series of experiments conducted at Calspan and the U of M in which the initial concentrations of hydrocarbons and nitric oxides were nearly identical[47]. Looking at the rate parameter for NO

*A range which includes >90 percent of all the aerosol volume observed in the experiments conducted in this study.

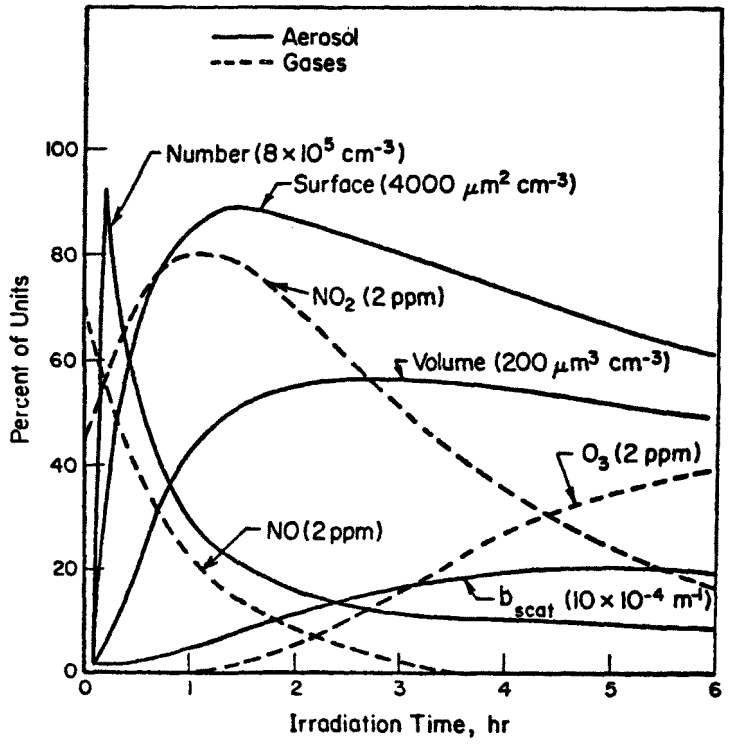

FIGURE 4. PROFILE OF AEROSOL FORMATION DURING IRRADIATION OF FILTERED AND DILUTED AUTO EXHAUST (16 ppmC HYDROCARBONS)

photooxidation (Table 2, NO_2-t_{max}) it appears that for the more slowly reacting hydrocarbons (toluene and 1-hexene) reactivity in the Calspan chamber is considerably less than in the U of M chamber, in spite of the fact that the light intensity of the Calspan chamber was substantially greater than that of the U of M chamber (k_d = 0.23 min^{-1} and 0.15 min^{-1}, respectively). The differences in reactivity in terms of NO photooxidation are less in the cases of m-xylene and cyclohexene, but again the rates are highest for Calspan. Differences in the maximum aerosol formation rate (Table 2) for "replicate" experiments are quite diverse; a factor of 10 for toluene, 20 for 1-hexene, 5 for m-xylene, and 2 for cyclohexene. Most disconcerting, perhaps, is the fact that the higher formation rate in each case is not occurring in the same chamber. The higher rates of aerosol

TABLE 2. COMPARISONS OF AEROSOL FORMATION AND REACTIVITY FOR SMOG CHAMBERS AT CALSPAN AND THE UNIVERSITY OF MINNESOTA

Run No.	Laboratory(a)	Initial Conditions: Hydrocarbon	ppm (vol/vol)	Initial Conditions: [NO], ppm	Reactivity Parameters: NO_2-t_{max}, min	Reactivity Parameters: Aerosol Volume Formation Rate (dV/dt), $\mu m^3/cm^3/hr$
6	Calspan	toluene	0.35	0.17	400	2.2
76	U. of Minn.	toluene	0.35	0.15	210	24.5
5	Calspan	1-hexene	0.33	0.15	420	2.1
92	U. of Minn.	1-hexene	0.35	0.12	280	0.09
15	Calspan	m-xylene	0.34	0.15	100	14.1
81	U. of Minn.	m-xylene	0.35	0.15	80	73
10	Calspan	cyclohexene	0.33	0.14	120	110
83	U. of Minn.	cyclohexene	0.35	0.13	90	50

(a) Laboratory Conditions: Calspan chamber volume = 20,800 ft^3, k_d = 0.23 min^{-1}; University of Minnesota chamber volume = 600 ft^3, k_d = 0.15 min^{-1}.

production with aromatic hydrocarbons (toluene and m-xylene) were observed in the U of M chamber while the higher aerosol rates for olefins (1-hexene and cyclohexene) were observed at Calspan.

There appears to be another peculiarity in the above study that needs attention. Figure 5 is a time-concentration profile of Calspan Run No. 5. Considering the normalcy of the HC/NO_x ratios in the experiment (ppmC/ppmV = 13/1 in the case of 1-hexene), the rate of NO photooxidation

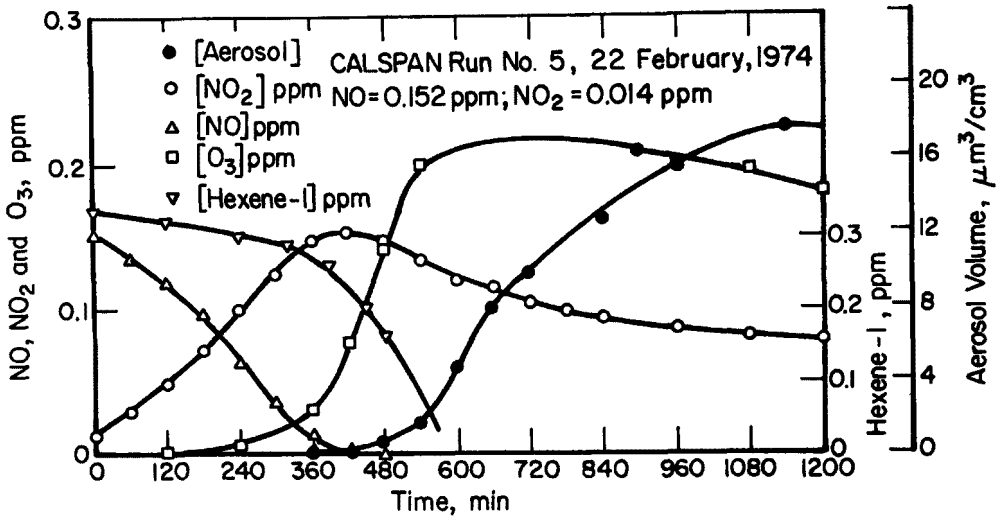

FIGURE 5. REPRODUCTION OF SMOG PROFILE FROM THE PHOTOOXIDATION OF 1-HEXENE AND NO IN THE CALSPAN CHAMBER

is unusually slow, and there is an unusually long induction period to aerosol formation (5 hours before any appreciable aerosol volume was observed in Calspan Run No. 5). As pointed out by comparisons made later in the report, these rates of oxidation are much slower than observed in the real atmosphere. The low light intensity in the Calspan chamber cannot be entirely responsible for the apparent lack of reactivity. In the real atmosphere, Jefferies, et al.[48] report an average k_1 value of

0.28 min^{-1} for the 5 hours between 0800 and 1300-EDT (latitude 35.72°, September 19, 1974) which is only twice as great as the k_1 value estimated for the Calspan chamber.

It is not likely that the peculiarities among smog-chamber results can be rationalized satisfactorily at this time. We would like to believe, however, that the major differences are related primarily to our insufficient knowledge of the chemical reactions taking place rather than to some mysterious artifacts involving "dirty chamber walls". As we attempt to provide a "current interpretation" of organic aerosol formation in the succeeding section of the report, we will try to explain some of the peculiarities and inconsistencies described above.

SECTION 4

CURRENT INTERPRETATION OF ORGANIC AEROSOL FORMATION

PRECURSOR CHARACTERISTICS OF ORGANIC AEROSOL FORMATION

With the history of earlier work and the data emanating from ongoing studies at several laboratories, it is possible to present an updated overview of the formation of photochemically derived organic aerosols.

In polluted urban atmospheres, the aromatics and the higher molecular-weight olefins have been shown to be the most important types of hydrocarbons in the formation of organic aerosols. It appears that these hydrocarbons react by different mechanisms in initiating the oxidation steps leading to condensable matter, and it is instructive to recognize these differences.

Differences in the simulated reaction profiles give evidence of the mechanistic differences. When tolulene is photooxidized with NO, NO_2, and water vapor in the Battelle smog chamber, aerosol formation results as shown in Figure 6. Toluene is oxidized more slowly than other aromatics (alkylbenzenes). The slower oxidation of toluene serves to illustrate an important characteristic we have seen with all aromatic hydrocarbons investigated; namely that, under proper conditions, toluene and the other alkylbenzenes produce aerosol during the period of NO oxidation and before appreciable O_3 formation. This, of course, is due to the fact that the aromatics react most exclusively with HO radicals under these conditions. The important role played by HO will be discussed shortly.

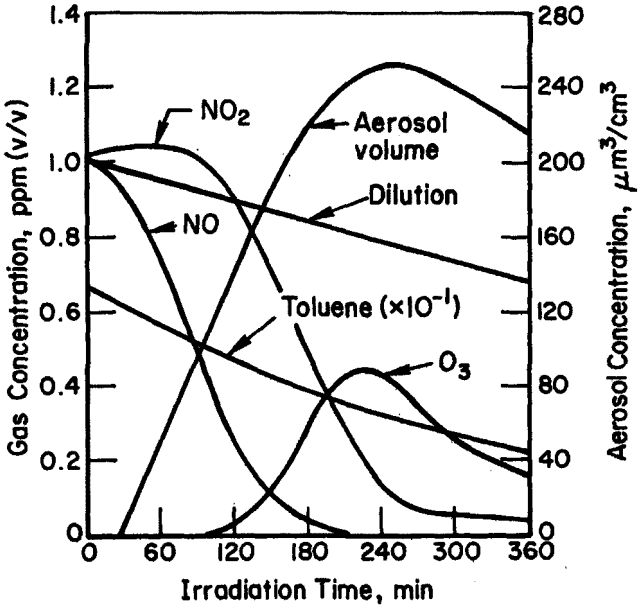

FIGURE 6. PHOTOCHEMICAL AEROSOL FORMATION DURING A SMOG-CHAMBER IRRADIATION OF A TOLUENE-NO_x-AIR MIXTURE

Figure 7 is a smog profile resulting from irradiation of 1-heptene, NO, NO_2, and water vapor. In this case, aerosol formation seems to be delayed until O_3 is formed, and we believe that in the case of olefins, the olefin-O_3 reaction may be more important overall to aerosol production than the olefin-HO reactions. Notice here that during the first 30 minutes of the irradiation, before appreciable O_3 is formed, a substantial amount of 1-heptene has been oxidized via 1-heptene-HO reactions, yet only a very small volume of aerosol was produced in this period. With the appearance of O_3, the rates of aerosol formation and 1-heptene oxidation increase.

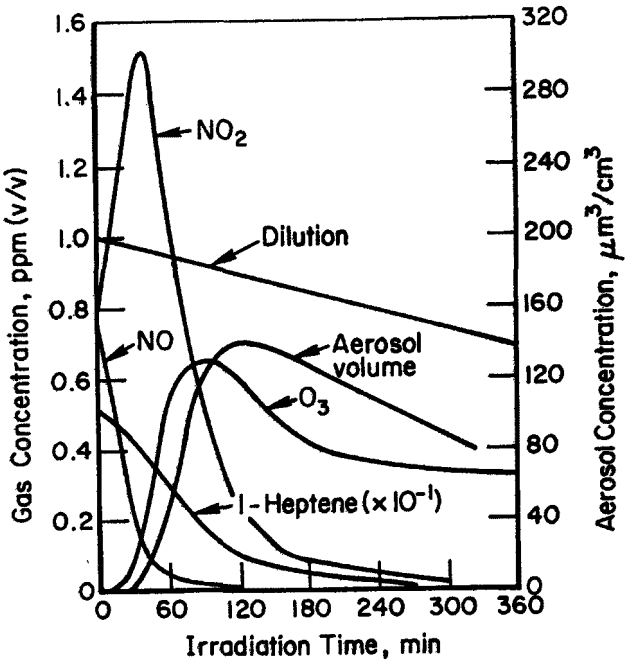

FIGURE 7. PHOTOCHEMICAL AEROSOL FORMATION DURING A SMOG-CHAMBER IRRADIATION OF A 1-HEPTENE-NO_x-AIR MIXTURE

Because we are now able to measure the volume of aerosol produced with irradiation time (i.e., the gas-to-aerosol conversion rate) it seems important to attempt to provide a quantitative (or at least semiquantitative) measure of reactivity of hydrocarbons with respect to aerosol formation. In the past (e.g., references 29 and 33) reactivities have been expressed on relative scales, and there has been no basis for assigning an absolute measure of aerosol production to any of the hydrocarbons. In an effort to provide quantification, we have defined a rather simple relationship called conversion efficiency (relationship A):

$$\text{Percent Conversion Efficiency (gas-to-aerosol conversion)} \equiv \frac{\text{Maximum Aerosol Formation Rate}}{\text{Maximum HC Oxidation Rate}} \times 100. \quad \text{(A)}$$

We define conversion efficiency for a particular hydrocarbon as the maximum aerosol formation rate divided by the maximum oxidation rate of the hydrocarbon during this occurrence; or the fraction of the hydrocarbon consumed which results in condensable matter. We have used *mass* as the basic unit of comparison. If the efficiency terms can be trusted (and there will no doubt be some variations of the values for different smog conditions; HC/NO_x ratios, etc.), then to predict aerosol formation under normal smog circumstances one might only have to multiply the observed hydrocarbon depletion rate by the appropriate conversion-efficiency value.

Table 3 shows some estimates of the efficiencies of a few hydrocarbons.

TABLE 3. ESTIMATED AEROSOL CONVERSION EFFICIENCIES FOR A FEW FAMILIAR HYDROCARBONS

Hydrocarbon	Efficiency, percent	
	HC + HO	HC + O_3
Toluene $k_{HC + HO} = 6 \times 10^3$(a)	7	very small
Butane $k_{HC + HO} = 4 \times 10^3$	very small ($<1 \times 10^{-2}$)	very small
Propylene $k_{HC + HO} = 2.5 \times 10^4$ $k_{HC + O_3} = 1.8 \times 10^{-2}$	very small ($<3 \times 10^{-3}$)	0.1
1-Heptene $k_{HC + HO} \sim 1 \times 10^5$ $k_{HC + O_3} \sim 5 \times 10^{-2}$	0.15	1.6
Cyclohexene $k_{HC + O_3} \sim 1 \times 10^{-1}$	?	28

(a) Rate units = $ppm^{-1}\ min^{-1}$.

For toluene we estimate a fairly substantial conversion efficiency of 7 percent. This value was established by both electrical aerosol analyzer data and gravimetric determinations of aerosols collected during smog-chamber experiments. Since toluene reacts almost exclusively with HO, the efficiency term is indicated under the HC+ HO column in Table 3. Under toluene, as well as under the other hydrocarbons listed, we have indicated a rate constant for the precursor reactions thought to be significant in each case. Thus by comparing the rate constants for two hydrocarbons (with a particular radical) coupled to the respective efficiency factor, one can appreciate the relative importance of the hydrocarbons to produce organic aerosols.

For butane, the efficiency factor is estimated to be very small, and its participation (as well as that of many alkanes) in aerosol production can be neglected. For propylene, which reacts much faster with HO, we nonetheless estimate a very small efficiency value for HO reactions, and this process can certainly be neglected. With ozone, however, a small but measurable ability to make aerosol is observed. Overall though, propylene can make only a very small contribution to the organic aerosol problem.

Because 1-heptene is a larger molecule than propylene it is appreciably more efficient in aerosol formation. Here again there is experimental evidence that the efficiency is greater upon reaction with O_3 compared to OH, but the distinction is not clear-cut since the reaction profiles are not clearly separable. By coupling the efficiencies with the respective rate constants for the O_3 reactions, 1-heptene is estimated to produce about 25 times as much aerosol as propylene. Cyclohexene is very unusual in its efficiency in producing aerosol for reasons discussed earlier. Here the efficiency value is a fairly crude estimate based on light scattering and gravimetric measurements.

As a final example of this analysis let us look at aerosol production in Figure 8 where a representative urban mixture of 17 hydrocarbons is irradiated at near-ambient conditions. Here too we arrive at an approximate efficiency value for the hydrocarbon mixture by

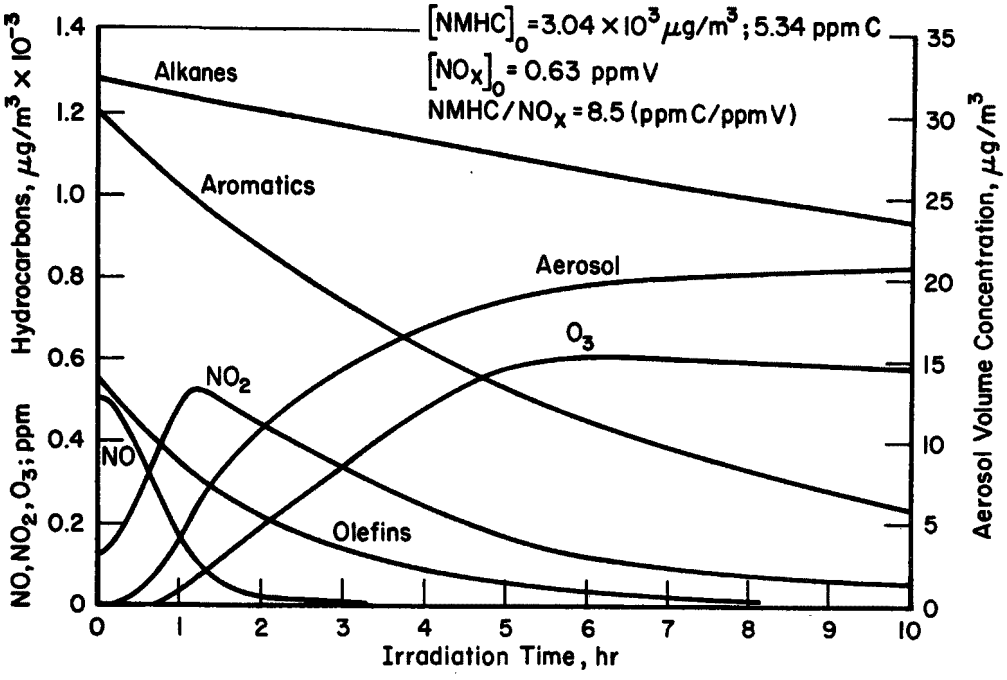

FIGURE 8. PHOTOCHEMICAL AEROSOL FORMATION DURING A SMOG-CHAMBER IRRADIATION OF A SURROGATE HYDROCARBON MIXTURE AND NO_x

averaging the hydrocarbon oxidation rates and dividing it into the aerosol formation rate. These quantities are summarized below.

Smog-Chamber Simulation

Maximum total HC oxidation rate = 400 μg/m^3/hr (13% hr)
Maximum aerosol formation rate = 10 μg/m^3/hr
Maximum conversion efficiency = 2.5 percent

Urban Conditions

Assume [total HC]$_o$ = 3 ppmC (1.7 x 10^3 μg/m^3)
Assume τ_{HC} = 4 hr
Maximum aerosol concentration after 4 hr ~ 20 μg/m^3

Dividing the maximum aerosol formation rate by the maximum total hydrocarbon oxidation rate results in an overall maximum conversion efficiency for the hydrocarbon mixture of 2.5 percent. If we extrapolate these findings to polluted urban conditions, as indicated above, and assume a typical mean hydrocarbon lifetime of 4 hours, we would predict a maximum organic aerosol concentration after 4 hours of 20 $\mu g/m^3$. Admittedly, much of this analysis is handwaving, but judging from the fairly good agreement between the simulated production of organic aerosols and the actual concentrations observed in urban areas it seems reasonable to conclude as follows:

(1) On the average, only a very small percentage (2-3) of the hydrocarbon that gets oxidized in the urban atmosphere ends up as aerosol, and it is possible to estimate the efficiency of certain hydrocarbons to make organic aerosols.

(2) Higher molecular weight olefins and aromatics are principally responsible for organic aerosol formation. Olefin-O_3 and aromatic-HO reactions appear to be the important precursor reactions in each case.

(3) The smog chamber appears reliable in simulating aerosol formation in photochemical smog, i.e., the rates of aerosol formation in the chamber are in accord with our expectations of the polluted atmosphere.

INTERLABORATORY COMPARISONS

If smog chambers are reliable in simulating photochemical aerosol formation then why do we see such divergent results among the different chambers? And why, in some cases, do we see rates of oxidation so

markedly different from the polluted atmosphere? In Los Angeles[49], for example, 55 percent of the olefins are consumed in a 4-hour period (0800-1200) while in the Calspan and U of Minn. chambers only a few percent of 1-hexene was oxidized in 4 hours. We feel that the answers to these questions are attributable to actual differences in chemical composition and other conditions of the simulated atmospheres compared to the real atmosphere. These differences may sometimes appear to be subtle, but they are believed to have rather profound effects on the radical concentrations responsible for aerosol production.

Let us examine some of the differences in reaction conditions which might explain the divergent rates of photooxidation observed between Calspan Run No. 5 (Figure 5) with 1-hexene and a Battelle experiment (Figure 7) with 1-heptene. Comparisons of some initial conditions and a few reactivity results are tabulated in Table 4.

TABLE 4. COMPARISONS OF SMOG-CHAMBER CONDITIONS AT CALSPAN AND BATTELLE AND SOME REACTIVITY RESULTS OF OLEFIN PHOTOOXIDATION

	Calspan	Battelle
Initial Conditions		
Chamber volume, ft^3	20,800	610
Lamps	blacklamps, sunlamps, whitelamps	blacklamps, sunlamps
Light intensity (k_d), min^{-1}	0.23	0.47
Hydrocarbon, ppmV	0.33	5.1
NO, ppmV	0.152	0.72
NO_2, ppmV	0.014	0.76
NO_2/NO_x	0.08	0.51
HC/NO_x, ppmV/ppmV	1.98	3.44
RH, percent	41	66
Photooxidation Parameters		
NO_2-t_{max}, min	420	36
Appearance time for aerosol vol, min	300	15
Aerosol production rate (dv/dt) max, $\mu m^3/cm^3/hr$	2.1	160
Aerosol conversion rate normalized to Calspan's pollutant concentrations	2.1	10.4

It is apparent in this case that there are large differences in initial reactant conditions as well as in experimental conditions. In the categories of light intensity and HC/NO_x ratio, the Battelle conditons are more favorable toward reactivity than Calspan's. The Battelle-to-Calspan ratio in these categories is 2/1 and 1.7/1, respectively. Another important factor here is the NO_2/NO_x ratio. The effect of this parameter on photooxidation rates is shown in Figure 9 for the 1-butene-NO_x system[27]. On the basis of the data in Figure 9, the difference between 8 percent NO_2 for Calspan and 50 percent NO_2 for Battelle could result in an additional factor of 2 difference for the NO_2-t_{max} rate. Coupling these three terms results in a predicted photooxidation rate 6.8 times greater for the Battelle conditions versus the Calspan conditions.

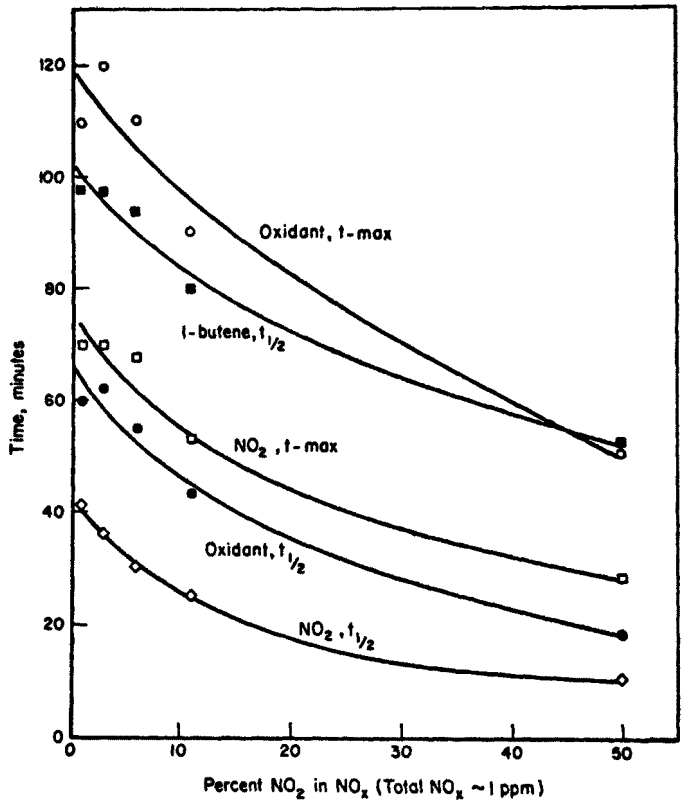

EFFECT OF NO_2/NO_x RATIO ON RATE PARAMETERS

1-Butene system.

FIGURE 9. EFFECT OF NO_2/NO_x RATIO ON PHOTOOXIDATION RATE PARAMETERS IN THE 1-BUTENE-NO_x-SYSTEM

In addition to the difference in the appearance time of aerosol in the two experiments, there is a tremendous difference in the maximum aerosol production rate. Differences in this rate should, however, be viewed after normalizing for the pollutant concentrations, and having done so, we see the aerosol formation rate is about 5 times greater for the Battelle experiment, in accord with the other differences in reactivity. The use of a higher molecular weight olefin (1-heptene) in the Battelle experiment is yet another reason to expect higher aerosol concentrations compared to the Calspan results. Thus, a large number of factors are important in attempting to conpare secondary aerosol results from different laboratories. If we had a better understanding of the chemical processes involved in aerosol formation, we might be able to provide a more accurate accounting for the differences.

One factor, namely nitrous acid (whose initial concentration is related to background air purification and chamber surfaces) is believed to be highly variable from chamber to chamber and may well account for some reactivity differences observed between seemingly similar experimental conditions. In the absence of light, nitrous acid (HONO) forms in the atmosphere and in smog chambers according to reaction 1a

$$NO_2 + NO + H_2O \underset{1b}{\overset{1a}{\rightleftharpoons}} 2\ HONO \quad . \qquad (1)$$

Decomposition of HONO, reaction 1b, limits its concentration. There is considerable evidence[50-52] that equilibrium concentrations of nitrous acid exist in the Battelle chamber prior to irradiation. If so, HO will be generated from HONO photolysis, and hydrocarbon oxidation is expected to occur at the moment of irradiation. The high rate of HO attack causes hydrocarbons to become radicals which both oxidize NO and regenerate HO to continue the chain sequence. This pattern of immediate oxidation is in contrast to that where no HONO exists as the irradiation

begins. In this case, NO_2 photodissociates, and nearly all of the O atoms produced serve to oxidize NO back to NO_2. If the hydrocarbons in the system are not successfully attacked by very low concentrations of O atoms or O_3 the generation of HO radicals (which are much more likely to react with hydrocarbons) proceeds rather slowly*. In instances where aromatic hydrocarbons are involved, it appears that a very long induction period to hydrocarbon oxidation might result where no HO source (e.g., HONO) was present initially. Indeed this seems to be the case with both the Calspan experiments and the U of M experiments. Because of the heterogeneous nature of reaction 1a** and the very large volume of the Calspan chamber, it is easy to understand why appreciable HONO is not formed prior to irradiation. In the U of M chamber where

---

*There are usually two reactions which predominate in HO production:

$$HONO + h\nu \longrightarrow HO + NO \quad (2)$$

$$HO_2 + NO \longrightarrow HO + NO_2 . \quad (3)$$

Therefore, aside from nitrous acid formation via reaction (1a), we must look for other sources of HONO and those for HO_2. The only important HONO sources are (4)

$$HO + NO(+M) \longrightarrow HONO(+M) \quad (4)$$

which leads to no net increase in HO radicals, and (5)

$$HO_2 + NO_2 \longrightarrow HONO + O_2 \quad (5)$$

which requires HO_2 radicals. The principal primary source of HO_2 is aldehyde photolysis, for example (6)

$$CH_2O + h\nu \longrightarrow H + HCO, \quad (6)$$

followed by reactions (7)

$$H + O_2(+M) \longrightarrow HO_2(+M) + HCO \quad (7)$$

and (8)

$$HCO + O_2 \longrightarrow HO_2 + CO . \quad (8)$$

Likewise, the reaction of alkoxy radicals with oxygen produces HO_2;

$$CH_3O + O_2 \longrightarrow HO_2 + CH_2O . \quad (9)$$

However, since the secondary reactions of CH_3O and H usually require an earlier reaction of HO (H from HO + CO $\longrightarrow$ H + CO_2 and RO from the sequence HO + RH $\longrightarrow$ H_2O + R; R + O_2 $\longrightarrow$ RO_2, RO_2 + NO $\longrightarrow$ RO + NO_2) we must look back at the sources of HO and stress the importance of the initial [HONO] in initiating photooxidation reactions in relatively unreactive systems.

**The heterogeneous nature of reaction (1a) to form HONO is suspected on the basis of kinetic data which show the reaction to be progressively slower as the reaction vessel is enlarged. The original rate constant obtained by Wayne and Yost for reaction (1a) is 4.3×10^{-6} $ppm^{-2}min^{-1}$(53). Using a chamber 40 times larger Graham and Tyler(54) obtained a much smaller value; 1.2×10^{-9} $ppm^{-2}min^{-1}$. Recently Calvert and associates at O.S.U. have observed consistent homogeneous behavior corresponding to a rate constant of 2.1×10^{-9} $ppm^{-2}min^{-1}$(55).

the S/V ratio is much greater, one would expect appreciable HONO formation unless mixing is poor or the Teflon surfaces are not conducive to the heterogeneous reaction. While there seems to be some basis for expecting different HONO concentrations in the Calspan and University of Minnesota chambers, that alone would not seem to adequately account for the differences observed in reactivity for toluene and m-xylene in the experiments compared earlier (Table 2). In the U of M chamber the initial [HONO] was perhaps significant enough to overcome the light intensity advantage of the Calspan chamber. For the experiments with olefins, light intensity was probably the dominate factor in accounting for the reactivity differences in these two chambers.

In a final analysis of smog-chamber performances, an important question to be addressed is, how do the rates of hydrocarbon oxidation in the polluted atmosphere compare with the smog-chamber results? This subject is treated in detail in the *Discussion* section of the report. The limited data from hydrocarbon mixtures indicate that the rates of oxidation of alkanes in the Battelle chamber are nearly identical to those found in the Los Angeles atmosphere[49] and in the 6-m^3 glass chamber at Riverside[56]. Compared to these two sources of rate data, olefin oxidation may be 50 percent greater in the Battelle chamber. On the average, the oxidation rates for aromatic hydrocarbons are about twice as great in the Battelle chamber as they are in the Los Angeles atmosphere (avg. rate, 0800-1200) and perhaps 50-100 percent greater than those observed in the Riverside chamber. Thus, the photooxidation rate data from the Battelle chamber, which have been emphasized in much of this discussion, are thought to be somewhat greater than the rates in the real atmosphere.

SECTION 5

EXPERIMENTAL APPROACH

In the planning of this program, much consideration was given to the appropriateness of including SO_2 and primary aerosols in the initial experimental program. Arguments were presented that nuclei, either those provided as primary aerosols or as secondary sulfuric-acid aerosols, might be necessary to cause nucleation of the organic vapors at low concentrations, and that experimental simulations of authentic organic aerosol formation might be meaningful only if these important variables were included. On the other hand, inclusion of SO_2 in the reactant mixture would not permit an accurate assessment of organic aerosol formation because analytical methods were not sophisticated enough to distinguish quantitatively between organic and sulfate aerosols. It was also well known that, although the HC-NO_x constituency of smog profoundly effects the rate of SO_2 oxidation, the corollary is not true; i.e., the presence of SO_2 in a HC-NO_x mixture has virtually no effect on the rate of hydrocarbon oxidation or even NO oxidation*. This is primarily due to the fact that hydrocarbons, particularly those involved in organic aerosol formation, out compete SO_2 for reactions with radicals by factors of 10 to 100. Furthermore, unpublished data from our laboratory indicate that sulfuric acid aerosols and organic aerosols are formed independently when mixtures of hydrocarbons, NO_x and SO_2 are irradiated in a smog chamber. For these reasons, SO_2 was excluded from the reaction mixture.

Primary aerosols were also excluded from the initial program for several reasons. First, the generation and control of primary aerosols is difficult, particularly where contamination from gases must be precluded. Secondly, the additional concentration of surface area provided by primary aerosol (generally 1-5 x 10^3 $\mu m^2/cm^3$ for aged aerosol) is very small relative to the surface/volume ratio of the smog chamber (2.6 x 10^6 $\mu m^2/cm^3$ for our 17.3 m^3 chamber). Thirdly, and most importantly,

*For example, confer reference 52 in which experimental evidence is presented showing insignificant effect of 0.5-3 ppm SO_2 on propylene and NO photooxidation rates.

results of our studies of secondary aerosol formation from auto exhaust teach that while primary aerosols do provide the surface upon which secondary aerosol preferentially condenses they do not significantly effect the degree of secondary organic aerosol formation, and they are not necessary to cause nucleation of organic vapors.

The principal effect of including primary aerosol is to alter the amount of light scattering attributable to secondary aerosol formation. An example is shown in Figure 10 in which auto exhaust was irradiated in the absence and presence of primary aerosol. With the exception of

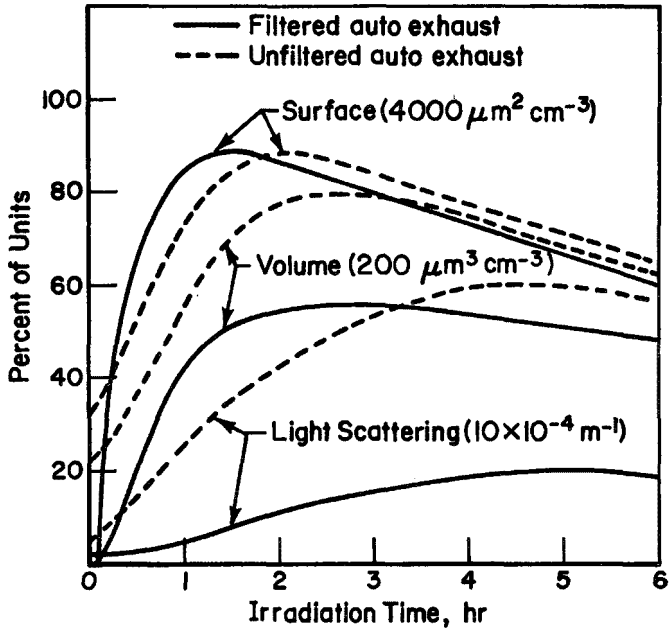

FIGURE 10. THE EFFECT OF PRIMARY AUTO EXHAUST AEROSOLS ON PHOTOCHEMICAL AEROSOL GROWTH AND LIGHT SCATTERING

the differences in primary aerosol concentration, the experiments were essentially identical, and the ensuing gas-phase reactions were also similar. The volume-concentration curves in Figure 10 indicate that the volumetric gas-to-aerosol conversion rates are fairly similar during the two experiments, and that at the end of the irradiations the difference

in total volume is nearly equal to the initial difference, i.e., the volume of primary aerosol. The difference in light scattering caused by primary aerosol can be rationalized on the basis of the consequent differences in the size distribution of the secondary aerosols and the strong dependence of light scattering on this parameter. Interpretative details of these data have been presented elsewhere[30,39,50] and will not be repeated here.

The propensity of organic vapor to nucleate under smog conditions is further illustrated in Figure 11 where auto exhaust (low sulfur fuel) was irradiated in a smog chamber. In this case, the surface distribution of aged primary-exhaust aerosol is represented by the hatched area. At

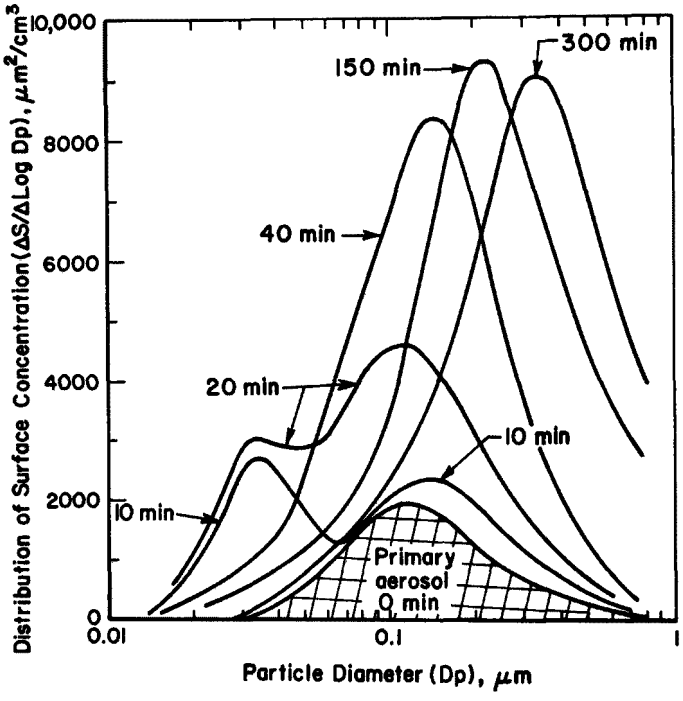

FIGURE 11. EVIDENCE OF PREFERENTIAL HOMOGENEOUS NUCLEATION OF PHOTOCHEMICALLY DERIVED AEROSOL IN AIR CONTAINING PRIMARY NUCLEI

the onset of irradiation we see that, in spite of the presence of primary aerosol surface, homogeneous nucleation of new aerosol occurred as is evident by the additional mode in the surface distribution at 0.03 μm. The aerosol formed in this "nucleation mode" is soon consumed by collisions with aerosols in the "accumulation mode" (0.1 to 1 μm) and thereafter it appears that all new aerosol growth occurs by condensation of vapor on the aerosol existing in the accumulation size region.

In summary, it was felt that the initial goal of establishing definitive relationships among the hydrocarbon and NO_x precursors of organic aerosols could best be achieved by irradiating pollutant mixtures of hydrocarbons and NO_x in otherwise clean air. Because the behavior of hydrocarbons in photochemical smog cannot be adequately simulated by a single hydrocarbon, a surrogate mixture of 17 hydrocarbons was used to simulate polluted urban atmospheres. Water vapor and CO were also added at constant levels to constitute what is referred to as a "reference atmosphere". The distribution of the pollutants in the reference atmosphere, including the hydrocarbons employed and the atmospheric hydrocarbons they represent, are indicated in Table 5. The hydrocarbon mixture was formulated mainly from the atmospheric data of Stephens[57].

Seventeen experiments were conducted varying the total hydrocarbon and NO_x concentration. The experimental design is shown in Figure 12. All irradiations were conducted for 10 hours.

TABLE 5. REFERENCE ATMOSPHERE

Carbon Monoxide = 2.5 ppm

Nitrogen Oxides (total) = 0.100 ppm
Nitric oxide = 0.083 ppm
Nitrogen dioxide = 0.017 ppm

Nonmethane Hydrocarbons = 1.00 ppm as CH_4

Hydrocarbons Represented	Reference Hydrocarbons	Molar Concentrations Relative to Total NMHC	
		Los Angeles Air[a]	Experimental Air[b]
acetylene	acetylene	.177	.136
ethane	ethane	.087	.100
propane	propane	.036	.040
2-methylpropane	2-methylpropane	.024	.023
n-butane	n-butane	.100	.099
2-methylbutane	2-methylbutane	.066	.070
n-pentane	n-pentane	.036	.037
2,2-dimethylbutane 2-methylpentane 2,3-dimethylbutane n-hexane	2-methylpentane	.063[c]	.044
ethylene	ethylene	.129	.162
propylene	propylene	.039	.035
1,3-butadiene 1-butene trans-2-butene cis-2-butene 2-methylpropene	trans-2-butene	.033[c]	.043
2-methylbutene-1 2-methylbutene-2 trans-2-pentene	2-methylbutene-2	.018[c]	.013
benzene	benzene	.024	.029
toluene	toluene	.054	.061
ethylbenzene p-xylene m-xylene o-xylene	m-xylene	.069[c]	.069
isopropylbenzene n-propylbenzene p-ethyltoluene m-ethyltoluene o-ethyltoluene	p-ethyltoluene	.024[c]	.025
1,3,5-trimethylbenzene 1,2,4-trimethylbenzene 1,2,3-trimethylbenzene	1,2,4-trimethylbenzene	.021[c]	.013

(a) Composition derived from that reported by E.R. Stephens [57].

(b) Initial concentrations from Run No. 8.

(c) The sum of the concentrations for groups of similar hydrocarbons in Los Angeles air are indicated opposite the reference hydrocarbon.

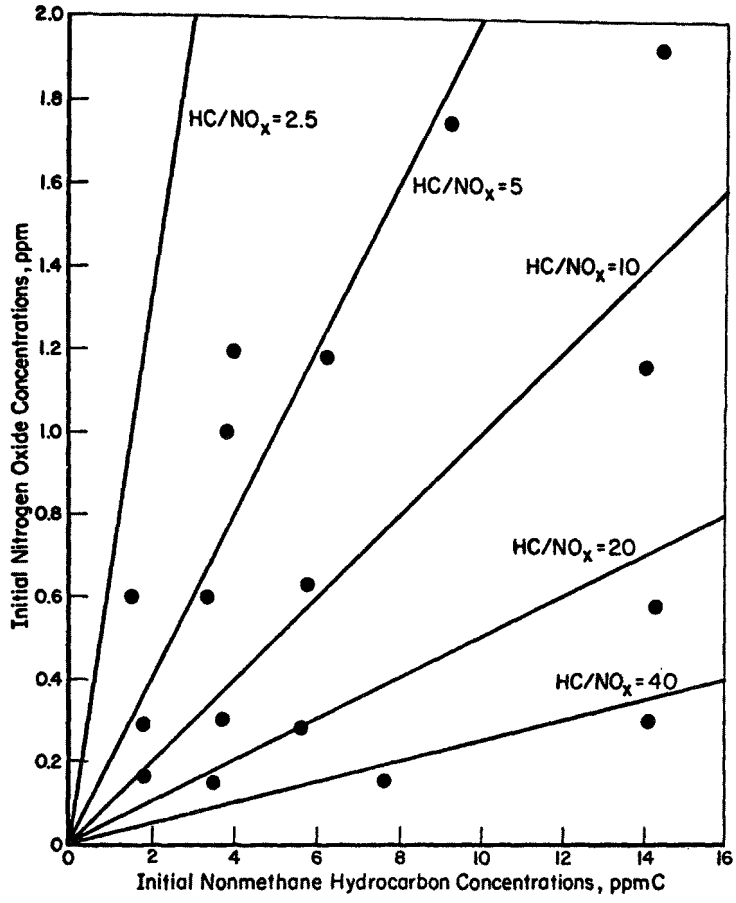

FIGURE 12. INITIAL HYDROCARBON AND NITROGEN OXIDE CONCENTRATION COORDINATES IN THE EXPERIMENTAL PROGRAM

SECTION 6

EXPERIMENTAL METHODS

SMOG-CHAMBER DESCRIPTION AND OPERATION

All irradiation experiments were conducted in Battelle-Columbus' 17.3-m^3 smog chamber having a surface-to-volume ratio of 2.6 m^{-1}; the surface is polished aluminum and FEP Teflon®. Direct irradiation through 5-mil Teflon windows is provided by a bank of 95 fluorescent blacklamps and 15 fluorescent sunlamps. The photon flux of the blacklamps is distributed unimodally in the uv region, with peak intensity at 370 mm; the sunlamp peak intensity occurs at 310 nm. Light-intensity measurements by NO_2 photolysis[58] and o-nitrobenzaldehyde photolysis[59] agree quite well, as described by Gordon[60]. Prior to the first series of experiments new fluorescent blacklamps were installed, and the k_d value was 0.48 min^{-1}. Four months later when the second series of experiments was conducted, the light intensity had diminished to a k_d value of 0.41 min^{-1}.

Background air supplied to the chamber is taken through a 10-m stack atop a three-story building and is passed through a purification system which includes a permanganate filter bed, a charcoal filter system, an absolute filter, and a humidification unit. After purification, background total hydrocarbon is generally 2-3 ppmC, with the majority being methane. Nonmethane hydrocarbons (relatively unreactive) are <0.2 ppmC, NO_x <0.02 ppm, CO <4 ppm, and particles <10^3 cm^{-3}.

Prior to each series of experiments, the chamber surfaces were thoroughly cleaned by washing with water. After cleaning, the chamber was dried by continuous purging with purified air, and then conditioned by prolonged irradiation of background air.

All experiments were conducted for about 10 hours. Typically, the chamber was first humidified with deionized, double-distilled water vapor followed by consecutive injections of NO, NO_2, CO, a low molecular-weight hydrocarbon mixture (C_2-C_4), a high molecular-weight hydrocarbon mixture (C_5-C_9), and tracer (SF_6). The inert tracer was added to determine the dilution rate. Continuous and intermittent sampling of the chamber

air together with a small unavoidable leak rate results in dilution of the original air volume. Makeup air is the same as the purified background air. For experiment Nos. 1-12, the dilution rate averaged about 8 percent/hr; for experiments 13-19, the rate was near 13 percent/hr. The chamber air is well mixed with a stirring fan during the injection period. The stirring fan is turned off when irradiation begins.

ANALYTICAL

The gas-phase chemistry of the smog experiments was monitored with conventional instrumentation. Carbon dioxide was determined by nondispersive IR, O_3 by chemiluminescence with ethylene, NO and NO_2 by automated Saltzman using a dichromate oxidizer for NO oxidation, CH_4 and total NMHC by flame ionization using a dual-flame analyzer. The latter analysis was used primarily to indicate the approximate hydrocarbon concentratins during chamber loading.

Detailed hydrocarbon analyses were obtained hourly with two flame ionization gas chromatographs. The C_1 to C_3 hydrocarbons and 2-methylpropane were chromatographed on a Duropak® phenylisocyanate column (10-ft long, 0.06-in. i.d. aluminum tubing) immersed in a wet ice bath. The sample size was 5 cc. The other C_4 hydrocarbons and all those $>C_4$ were chromatographed on a capillary column (300-ft long, 0.01 in. i.d. stainless steel tubing) with programmed temperatures from -100 to 136 C. The sample size was 20 cc. SF_6 was determined by electron-capture gas chromatography. The analysis was performed on a silica gel and carbosieve column (3-ft long, 0.06 in i.d. stainless steel tubing) maintained at 120 C. The sample size was 1 cc. Figure 13 is a reproduction of a typical chromatogram showing good resolution. Only the propylene peak was troublesome in that integration was sometimes inaccurate at low concentrations. Typically, unknown hydrocarbon concentrations (excluding the impurity in the helium carrier gas) were in the range 0.01-0.5 percent by weight.

The ozone instrument was calibrated by the neutral-buffered-KI method. The $NO-NO_2$ analyzer was calibrated by an O_3-NO titration procedure[61]. The chromatographs were calibrated each day from a NBS certified bottle of propane in nitrogen.

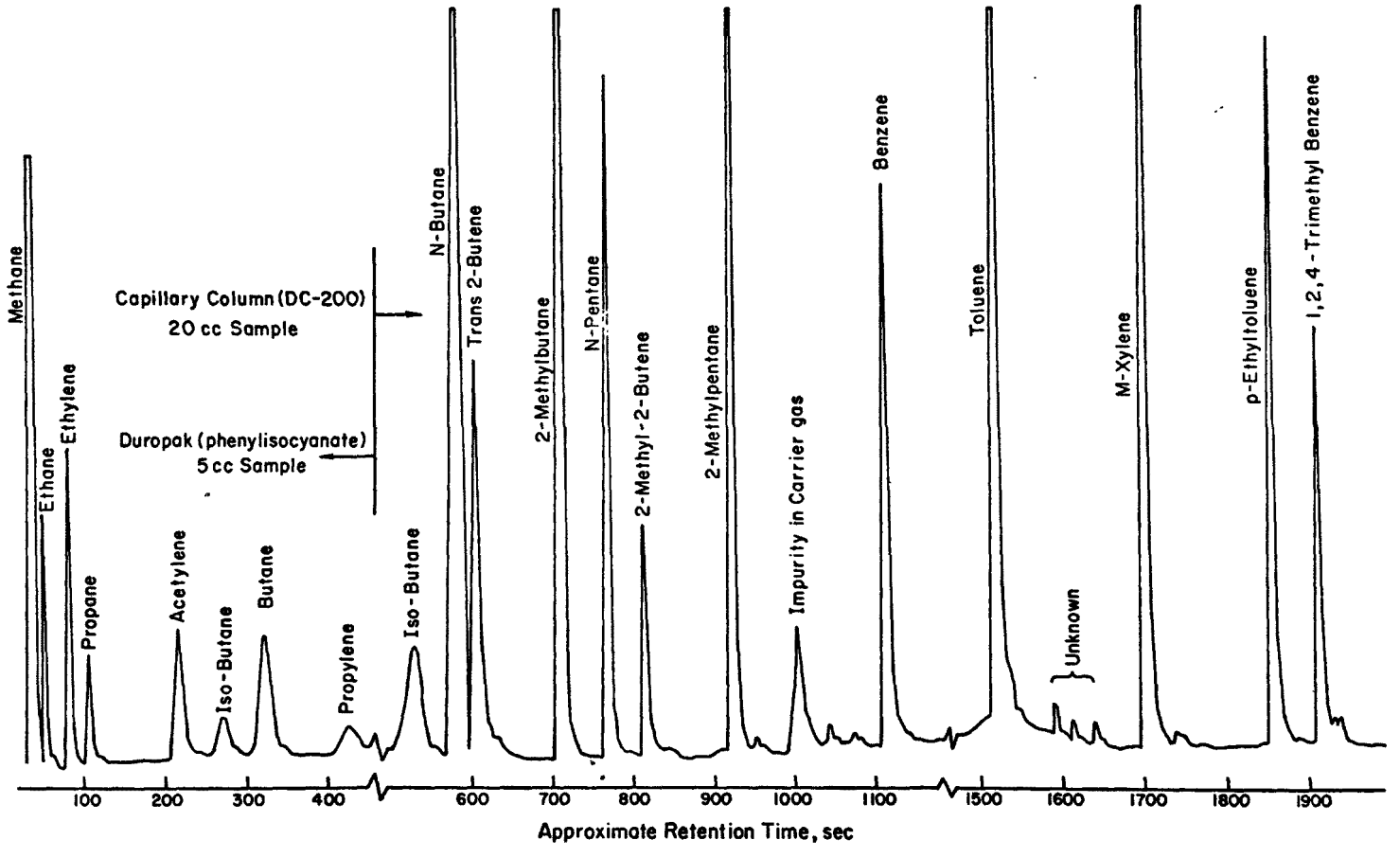

FIGURE 13. REPRESENTATIVE CHROMATOGRAM SHOWING RESOLUTION OF THE SURROGATE HYDROCARBON MIXUTRE OBTAINED WITH TWO GAS CHROMATOGRAPHS

Aerosol measurements were made with an integrating nephelometer and an electrical aerosol analyzer (EAA). Aerosol growth into the light-scattering size range occurred in only a couple of experiments, so the EAA data was the principal method of aerosol analysis. The EAA measures in situ the size distribution of aerosols in the 0.005 to 0.3-μm diameter size range. The instrument operates on the principle of unipolar electric diffusion charging followed by mobility analysis. All data are based on the recent calibration data reported by Liu and Pui[46]. The application of this instrument in numerous atmospheric aerosol studies has been reviewed by Willeke and Whitby[62].

Data from the EAA were examined to determine if substantial truncation errors existed due to the analyzer's cut-off size at 0.3 μm diameter. Assuming a log-normal distribution of aerosol volume in the 0.03 to 0.3 μm-diameter range, the projected aerosol volume extending beyond the 0.3-μm size range was always < 10 percent of the total integrated volume and thus no corrections for truncation were necessary.

Examples of the development of photochemical aerosol under the conditions employed are shown in Figure 14 where the changes in the surface-area and volume-concentration size distributions are plotted against irradiation time.

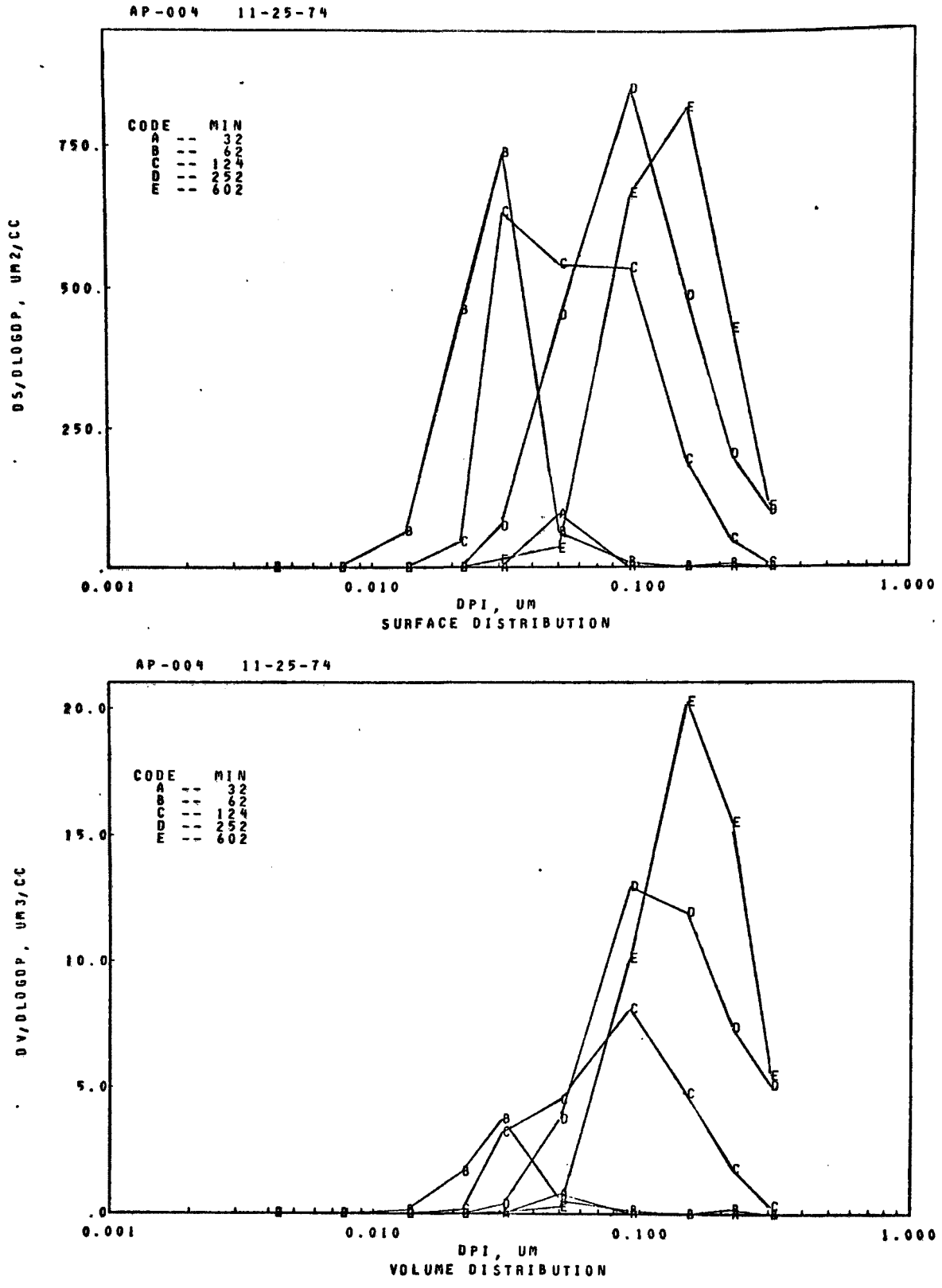

FIGURE 14. COMPUTER-GENERATED GRAPHS OF THE CHANGES IN THE AEROSOL SURFACE-AREA AND VOLUME-SIZE DISTRIBUTION THAT OCCUR AS A FUNCTION OF IRRADIATION TIME

SECTION 7

RESULTS

At the request of EPA, a comprehensive file of data was prepared as a supplement to this report*. In this section of the report we have included summary tables of initial experimental conditions and results pertinent to our discussions. In addition, smog profiles (continuous time-concentration profiles of NO, NO_2, O_3, and aerosol) are presented in Appendix A, and cumulative hourly profiles of hydrocarbon depletion are presented in Appendix B.

The relative composition of the atmosphere irradiated in each experiment was approximately that described in Table 5. The only intended variables in the experiments were the total NMHC and the total NO_x concentrations. Efforts were made to maintain constant distributions among the hydrocarbon and NO_x (NO and NO_2) mixtures. The measured initial concentrations of the reactants are presented in Table 6. There was some inadvertent variation in $[CO]_o$, but this should not have had a substantial effect on the results of interest. According to the data in Table 6, there are also slight variations in the initial hydrocarbon distributions, but in view of the calibrated volume injection procedure employed, these variations may reflect analytical inaccuracies as much as actual discrepencies. Here, too, small variations in the relative distributions of these reactants are thought to have been inconsequential.

---

*The data file consists of both magnetic tapes and conventional computer printouts. One magnetic tape (No. 230) contains all the gas-phase data, with the exception of the gas chromatographic data, acquired during the course of the smog experiments. A second magnetic tape (No. 268) contains the aerosol-size-distribution data for all samples taken during the experiments. This record includes tabulations of the surface-area and volume size distribution of each sampling and an integrated value for the total number, total volume, and total surface area concentrations. As requested, 9-track tapes were prepared at 800 BPI, odd parity in EBCDIC code with no labels. Instructions for reading the tapes were included in the package. The gas chromatographic data is complied entirely as printed output and bound separately. The output includes the concentration of each hydrocarbon (expressed as ppmC, percent carbon, ppmV, and percent volume) for every hour of the irradiation. For each experiment there are summary tables of the average rates of decay fitted to first-order kinetics.

TABLE 6. INITIAL POLLUTANT CONCENTRATIONS[a]

	Run Number																
	1	2	3	4	5	6	7	8	9	10	13	14	15	16	17	18	19
Carbon monoxide	16	10	14	14	14	15	15	14	14	14	10	12	10	12	11	15	10
Nitrogen oxides	0.63	0.28	1.75	1.18	0.30	0.60	1.19	0.58	1.16	0.30	1.93	0.99	0.60	0.29	0.16	0.15	0.15
Nitric oxide	0.50	0.23	1.43	0.99	0.25	0.51	0.99	0.48	0.96	0.25	1.52	0.83	0.50	0.25	0.13	0.13	0.13
Nitrogen dioxide	0.13	0.05	0.32	0.19	0.05	0.09	0.20	0.10	0.20	0.05	0.41	0.16	0.10	0.04	0.03	0.02	0.02
Nonmethane hydrocarbons (as CH_4)	5.742	5.642	7.221	6.244	3.731	3.482	3.957	14.294	13.922	14.136	14.352	3.826	1.766	1.819	1.847	3.457	7.600
acetylene	0.401	0.335	0.555	0.452	0.247	0.266	0.265	0.964	1.047	1.039	0.932	0.216	0.110	0.119	0.131	0.221	0.520
ethylene	0.528	0.520	0.683	0.526	0.290	0.300	0.299	1.150	1.153	1.193	1.105	0.317	0.148	0.146	0.152	0.273	0.588
propylene	0.125	0.109	0.224	0.112	0.123	0.078	0.094	0.370	0.372	0.406	0.333	0.088	0.029	0.032	0.025	0.080	0.176
trans-2-butene	0.211	0.202	0.313	0.236	0.126	0.117	0.134	0.606	0.589	0.576	0.609	0.152	0.036	0.046	0.044	0.119	0.348
2-methyl-2-butene	0.091	0.088	0.129	0.099	0.057	0.052	0.058	0.238	0.228	0.227	0.226	0.060	0.027	0.026	0.027	0.048	0.121
ethane	0.314	0.310	0.414	0.278	0.174	0.194	0.179	0.715	0.699	0.727	0.665	0.222	0.099	0.100	0.111	0.179	0.356
propane	0.195	0.196	0.253	0.192	0.110	0.126	0.113	0.426	0.431	0.471	0.433	0.131	0.060	0.056	0.063	0.106	0.246
n-butane	0.563	0.541	0.756	0.610	0.358	0.318	0.416	1.409	1.349	1.329	1.390	0.432	0.189	0.179	0.189	0.336	0.801
2-methylpropane	0.110	0.128	0.181	0.125	0.072	0.079	0.093	0.324	0.344	0.353	0.327	0.107	0.040	0.034	0.041	0.082	0.178
n-pentane	0.249	0.257	0.270	0.297	0.175	0.148	0.181	0.658	0.628	0.614	0.622	0.179	0.079	0.078	0.077	0.151	0.326
2-methylbutane	0.477	0.489	0.514	0.561	0.326	0.276	0.353	1.252	1.185	1.175	1.213	0.332	0.154	0.155	0.155	0.293	0.640
2-methylpentane	0.340	0.352	0.385	0.414	0.248	0.207	0.255	0.933	0.889	0.874	0.864	0.228	0.109	0.115	0.114	0.211	0.444
benzene	0.406	0.237	0.544	0.273	0.163	0.149	0.177	0.628	0.600	0.587	0.591	0.148	0.072	0.081	0.075	0.144	0.299
toluene	0.575	0.594	0.631	0.715	0.419	0.364	0.420	1.529	1.478	1.459	1.508	0.358	0.170	0.200	0.212	0.371	0.774
m-xylene	0.753	0.857	0.898	0.883	0.552	0.507	0.573	1.944	1.825	1.881	1.994	0.486	0.245	0.263	0.252	0.486	1.000
p-ethyltoluene	0.249	0.279	0.304	0.294	0.185	0.187	0.214	0.711	0.679	0.741	0.901	0.215	0.109	0.107	0.104	0.204	0.451
1,2,4-trimethylbenzene	0.146	0.140	0.159	0.168	0.097	0.105	0.126	0.429	0.420	0.475	0.631	0.146	0.080	0.075	0.068	0.142	0.324

(a) All concentration units are ppm (vol/vol); hydrocarbon units expressed as ppm CH_4 or ppmC.

Experimental results are summarized in Table 7. The reactivity parameters are defined by footnotes. Three principal manifestations, the concentrations of ozone and aerosol and the hydrocarbon depletion rates were corrected for dilution of the smog chamber. This was necessary because the dilution rate varied somewhat from run-to-run. The dilution rate was particularly great (~13%/hr) for Run Nos. 13-19 due to a small leak in a Teflon window that went undetected.

The units of aerosol volume concentration used throughout this report, $\mu m^3/cm^3$, are convenient in that they correspond to familiar mass concentration units of $\mu g/m^3$ if the density of the aerosols is unity. Unless otherwise specified units of ppm and ppb refer to parts-per-million or parts-per-billion by volume (ppmV and ppbV) while ppmC refers to hydrocarbon concentrations of parts-per-million equivalent in carbon atoms to methane; e.g., 1 ppm propane = 3 ppm as CH_4 or 3 ppmC.

TABLE 7. SUMMARY OF EXPERIMENTAL RESULTS

Run No.	Initial Conditions		Smog Reactivity Parameters							
	NMHC, ppmC	NO_x, ppm	NO_2-t_{max},[a] min	NO_2 rate,[b] ppb/min^{-1}	$[O_3]_{max}$,[c] ppm	HC rate,[d] %/hr	Aerosol Volume Concentration,[e] $\mu m^3/cm^3$ 2 hr	4 hr	8 hr	Aerosol rate[f] $\mu m^3/cm^3/hr$
1	5.74	0.63	74	7	0.60	13.4	9.9	16.6	20.3	6.2
2	5.64	0.28	38	7	0.42	11.2	14.6	17	17	11.5
3	7.22	1.75	210	5	0.16	11.4	2.6	6.6	10.1	2.7
4	6.24	1.18	150	5	0.48	12.5	5.2	9.9	14.3	4.2
5	3.73	0.30	45	8	0.51	15.8	11.8	15.0	15.8	6.5
6	3.48	0.60	112	3	0.53	13.8	6.8	10.2	13.3	4.2
7	3.96	1.19	285	3	0.14	12.6	2.6	4.4	5.8	2.1
8	14.29	0.58	38	13	0.50	10.2	29.3	30.5	29.7	32.0
9	13.92	1.16	85	12	0.82	17.5	12.5	19.8	24.3	10.0
10	14.14	0.30	22	11	0.45	5.2	24.6	23.6	23.3	25.5
13	14.35	1.93	150	6	0.92	11.7	6.2	12.8	19.0	5.1
14	3.83	0.99	157	2	0.30	12.3	2.2	5.6	8.7	2.2
15	1.77	0.60	180	1	0.30	8.7	1.8	5.4	9.1	2.5
16	1.82	0.29	90	2	0.43	12.7	5.8	9.1	14.3	3.5
17	1.85	0.16	65	2	0.39	12.3	10.1	13.5	14.2	3.2
18	3.46	0.15	43	4	0.35	12.8	9.9	13.1	13.6	8.5
19	7.60	0.15	23	5	0.40	5.2	12.6	12.6	12.6	14.4

(a) Time to reach the maximum $[NO_2]$.

(b) $\{[NO_2]_{max} - [NO_2]_1\}$/time to $[NO_2]_{max}$.

(c) Maximum $[O_3]$ corrected for the smog-chamber dilution rate.

(d) NMHC depletion rate corrected for dilution; the data fitted to a first-order decay expression.

(e) Aerosol volume inferred from the size-frequency distribution of aerosols assuming spherical shape; the volume concentrations corrected for dilution.

(f) Maximum aerosol volume formation rate during the 10-hour irradiation; the rates corrected for dilution.

SECTION 8

DISCUSSION

OVERALL REACTIVITY

Before turning to the discussion of aerosol precursor relationships it is of interest to comment on some measures of reactivity in general and make some comparisons with other smog-chamber and atmospheric results.

Linear regressions of two-variable combinations of various reactivity parameters were performed on our data, and the results appear in Table 8. It is noted that the rate parameters designated (A), (G), (H), and (I) are concentration normalized, i.e., the dimensions do not contain a concentration term. The other rate parameters, (B) and (F), do include a concentration term, and, of course, parameters (C), (D), and (E) have concentration units.

TABLE 8. CORRELATION COEFFICIENTS AMONG MEASURED REACTIVITIES

Parameters[a]	(A)	(B)	(C)	(D)	(E)	(F)	(G)	(H)	(I)
(A) NO_2-t_{max}	1.0	-0.82	-0.36	-0.73	-0.63	-0.61	0.18	0.06	0.05
(B) NO_2-rate		1.0	0.04	0.64	0.44	0.71	-0.44	-0.14	-0.38
(C) O_3-max			1.0	0.47	0.67	0.19	0.29	0.25	0.18
(D) Aerosol-4 hr				1.0	0.95	0.89	-0.12	0.19	-0.32
(E) Aerosol-8 hr					1.0	0.77	0.02	0.24	-0.22
(F) Aerosol-rate						1.0	-0.47	-0.03	-0.64
(G) NMHC-rate							1.0	0.77	0.78
(H) Olefin-rate								1.0	0.26
(I) Aromatic-rate									1.0

(a) Dimensions are: (A), (G), (H), and (I) time; (B) and (F) concentration/time; (C), (D), and (E) concentration.

A normalized rate parameter for NO photooxidation (NO_2-t_{max}) correlates fairly well with the absolute NO-photooxidation rate (NO_2-rate) and the aerosol parameters (D, E, and F), but rather poorly with peak ozone (C) and the fractional rates of hydrocarbon decay (G, H, and I). Rather surprisingly, NO_2-rate shows no improvement in correlating with maximum O_3 concentrations, and the correlations with the rates of hydrocarbon decay were low and negative. In a study by Heuss and Glasson[6] with individual hydrocarbons, the correlation of NO_2-rate with peak O_3 was 0.61, and between NO_2-rate and percent hydrocarbon reacted (parameter G) it was 0.56. Perhaps the higher correlations in their work are related to constant initial concentrations of reactants.

Maximum ozone concentration does not correlate highly with the other measures of reactivity, although there is fairly good correlation with aerosol concentrations at 8 hours irradiation. One sees from the smog profiles (Appendix A) that aerosol formation often precedes O_3 formation, and even less correlation between these dependent variables would be expected for instantaneous data. These relationships will be discussed more fully in the sections to follow.

Aerosol concentrations at 4 and 8 hours are well correlated with each other and with the maximum rate of aerosol formation, but they are not correlated with the fractional rates of hydrocarbon decay. The latter finding is not surprising since the hydrocarbon parameters are normalized. A more meaningful comparison can be made on the basis of the total amount of hydrocarbon reacted and the amount of aerosol produced. Therefore, linear regressions were performed between time integrals of hydrocarbon decay and the concentrations of aerosols at the respective time limits (e.g., $\int_{0\,hr}^{4\,hr} d(HC)/dt$ vs aerosol volume concentration at 4 hr). The results are shown in Table 9. While none of the correlations are especially good there is considerable improvement over the previous analysis. In all categories the correlation coefficients increase with irradiation time.

TABLE 9. CORRELATION COEFFICIENTS BETWEEN AEROSOL CONCENTRATION AND THE TIME INTEGRALS OF HYDROCARBON DECAY

Integral Variable	Integral Period		
	2 hr	4 hr	8 hr
Olefins	0.50	0.65	0.76
Aromatics	0.33	0.53	0.70
NMHC	0.27	0.48	0.68

HYDROCARBON OXIDATION

In nearly all of the experiments conducted, the observed hydrocarbon depletion rates could be fitted satisfactorily to first-order kinetics. Therefore, fractional first-order rates are used throughout the report in summarizing the hydrocarbon data. Examples of the decay rates are shown in Figure 15. The rates were corrected for the first-order dilution of the chamber air and they therefore can be no more accurate than the determinations of the dilution rate. As indicated in Figure 15, benzene, acetylene, ethane, and propane are oxidized very slowly--generally at rates <1 percent/hr. Other alkanes, ethylene, and toluene decayed at rates in the range of 2-10 percent/hr. The ethylene and toluene rates were often quite similar. The other olefins and aromatics disappeared at substantially higher rates.

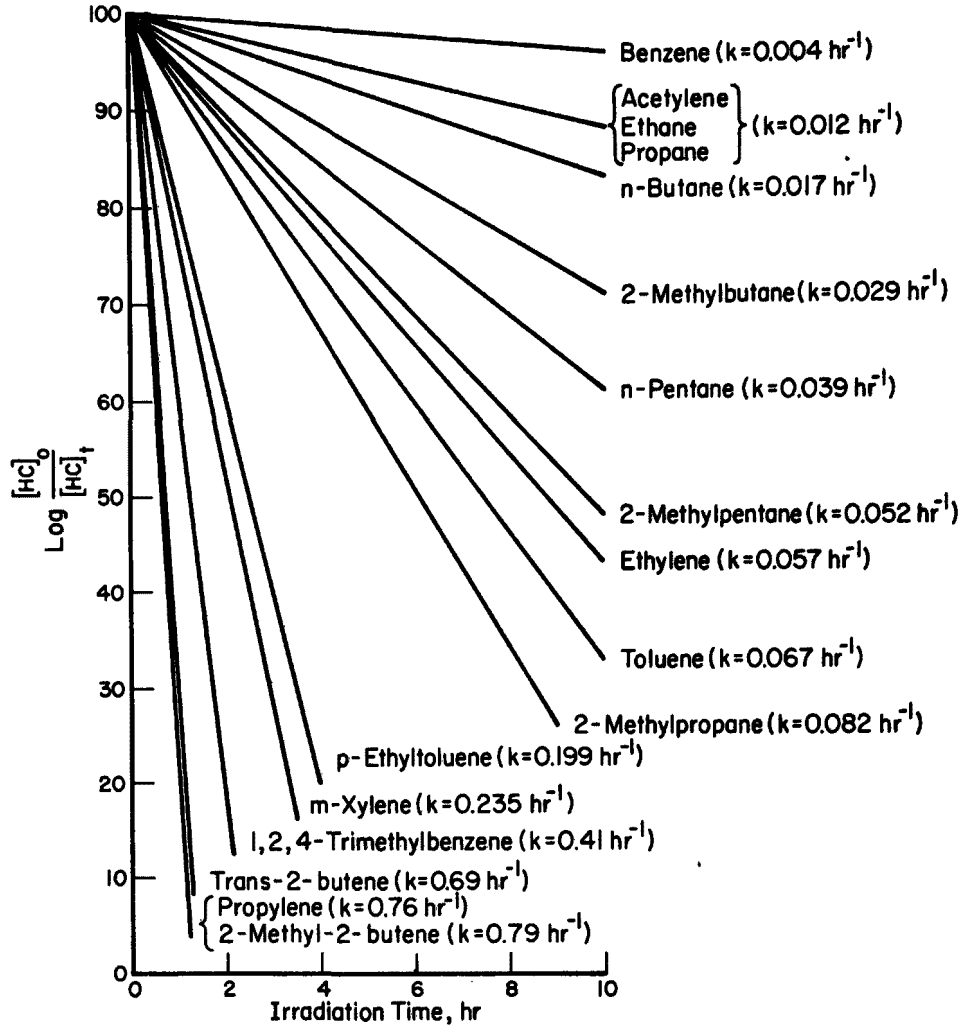

FIGURE 15. FRACTIONAL HYDROCARBON DECAY RATES AT 9.1/1 NMHC/NO_x RATIO, RUN NO. 1

There were two peculiar results which were consistently observed. (1) Propylene disappeared at unusually rapid rates. In many cases this appeared to be the result of peak broadening and inaccurate electronic integration at low concentrations. (2) At initial NMHC concentrations <4 ppmC, the ethylene concentration actually increased late in the irradiations. We confirmed that this anomaly was not due to ethylene leaks to the chamber or to ethylene in the make-up air. The possibility of ethylene being produced via aldehyde photolysis has been discussed

by Altshuller, et al.[63], but its presence was not detected in their work. Other explanations appear equally speculative.

Table 10 summarizes some of the pertinent data on hydrocarbon disappearance rates when typical urban mixtures of hydrocarbons are irradiated naturally or with artificial sunlight. Footnotes (a)-(c) describe three studies cited for comparison with our smog-chamber results. In the study with Los Angeles air, the average NMHC/NO_x ratio was 8.8/1. In the other study with actual urban air [footnote (b)], the ratio was not stated. Smog-chamber experiments at NMHC/NO_x ratios of 9.1/1, 4.1/1, and 24/1 were selected for comparison. All of the rate data in Table 10 are normalized with respect to the rate of n-butane decay. Measured rates for n-butane are given in footnote (d).

In comparing first the rates of hydrocarbon decay in the three smog-chamber experiments of this study, there is remarkable similarity in the overall rates in view of the wide range of NMHC/NO_x ratios. It is important to note that the absolute rates for butane are also very similar, as are the relative rates for the other alkanes (propane and 2-methylbutane) and acetylene, ethylene, and benzene. Because the propylene data is questionable it will not be compared. 2-methyl-2-butene shows slightly increased decay rates with increasing NMHC/NO_x ratios. Rather interestingly, the alkylbenzenes all show a maximum rate of decay for the NMHC/NO_x condition of 9.1/1. This trend is further illustrated in Figure 16 where the average fractional decay rate of all aromatics is plotted against the NMHC/NO_x ratio for 17 experiments. Although there is considerable scatter because of the dependency on the absolute hydrocarbon and NO_x levels, there appears to be a trend of maximum decay rate near the NMHC/NO_x ratio of 10/1. The same type plot for total olefins did not reveal a reasonable trend.

TABLE 10. HYDROCARBON OXIDATION RATES IN POLLUTED AIR AND IN SMOG-CHAMBER SIMULATIONS

	Oxidation Rates Relative to n-Butane					
	Los Angeles[a] Air	Riverside[b] Air	Riverside[c] Smog Chamber	Battelle Chamber--This Study Run No. 1	Run No. 3	Run No. 8
$NMHC/NO_x$ (ppmC/ppmV):	8.8	-	7.7	9.1	4.1	24
Acetylene	0.5	-	-	0.7	0.7	0.5
Ethylene	3.7	3.8	-	3.3	-	4.0
Propylene	8.6	16.1	-	44	26	43
2-Methyl-2-Butene	34.7	-	-	46	44	75
Propane	0.6	-	-	0.7	0.4	-
n-Butane[d]	1.00	1.00	1.00	1.00	1.00	1.00
2-Methylbutane	1.6	1.8[e]	-	1.7	1.6	1.6
Benzene	-	-	<1	0.23	<0.2	0.23
Toluene	2.1	-	1.4	3.9	2.5	1.9
m-Xylene	4.2	-	7.5	13.8	10.1	10.3
1,2,4-Trimethylbenzene	-	-	11	24	20	18

(a) Downtown L.A. air collected at 0800 and irradiated naturally in Tedlar bags. Oxidation rates are 4-hr avg (0800-1200)[49].

(b) Central Riverside air collected at 0630 and irradiated naturally in borosilicate carboys. Oxidation rates are 8-hr avg (0730-1530)[57].

(c) Surrogate HC mixture irradiated with blacklamps (k_1 = 0.20 min^{-1}) in 6-m^3 chamber at U of Calif. (Riverside). Oxidation rates are 2-hr avg[56].

(d) Rates normalized to n-butane. Absolute rates for n-butane are: ref. (a), k = 0.023 hr^{-1} (6-hr avg); ref. (b), not given; ref. (c), k = 0.023 hr^{-1} (estimated from published data, 2-hr avg); run no. 1, k = 0.017 hr^{-1} (10-hr avg); run no. 3, k = 0.013 hr^{-1} (10-hr avg); run no. 8, k = 0.017 hr^{-1} (10-hr avg).

(e) Value indicated was for n-hexane.

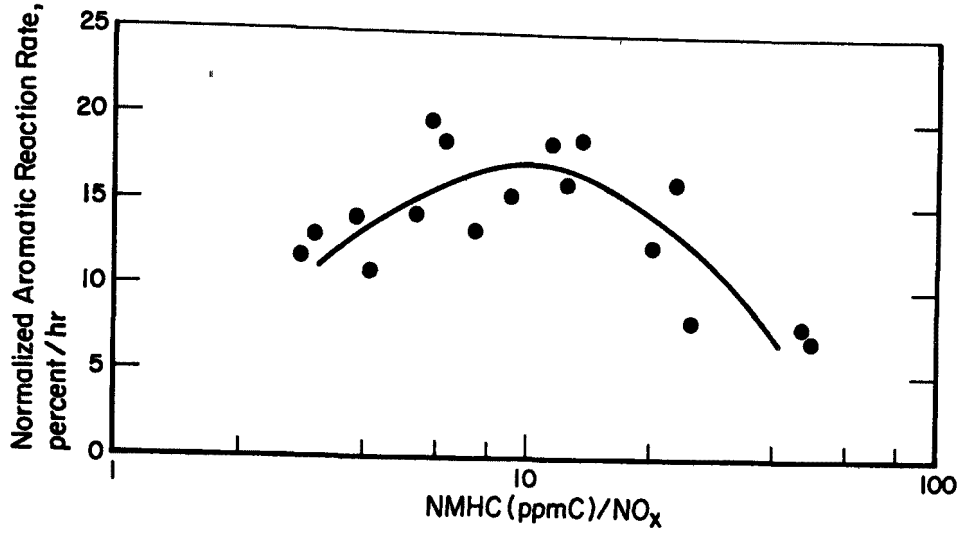

FIGURE 16. EFFECT OF NMHC/NO_x RATIO ON THE RATE OF AROMATIC HYDROCARBON DECAY

With Run No. 1 data (NMHC/NO_x = 9.1) as the comparable Battelle-chamber data, it appears that the absolute rate for butane decay is in satisfactory agreement with the results of the Los Angeles air study, with which the Riverside-chamber rate is in perfect agreement. It must be kept in mind here that the rates reported with natural irradiation [studies footnoted (a) and (b)] are averages over a period of variable irradiation intensity while the rates reported from the Riverside and Battelle chambers are average rates over periods of constant irradiation intensity. For acetylene, ethylene, 2-methyl-2-butene, propane, and 2-methylbutane there is good agreement between the Battelle-chamber data and the Los Angeles air data. However, at the 9.1/1 NMHC/NO_x ratio, the rate of toluene disappearance was nearly twice as large in the Battelle chamber, and the rate for m-xylene was about 3 times larger than the rate observed in Los Angeles air. At the NMHC/NO_x ratios of 4.1/1 and 24/1, the rates were more comparable.

The Riverside air study [footnote (b)] showed good agreement with the Los Angeles air study for the limited data. In the Riverside

smog-chamber study [footnote (c)] the decay rate reported for toluene is somewhat less than that measured in Los Angeles air, but the rate for m-xylene is nearly a factor of 2 larger. The ratio of the rates of m-xylene to toluene are about 5/1 in the Riverside chamber, and they ranged from 3.5/1 to 5.5/1 in the Battelle chamber. In Los Angeles air the ratio was only 2/1.

As a final indication of the comparability of the smog-chamber data with the atmospheric data, averages of the decay rates of paraffins, olefins, and aromatics are shown in Table 11. Based on these averages, there is good agreement between the decay rates for paraffins, the olefin rate is somewhat higher (perhaps inaccurately higher because of propylene uncertainties) in the Battelle chamber, and the aromatic rate is about a factor of 2 greater in the Battelle chamber when the data are compared to the Los Angeles atmospheric rates averaged over the period of 0800-1200 hours at full sunlight intensity.

TABLE 11. AVERAGE HYDROCARBON LOSS RATES UNDER NATURAL AND SIMULATED IRRADIATION CONDITIONS

Hydrocarbon Class	Hydrocarbon Decay Rate, percent/hr	
	Los Angeles Air[a] Natural Irradiation	Battelle Smog Chamber[b] Blacklamp Irradiation
Paraffins	2.8	3.0
Olefins	20	37
Aromatics	8.5	15

(a) Reference No. 49

(b) Run No. 1, this study.

In conclusion, we feel that the data obtained in this smog-chamber program are highly representative of that associated with intense photochemical smog conditions which manifest in some urban areas. Since the photochemically induced rates of organic aerosol formation have never been measured in polluted atmospheres direct comparisons of the smog chamber's aerosol data are not possible. Although the correlation results are not impressive, it nonetheless seems reasonable to presume that organic aerosol formation in the smog chamber is closely related to the rates of hydrocarbon oxidation. By deduction then it would appear that the harmony observed between the hydrocarbon rate data in the atmosphere and in the smog chamber lends credence to the relevancy of the aerosol data presented next.

AEROSOL PRECURSOR RELATIONSHIPS

The principal objective of this study was to establish the relationships that exist between nonmethane hydrocarbon, nitrogen oxides concentrations, and the subsequent development of photochemically related aerosols. As discussed earlier, the relationships sought thus far relate to the formation of organic aerosols and not to sulfate aerosols. Experiments were conducted for 10 hours, and it is apparent from the data that there are significant changes in the aerosol growth dependency on NMHC and NO_x concentrations as the irradiations progress. While irradiation time normally indicates the duration of a smog reaction at constant irradiation intensity, it is possibly justifiable to think of the irradiation period as the density or total flux of irradiation. In other words, the results of a 2-hour simulation in a smog chamber may be representative of smog conditions that would result at some reduced level of irradiation on a cloudy day.

Two methods were adopted for illustrating the simultaneous effects of the independent variables (NMHC and NO_x) on the dependent aerosol variables. In one case, 2-dimensional contour diagrams are drawn depicting isopleths of the response surface (dependent variable) as a function of the independent variables. An example of this analysis

is shown in Figure 17 where the maximum rate of formation of aerosol volume is represented by the contour lines (isopleths) and NMHC and NO_x concentrations are represented on the abscissa and ordinate, respectively. Each contour line represents intervals of the rate of aerosol volume formation in units of 2 $\mu m^3/cm^3/hr$. The second graphical method involves making projections of the response surface as it would appear in 3 dimensions. With this method a realistic impression of the response is conveyed but at some sacrifice of the numerial value of the surface height. However, since the emphasis in our interpretations is on relative functions and values, the 3-dimensional projections seem to be particularly descriptive. Figure 18, for example, shows the aerosol rate data (same as Figure 17) as a surface projection. In viewing these illustrations it is important to establish the proper orientation. In Figures 17 and 18, [NMHC] and [NO_x] both increase in the directions away from the 0 point. In all projections, the response surface is in a positive-Z orientation*.

Figure 18 shows that the maximum rate of aerosol formation lies along a NMHC/NO_x line of about 30/1 for [NMHC] <9 ppmC. Above 9 ppmC, the crest in the surface shifts to a NMHC/NO_x ratio of 18/1. Although the maximum aerosol formation rate is nearly linear with respect to [NMHC], the [NMHC] regions of 0-3.5 ppmC and 9.0-14.25 ppmC appear to have slightly greater inclinations. In the [NMHC] range 0-9 ppmC, the maximum aerosol formation rate normalized to NMHC is about 1.9 $\mu m^3/cm^3/hr$ per unit ppmC hydrocarbon.

Figure 18 also shows that the maximum aerosol formation rate goes through a maximum with respect to initial [NO_x], with NO_x showing a strong inhibition effect at the higher pollutant concentrations. In the NMHC region between 0 and 3 ppmC, however, the maximum rate dependence

*The graphic surfaces in perspective were generated on a CDC 6400 computer and are the culmination of a 3-step process. First, a triangulation program (CNTOUR) was used to generate isopleths of the dependent variables from the original data. Smoothing programs were used to smooth the data and generate a symetric data base. The dimension of surface was then produced with a computer program (SRFACE) obtained from the National Center for Atmospheric Research.

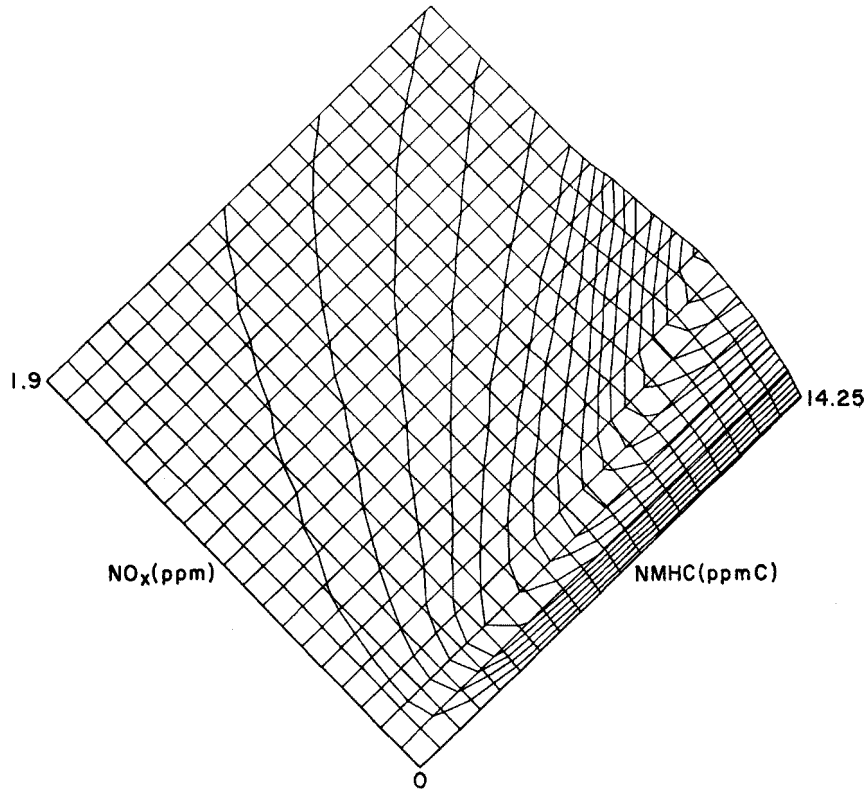

FIGURE 17. ISOPLETHS OF MAXIMUM RATES OF AEROSOL FORMATION AS A FUNCTION OF THE INITIAL CONCENTRATIONS OF NMHC AND NO_x (Isopleths correspond to intervals of volume production rates of 2 $\mu m^3/cm^3/hr$.)

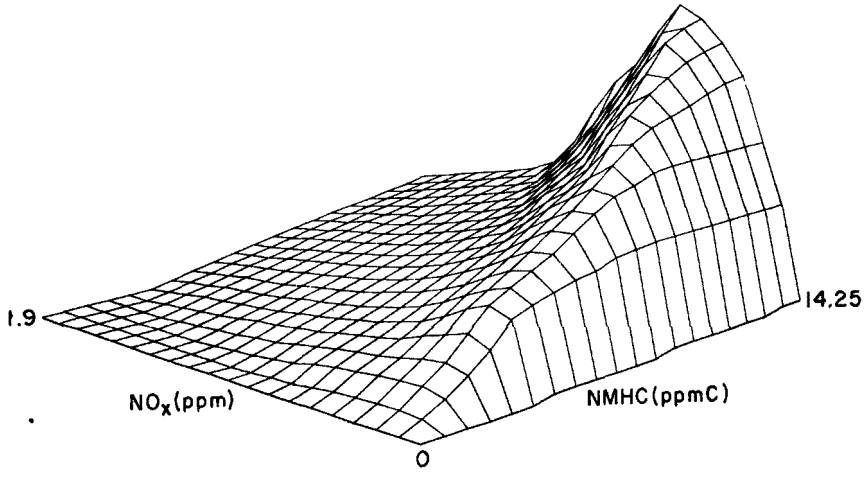

FIGURE 18. A SURFACE PROJECTION REPRESENTING MAXIMUM RATES OF AEROSOL FORMATION AS FUNCTIONS OF THE INITIAL CONCENTRATIONS OF NMHC AND NO_x

on [NO_x] is not so pronounced. These precursor trends will be examined in more detail as we look at the relationships between the instantaneous aerosol concentations as functions of [NMHC], [NO_x], and irradiation time.

Surface diagrams and contour plots of aerosol concentrations at 2-hour, 6-hour, and 10-hour irradiation periods are shown in Figure 19a,b,c and Figure 20a,b,c, respectively. (Our discussions relate primarily to the surface projections; the contours plots are included to provide quantitative intervals of the dependent variables.) The surface depicting aerosol concentrations at 2 hours shows relationships with [NMHC] and [NO_x] which are similar to those for the maximum aerosol formation rate (Figure 18). This is because the maximum formation rate usually occurred during the first 2 hours of the experiments. There are some subtle differences however. Most noteworthy is the relatively greater dependence of the 2-hour aerosol concentration on the initial concentrations of both NMHC and NO_x in the lower concentration regions. Here the NO_x dependence is particularly striking.

Figures 19b and 20b show the aerosol concentrations at 6 hours. Compared to the 2-hour situation a much expanded surface area has emerged corresponding to NO_x dependence. In other words, the inhibiting effect of NO_x on aerosol formation becomes less significant as the irradiation time increases. It is also interesting to compare the position of the ridges of maximum aerosol concentration at 6 hours and 2 hours. At 2 hours, the ridge follows a NMHC/NO_x line of 15/1 up to [NMHC] of about 3 ppmC. The ridge then flattens out and turns toward a much higher NMHC/NO_x ratio (34/1). At NMHC concentrations of about 7.5 ppmC, the ridge rises again to a peak. At 6 hours, the ridge follows a NMHC/NO_x line of 13/1 up to [NMHC] of 5.5 ppmC, and then it turns and follows a ratio line of 44/1.

At 10 hours, (Figures 19c and 20c) the aerosol "mound" fills out further than at 6 hours, but the surface and ridge seem to maintain the shapes established at the 6-hour period. The NMHC/NO_x ratio at peak aerosol concentration is 10/1 for [NMHC] <7.5 ppmC, and it approaches infinity for higher pollutant concentrations.

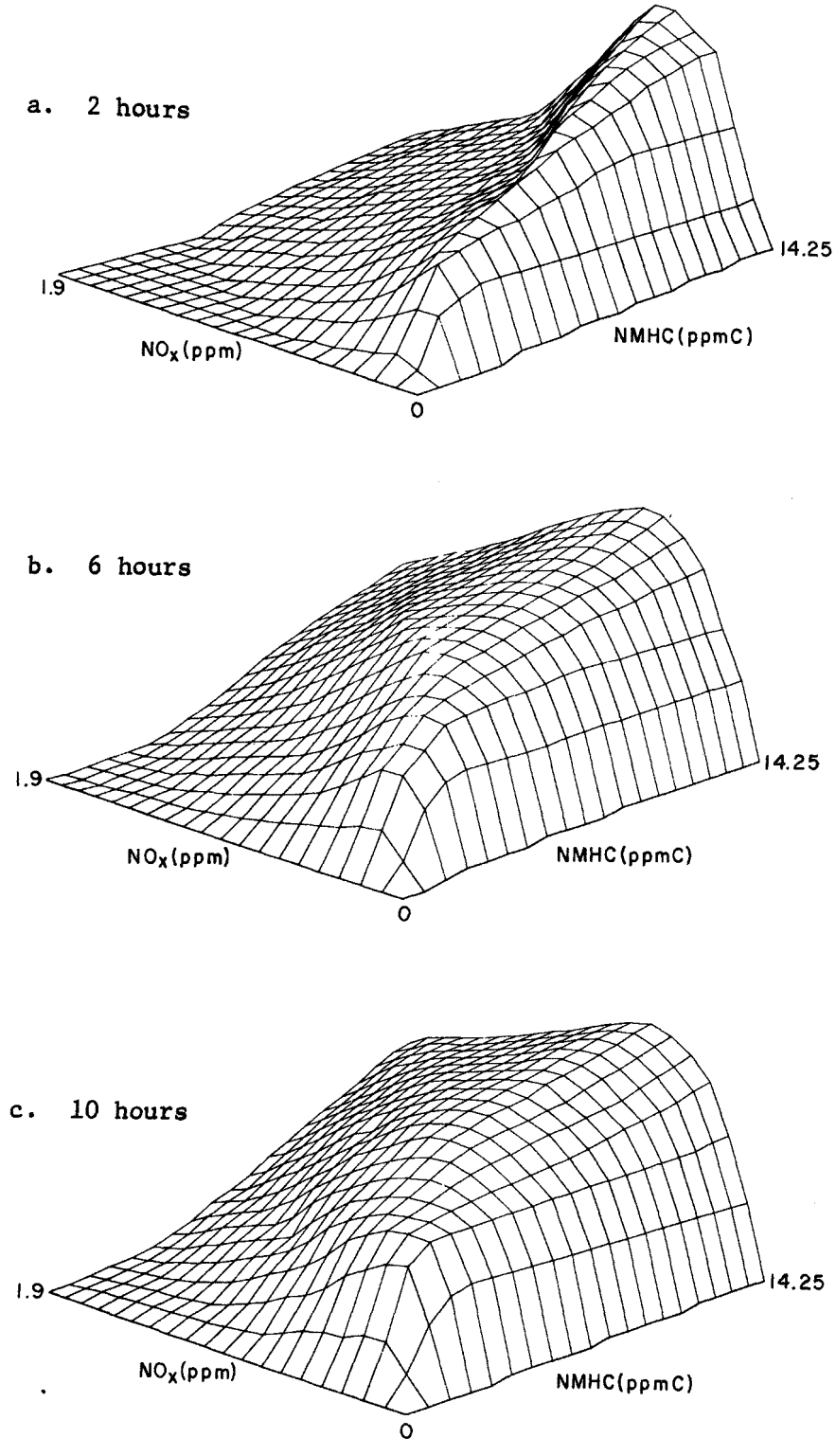

FIGURE 19. SURFACE PROJECTIONS REPRESENTING AEROSOL VOLUME CONCENTRATIONS AS FUNCTIONS OF THE INITIAL CONCENTRATIONS OF NMHC AND NO_x AT IRRADIATION TIMES OF 2, 6, AND 10 HOURS

a. 2 hours

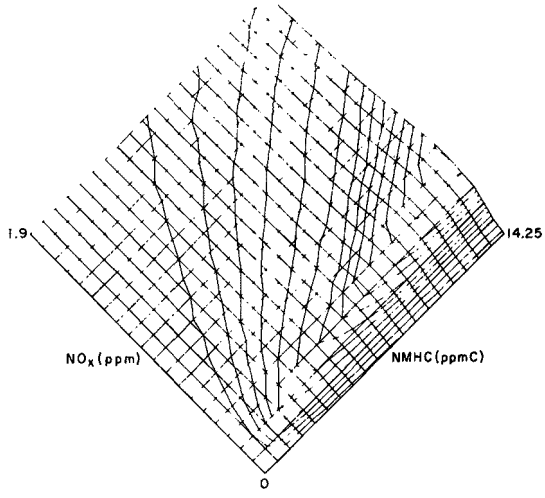

b. 6 hours

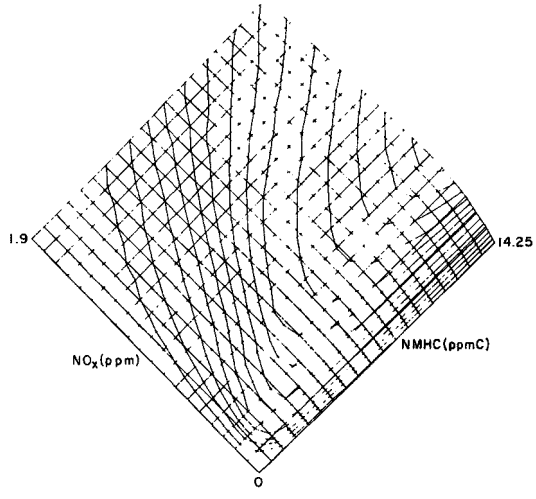

c. 10 hours

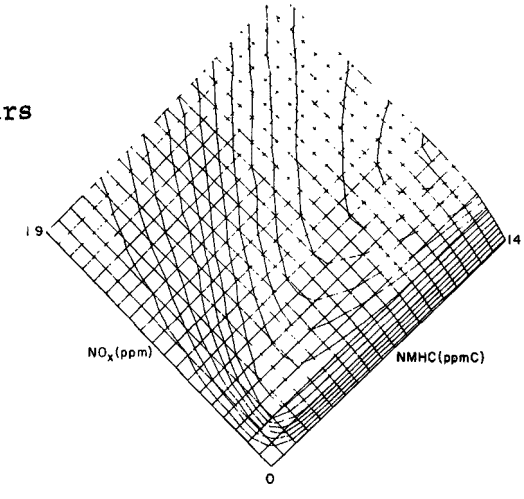

FIGURE 20. ISOPLETHS OF AEROSOL VOLUME CONCENTRATION AS FUNCTIONS OF INITIAL CONCENTRATIONS OF NMHC AND NO_x AT IRRADIATION TIMES OF 2, 6, AND 10 HOURS (Isopleths correspond to volume concentration intervals of 2 $\mu m^3/cm^3$.)

Aside from concentrating on the overall structure of the response surfaces and the crests of maximum response it is important to examine trends corresponding to distributions of NMHC and NO_x that currently exist in our polluted atmospheres and to the distributions predicted for future years. Unfortunately it appears that there is no typical NMHC/NO_x distribution among major urban areas where smog is a problem. The reliability of much atmospheric data has been questioned, and the reasons given for the apparent wide ranges of NMHC/NO_x ratios are controversial and will not be dealt with here. A few examples of atmospheric data with which we are familiar are shown in Table 12. References of data sources are indicated next to the sampling year.

TABLE 12. SELECTED DATA ON THE NMHC AND NO_x DISTRIBUTIONS IN URBAN AREAS

Sampling Site	Year	Averaging Period	Average NMHC, ppmC	Average NO_x, ppm	Average NMHC/NO_x
Welfare Is. (NY)	1972[1]	20 days	2.6	0.098	26/1
St. Louis	1973[64]	5 days	0.62	0.055	11.3/1
South Coast Basin	1973[65]	90 days (many stations)	3.9(1.7)[a]	0.14	12.1/1
Dayton, Ohio (downtown)	1974[66]	30 days	1.76	0.105	16.7/1
New Carlisle, Ohio[b]	1974[66]	30 days	0.67	0.022	30.4/1

(a) Total hydrocarbon reported at 3.9 ppmC. NMHC estimated at 1.7 ppmC.

(b) Semirural area 30 miles NE of Dayton, Ohio.

During the past couple of years it appears that NMHC/NO_x ratios have been >10/1 in most areas. Let's arbitrarily select 10/1 as a ratio to examine the NMHC and NO_x effects on aerosol formation. To do this we have "sliced" the response surfaces corresponding to the 10/1 NMHC/NO_x

section, and we have removed part of the mound to expose the section face*. The sections are shown in Figure 21a,b,c as a function of time from two vantage points; nearly normal to the ordinate (NO_x) and nearly normal to the abscissa (NMHC). Judging from the 2-hour data, the response surface (aerosol concentration) at the 10/1 ratio is constant over a large range of NMHC and NO_x concentrations. Only when the NMHC and NO_x concentrations become small is any reduction in the aerosol concentration noticeable. For 6-hour irradiations the trend changes (Figure 21b). Here the aerosol concentration is also constant at high pollutant concentrations, but there is a gradual reduction in aerosol concentration for NMHC and NO_x levels <5 and 0.5 ppm, respectively. However, the reduction in aerosol concentrations becomes precipitous only where NMHC and NO_x concentrations become <2 and 0.2 ppm, respectively. Similar trends are obvious for the 10-hour irradiation periods. Again only moderate reduction in aerosol concentration occurs until low pollutant concentrations are reached. At 2 ppmC NMHC levels, the aerosol concentration increases 60 percent during the period from 2 hours to 6 hours, and 90 percent during the period from 2 hours to 10 hours of irradiation. Thus most of the organic aerosol is formed during the more typical irradiation period of 6 hours.

All predictions of the direction of future NMHC/NO_x ratios are toward lower values due primarily to emphasis on hydrocarbon emission controls. To estimate the effect of these atmospheric trends, we have rather arbitrarily sliced the response surface to reveal the 5/1 NMHC/NO_x section. The results are shown in Figure 22a,b,c. For the 2-hour irradiation period at the 5/1 ratio, Figure 22a indicates that aerosol concentrations actually increase slightly with decreasing NMHC and NO_x

*The computer program does not permit perfect slicing rather only sectioning of the smallest dimensions of the array. Thus where truncation is used to reveal a particular edge of the response surface, array points are accepted or rejected based on integral values, and a jagged edge results. The heavy lines outlying the sections are interpolations between the array points, and they are particularly necessary in interpreting the data at very low concentrations where the number of significant figures becomes seriously limited. Sometimes the interpolation curve lies across the peaks of bisection edges and sometimes is passes through the valleys.

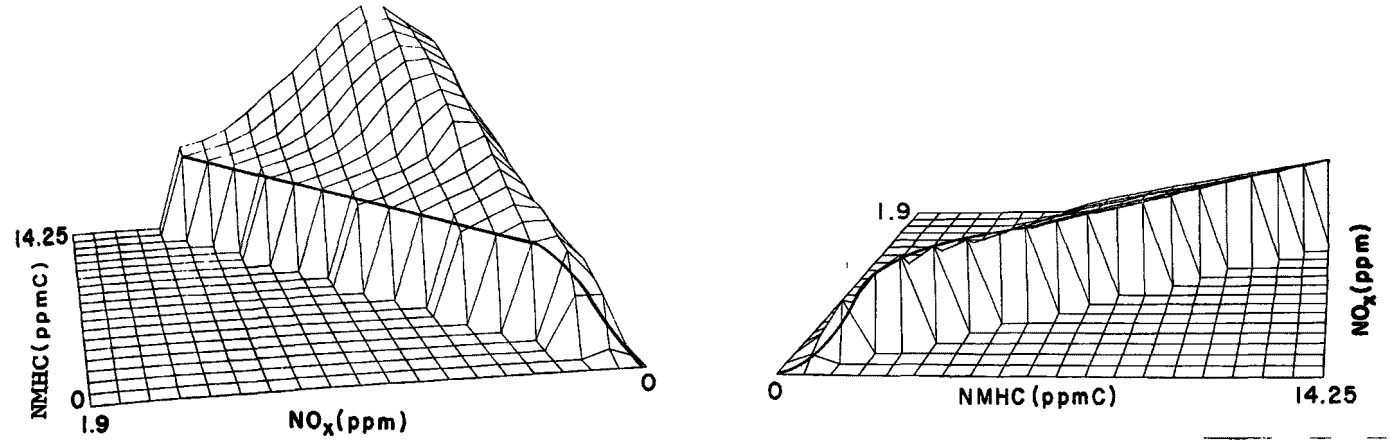

a. 2 hours

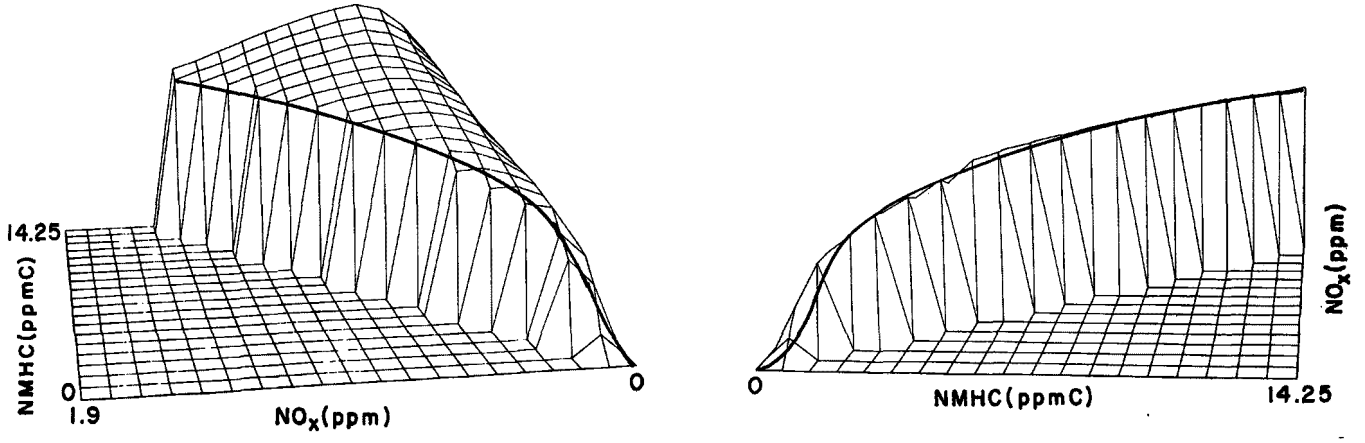

b. 6 hours

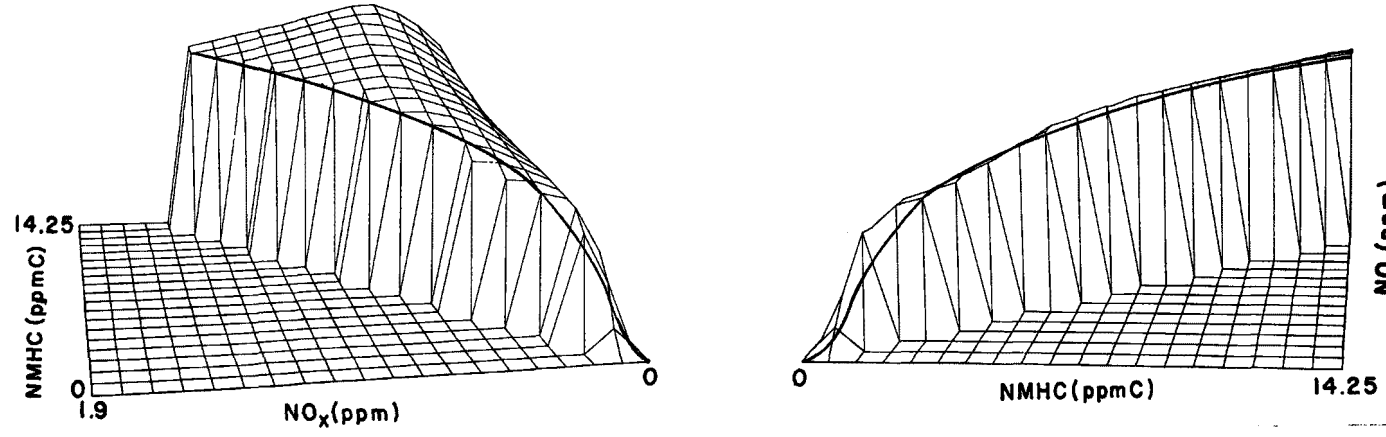

c. 10 hours

FIGURE 21. SURFACE PROJECTIONS REPRESENTING AEROSOL VOLUME CONCENTRATIONS AS FUNCTIONS OF INITIAL POLLUTANT CONCENTRATIONS AT A CONSTANT NMHC/NO_x RATIO OF 10/1 AND IRRADIATION TIMES OF 2, 6, AND 10 HOURS

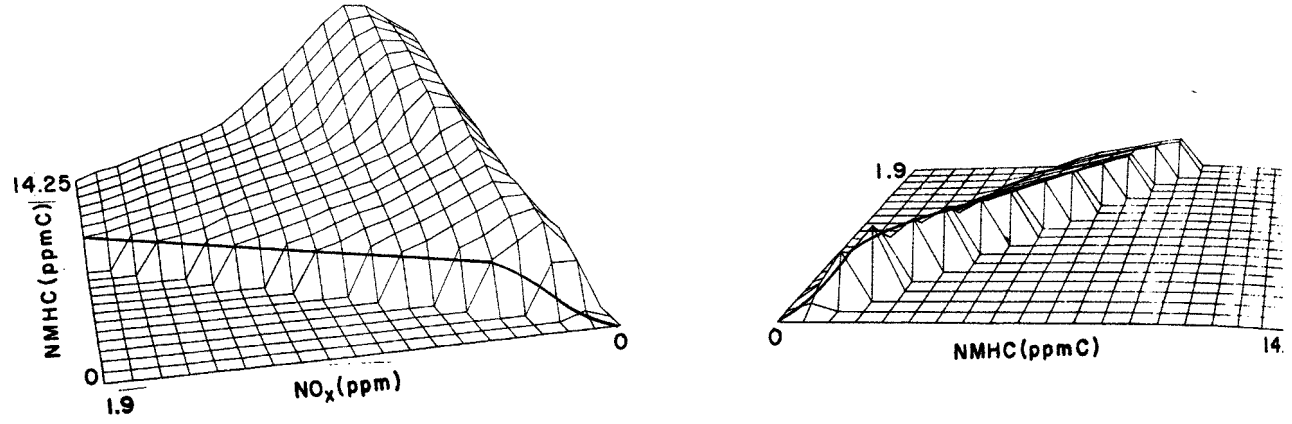

a. 2 hours

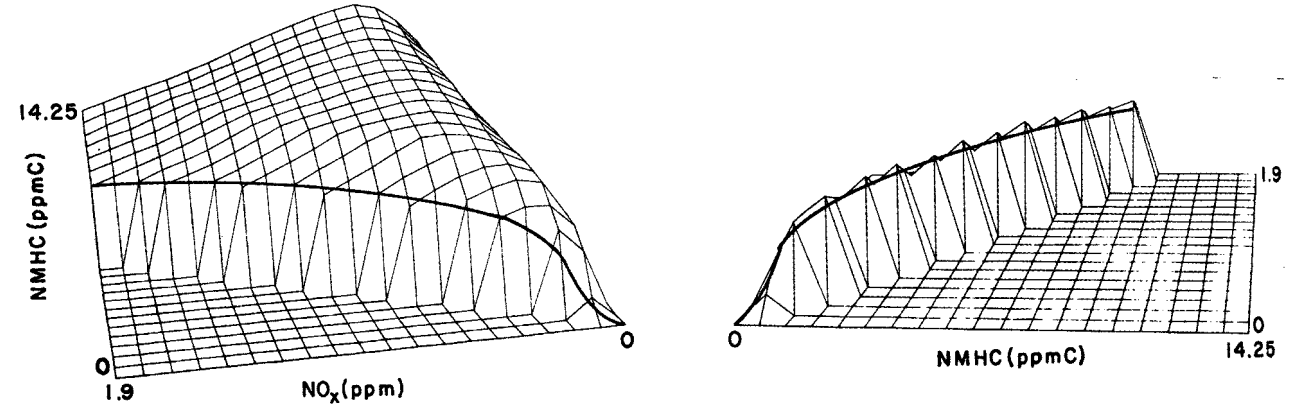

b. 6 hours

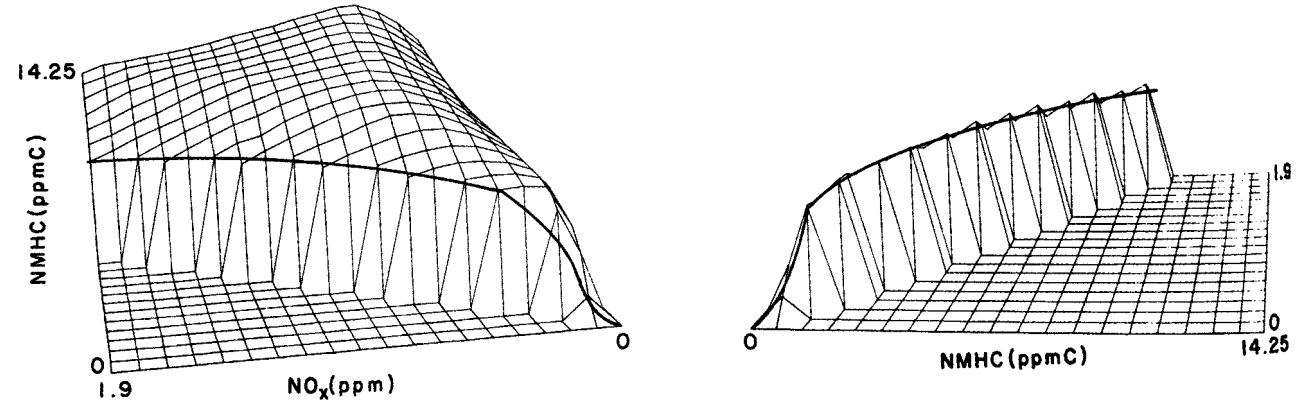

c. 10 hours

FIGURE 22. SURFACE PROJECTIONS REPRESENTING AEROSOL VOLUME CONCENTRATIONS AS FUNCTIONS OF INITIAL POLLUTANT CONCENTRATIONS AT A CONSTANT NMHC/NO_x RATIO OF 5/1 AND IRRADIATION TIMES OF 2, 6, AND 10 HOURS

concentrations down to a point of maximum aerosol concentration near the region of 2 ppmC NMHC and 0.4 ppm NO_x. Then there is a nearly linear reduction in aerosol concentration as zero pollutant concentrations are approached. At 6 hours (Figure 22b), the plateau of maximum aerosol concentration still persists until NMHC and NO_x are reduced below 2.0 and 0.4 ppm, respectively. At the 10-hour irradiation period (Figure 22c), the picture is unchanged except that the aerosol concentrations have increased slightly.

In the plateau regions of constant aerosol concentrations along the specified NMHC/NO_x ratios, the relative reduction in aerosol concentration in going from 10/1 to 5/1 ratios is only about 25 percent.

In conclusion, we see that the dependence of aerosol concentration goes through a maximum with respect to initial NO_x concentrations, particularly at low NO_x concentrations or high NMHC/NO_x ratios. As the irradiation exposure increases from 2 hours to 6 hours and 10 hours, the NMHC/NO_x ratios corresponding to peak aerosol concentrations change from 15/1 to 13/1 to 10/1, respectively, in the pollutant concentration ranges common to our atmosphere. At higher pollutant concentrations the ratios at peak aerosol concentrations are much higher. At NMHC/NO_x ratios >10/1, there is a strong dependence of aerosol formation on the initial pollutant levels. In general, the pollutant level effect is more pronounced as the NMHC/NO_x ratio increases. At ratios <10/1, the pollutant loading effect is slight except at [NMHC] <2 ppmC. Looking back at Figure 19b and c, we see that the pollutant concentrations in the atmosphere must get into the regions of NMHC <2 ppmC and NO_x <0.2 or >0.6 ppm before photochemical aerosol formation is greatly suppressed.

OZONE PRECURSOR RELATIONSHIPS

The results of several smog-chamber studies have provided guidance in establishing the relationships of hydrocarbons and nitrogen oxides in the formation of ozone in smog. The results of a study by

Romanovsky, et al.[5], reproduced in Figure 23, well established the relative roles of hydrocarbon and nitric oxide with respect to peak O_3 concentration. Computer simulations of O_3 formation in smog have also been useful. Simulation results of Hecht[67] are reproduced in Figure 24. N-butane (75%) and propylene (25%) were used in the computer simulation. Propylene was the hydrocarbon employed in the Romanovsky study. There are similarities in the trends of O_3 dependency shown by the data in the two studies, but, owing to different conditions and assumptions, there are major differences in the quantitative results.

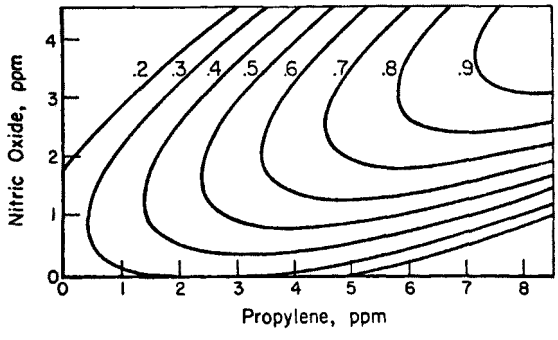

FIGURE 23. ISOPLETHS OF CONSTANT OZONE CONCENTRATION (ppm) DEVELOPED FROM PEAK OZONE CONCENTRATIONS IN AN EARLIER SMOG-CHAMBER STUDY Romanovsky, et al.[5].

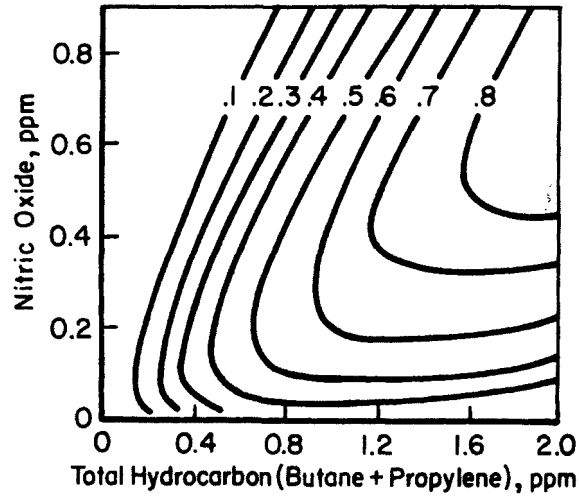

FIGURE 24. ISOPLETHS OF CONSTANT OZONE CONCENTRATION (ppm) BASED ON 5-HR DATA PREDICTED BY A KINETIC SMOG MODEL Hecht[67].

Several studies have demonstrated that simplified smog systems containing only one or two hydrocarbons do not adequately simulate the smog manifestations representative of actual urban conditions. Thus,

more realistic smog-chamber experiments have been conducted with auto exhaust emissions or surrogate mixtures of typical 6-9 a.m. hydrocarbon distributions in cities. The smog-chamber results used by the Los Angeles County Air Pollution Control District (LACAPCD) to predict future trends in peak ozone[68] are reproduced in Figure 25 alongside a drawing (Figure 26) of our results. Direct comparisons of the LACAPCD results with the history of smog episodes in that area have shown that their smog-chamber model underestimates actual peak ozone concentrations. Efforts to adjust the model to fit atmospheric data have met with criticism[69].

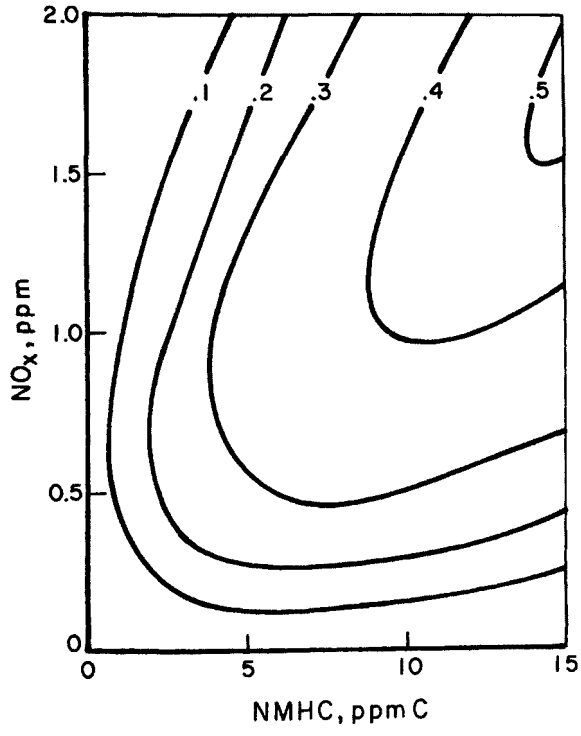

FIGURE 25. ISOPLETHS OF CONSTANT OZONE CONCENTRATIONS (ppm) DERIVED FROM THE LACAPCD SMOG-CHAMBER STUDIES Hamming, et al.[68].

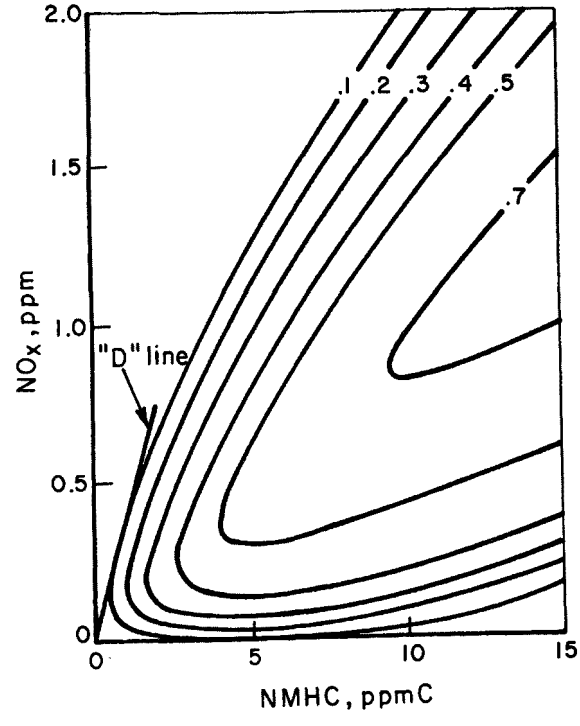

FIGURE 26. ISOPLETHS OF CONSTANT OZONE CONCENTRATIONS (ppm) DERIVED FROM INSTANTANEOUS OZONE CONCENTRATIONS AT 6-HR OF IRRADIATION This Study.

Our model shows higher O_3 concentrations for the corresponding LACAPCD conditions, but it too is undoubtedly imperfect (no model so simple is expected to be extremely accurate). The "D" line in Figure 26, a boundary established in a study by Dimitriades[15], represents a NMHC/NO_x ratio required to meet the present air quality standard for ozone. Dimitriades' smog-chamber study utilized auto exhaust mixtures. His results, at least those defining the "D" lines, are in accord with the results of this study.

Presumably, atmospheric conditions resulting in worst-case incidents of ozone occurrence are those where a highly polluted air mass is confined in space throughout a day-long irradiation period. An air mass stagnant over Los Angeles, for example, does not necessarily meet this criteria because in the late afternoon automotive emissions are added to the stagnant atmosphere under attentuated irradiation, and the additional NO emission effectively reduces the afternoon O_3 level. A condition more nearly representative of a worst case occurs when a highly polluted air mass from an urban area like Los Angeles travels into a more remote area (like Riverside or Azusa), and the full ozone-forming potential of the air mass is realized. This situation is akin to the smog-chamber conditions where a static or moderately diluted condition is simulated over prolonged irradiation periods.

Accepting the hypothetical similarity between the smog chamber and atmospheric conditions we can compare to the model a few data points that were reported as "worst case" incidents of ozone for the Pasadena area in 1969 and 1970[70]. The data are shown in Table 13. In most cases, the atmospheric data points are quite close to the O_3 concentrations predicted by the smog-chamber model. Again, these data are not convincing that the smog model is always accurate, but the agreement does provide an additional element of confidence.

TABLE 13. WORST-CASE OZONE EPISODES IN PASADENA (1969-1970) AND THE PRECURSOR HYDROCARBON AND NO_x CONCENTRATIONS(a)

Date	Initial Concentrations		Ozone Maximum, ppm	
	NMHC, ppmC	NO_x, ppm	Pasadena	6-hr Model Prediction
9-10-69	4.0	0.43	0.60	0.55
9-29-69	4.5	0.75	0.59	0.42
8-6-70	3.9	0.32	0.56	0.54
8-31-70	3.0	0.31	0.51	0.47
10-1-70	4.3	0.75	0.52	0.40

(a) Data are 6-9 a.m. NMHC and NO_x concentrations measured in downtown Los Angeles and maximum hourly average O_3 measured in Pasadena on days when the airflow trajectory was predominantly from Los Angeles to Pasadena.

A more thorough appreciation of the ozone precursor model can be gained by viewing 3-dimensional graphs as we did for the aerosol model. One of the most interesting features of the data is the irradiation-time effect on the NMHC/NO_x ratios corresponding to maximum ozone concentrations. This is depicted in Figure 27a,b,c in which the response surfaces represent the instantaneous O_3 concentrations for all initial concentrations of NMHC and NO_x. For quantitative reference isopleths of constant O_3 concentration are presented in Figure 28a,b,c; each isopleth represents 0.05 ppm O_3. At the 2-hour irradiation interval the ozone concentration is nearly zero for low NMHC/NO_x ratios. The NMHC/NO_x ratio at peak ozone concentrations lies along the 28/1 plane over the entire range of precursor concentrations. Thus there is a pronounced effect of NO_x inhibiting O_3 formation over this irradiation period. By 6 hours, there are striking differences. In addition to the response surface "swelling up" in the NO_x region of the diagram, the NMHC/NO_x ratio of the ridge (maximum O_3) shifts to 11.5/1. At 10 hours, the

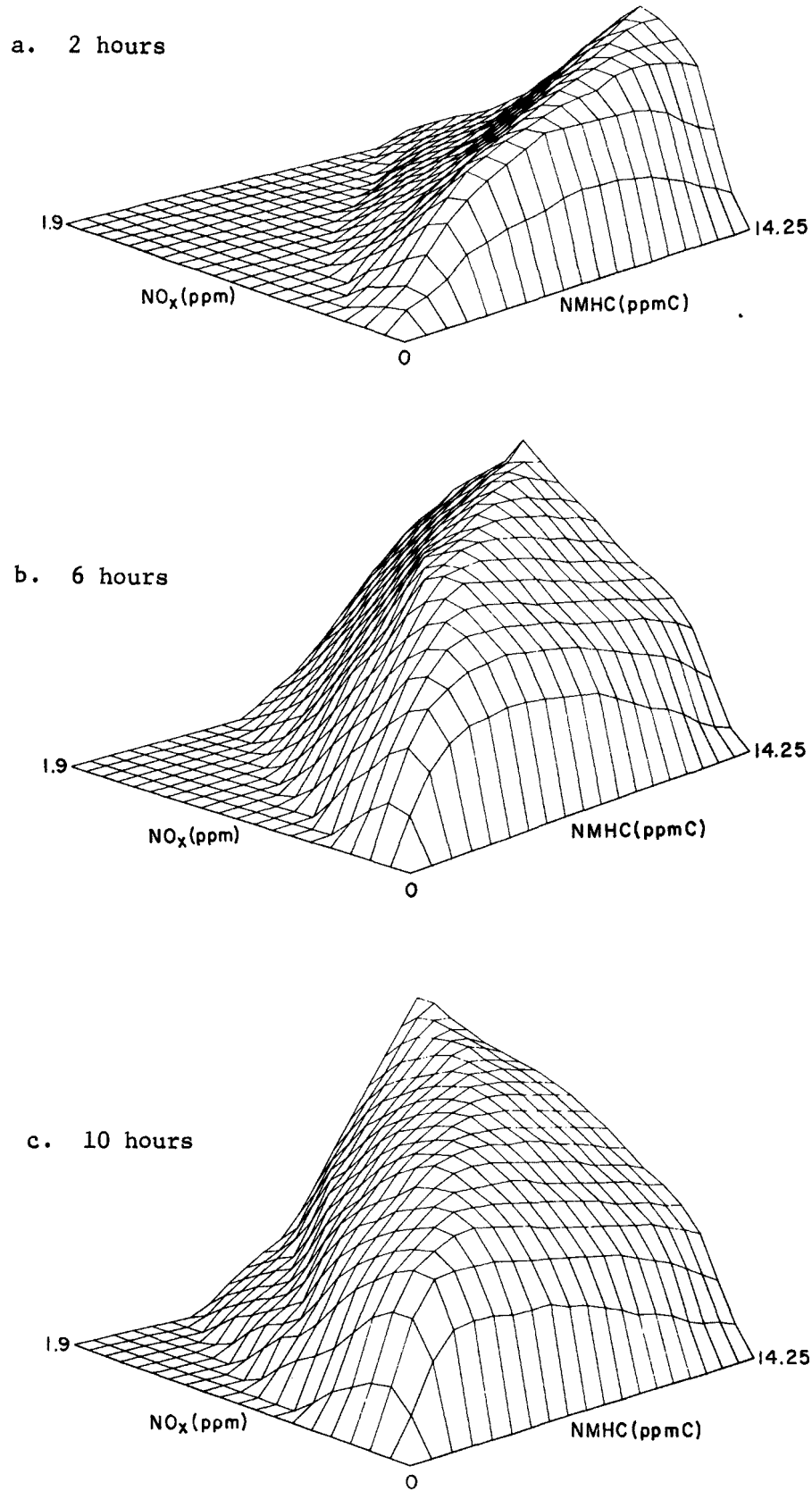

FIGURE 27. SURFACE PROJECTIONS REPRESENTING OZONE CONCENTRATIONS AS FUNCTIONS OF INITIAL CONCENTRATIONS OF NMHC AND NO_x AT IRRADIATION TIMES OF 2, 6, AND 10 HOURS

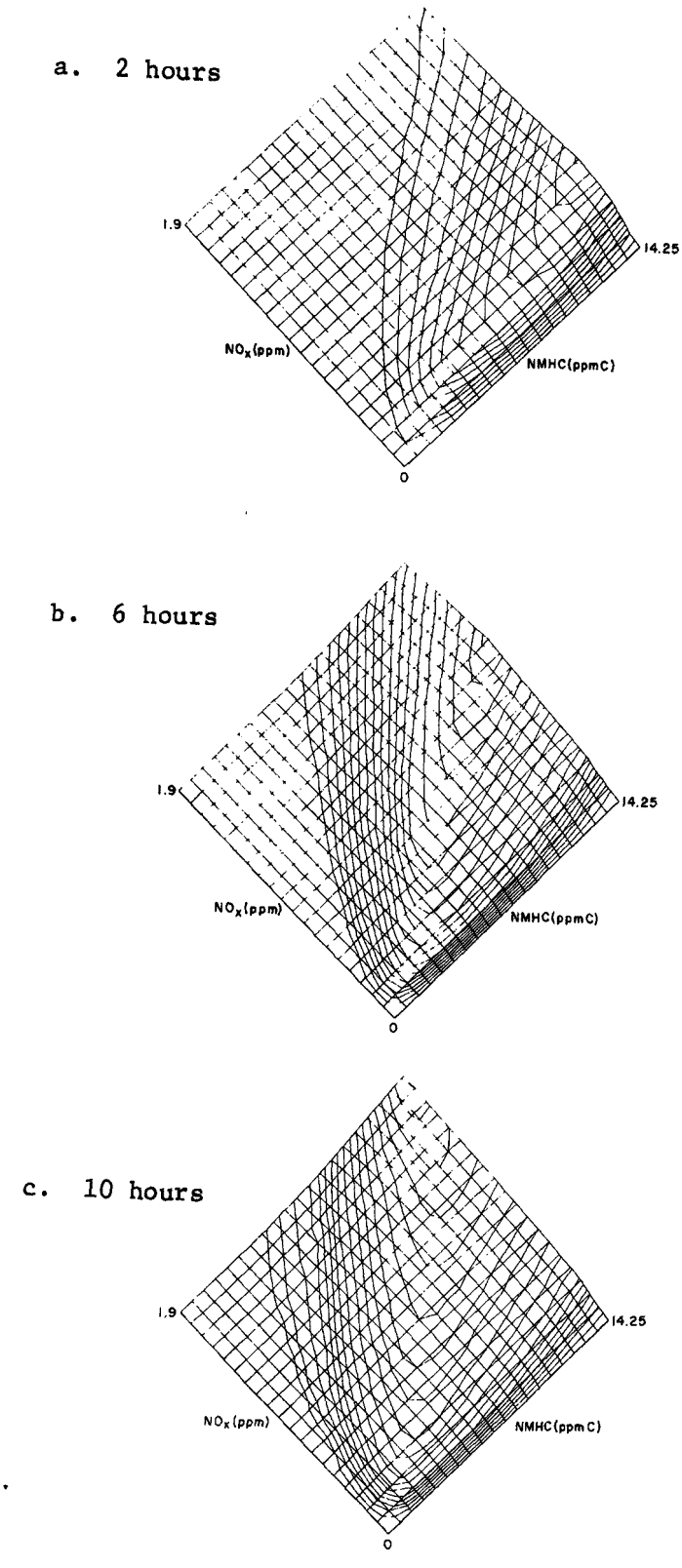

FIGURE 28. ISOPLETHS OF OZONE CONCENTRATIONS AS FUNCTIONS OF INITIAL CONCENTRATIONS OF NMHC AND NO_X AT IRRADIATION TIMES OF 2, 6, AND 10 HOURS (Isopleths correspond to concentration intervals of 0.05 ppm O_3.)

ridge swings further in the NO_x direction to a NMHC/NO_x ratio of 8/1. Thus as the irradiation time is extended, the inhibiting effect of NO_x on peak O_3 continually diminishes in agreement with the modeling results of Hecht[67]. Hecht points out that true suppression of O_3 occurs only when all the reactive hydrocarbon is consumed without complete conversion of NO to NO_2.

Although somewhat academic it is interesting to note that at very high NMHC/NO_x ratios the O_3 dependency on NMHC goes through a maximum at all irradiation periods. At the 2-hour, 6-hour, and 10-hour periods the maximum occurs near [NMHC] of 7 ppmC, 4.5 ppmC, and 2.3 ppmC, respectively. Such conditions are possibly relevant to rural situations where high HC/NO_x ratios may be encountered. The dependency of ozone on NO_x also goes through a maximum, as it did for aerosol, with the functionality broadening with increasing irradiation time and increasing pollutant concentrations.

To illustrate the changes in the O_3 precursor relationships at constant NMHC/NO_x ratios, ozone response surfaces were "sliced and exposed" at 10/1 and 5/1 ratios. The results are presented in Figures 29a,b,c and 30a,b,c; the ordinate (NO_x) and the abscissa (NMHC) are the vantage points in each pair of graphs. Presumably, this type of illustration is becoming more familiar and self explanatory.

Looking first at the 10/1 data, one sees that at 2 hours there is a O_3 plateau which does not decline until NMHC and NO_x concentrations < 3 ppm and < 0.3 ppm are reached. At 6 hours, there is a gradual dependence of O_3 on the pollutant concentration corresponding to [NO_x] < 0.8 ppm and [NMHC] < 8 ppmC. At 10 hours, increasing O_3 concentration occurs with increasing pollutant concentrations over the entire range of initial concentrations, but the slope is steep only for NMHC < 2 ppmC and $NO_x < 0.2$ ppm.

At the 5/1 ratio, almost no O_3 is present at 2 hours of irradiation, but the small peak which does exist occurs at relatively low pollutant concentrations. At 6 hours, the ozone maximum is still below 0.3 ppm for all pollutant concentrations. The peak ozone concentration goes through a maximum with respect to the initial pollutant concentration--the maximum O_3 occurring in the pollutant concentration range from 2 ppmC NMHC and 0.4 ppm NO_x to 5 ppmC NMHC and 1 ppm NO_x.

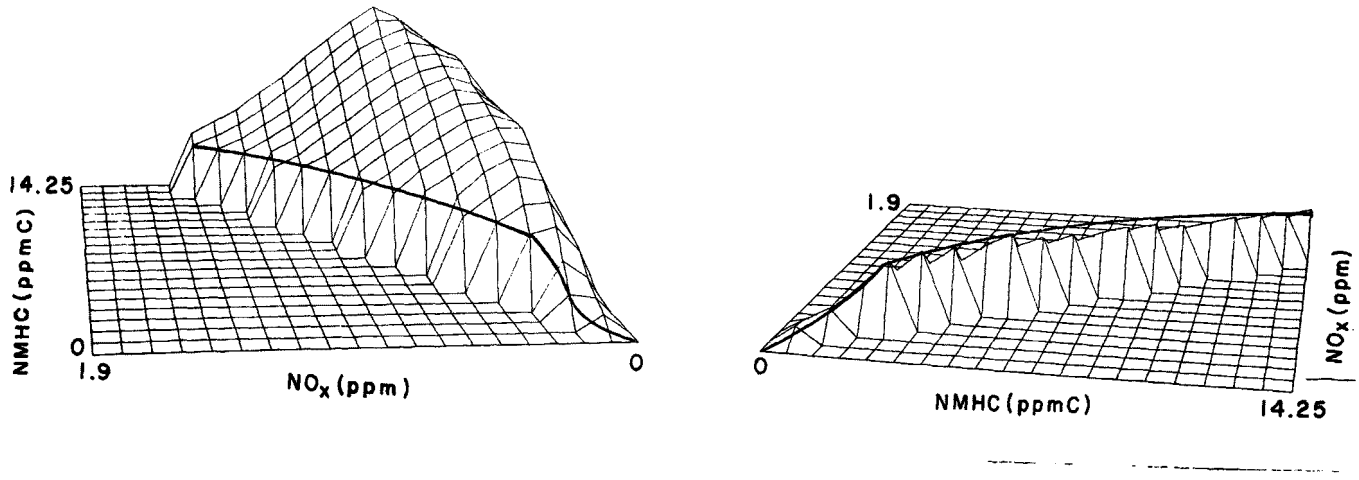

a. 2 hours

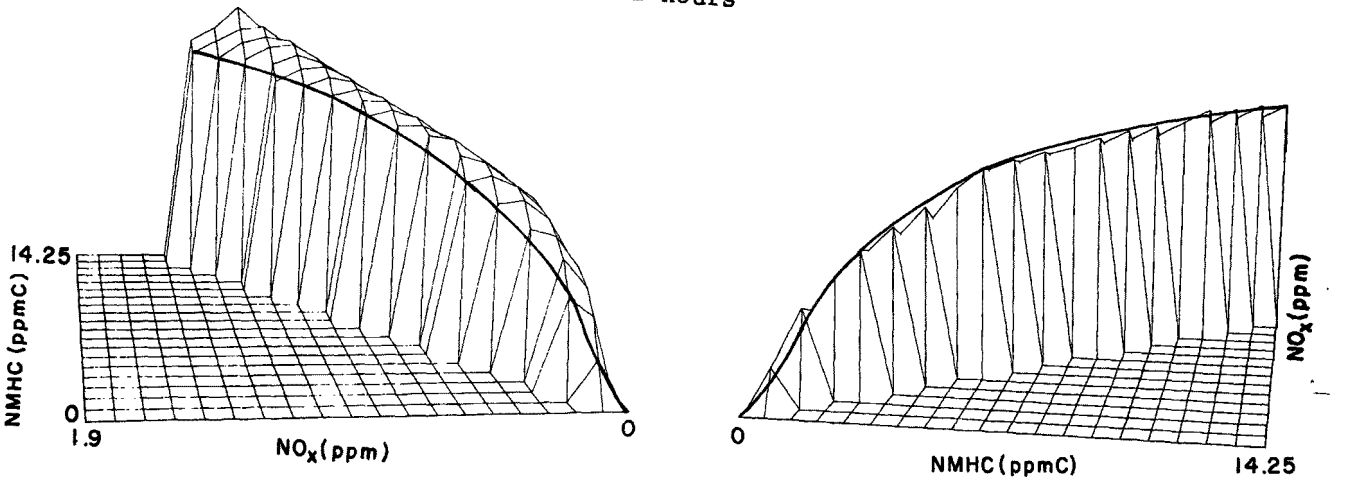

b. 6 hours

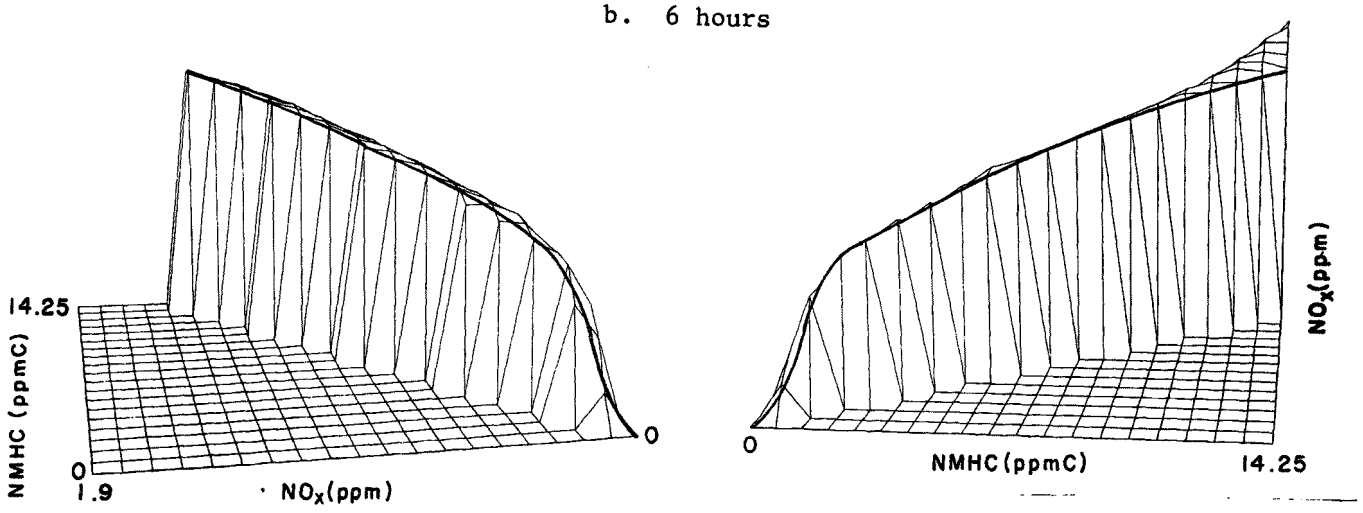

c. 10 hours

FIGURE 29. SURFACE PROJECTIONS REPRESENTING OZONE CONCENTRATIONS AS FUNCTIONS OF INITIAL POLLUTANT CONCENTRATIONS AT A CONSTANT NMHC/NO_x RATIO OF 10/1 AND IRRADIATION TIMES OF 2, 6, AND 10 HOURS

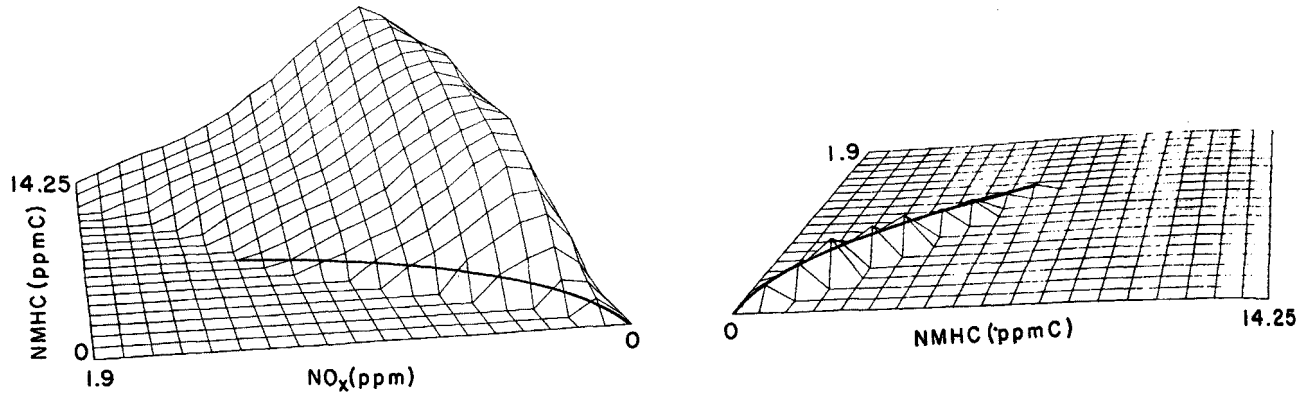

a. 2 hours

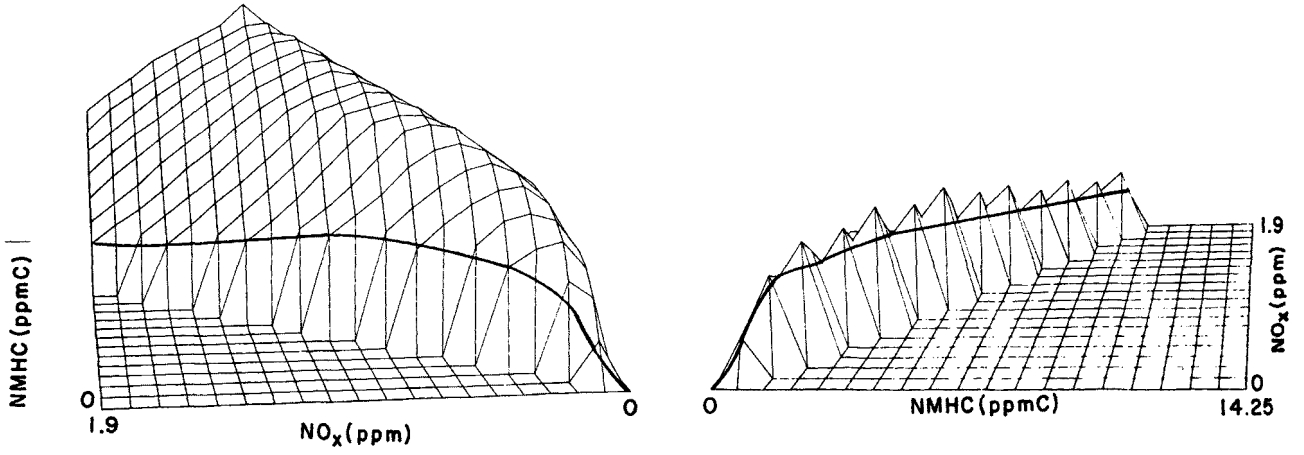

b. 6 hours

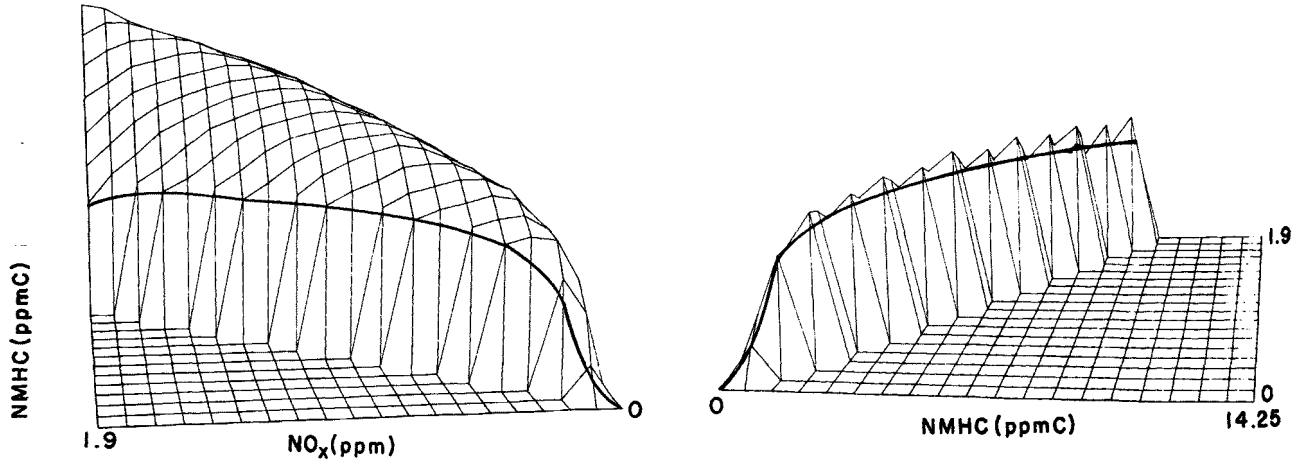

c. 10 hours

FIGURE 30. SURFACE PROJECTIONS REPRESENTING OZONE CONCENTRATIONS AS FUNCTIONS OF INITIAL POLLUTANT CONCENTRATIONS AT A CONSTANT NMHC/NO_x RATIO OF 5/1 AND IRRADIATION TIMES OF 2, 6, AND 10 HOURS

Results over prolonged irradiations of 10 hours are similar to those at 6 hours except that an even greater range of constant maximum ozone concentrations and a 25 percent greater maximum value are evident. A precipitous decline in the ozone concentration does not occur until pollutant levels < 1.5 ppmC NMHC and < 0.3 ppm NO_x are reached.

AEROSOL AND OZONE--MUTUAL BENEFITS FROM PRECURSOR CONTROLS

At first glance, the precursor relationships of aerosol formation with NMHC and NO_x may appear similar to those for ozone formation. In many respects they are, however, the fact that peak aerosol and ozone concentrations do not correlate well is a clue that there must be substantial differences. Side-by-side comparisons of the response surfaces of aerosol and ozone for identical precursor conditions will be used to identify the differences as well as the many similarities in the relationships, and they will likewise be useful in estimating benefits anticipated from precursor controls.

Figure 31a-f shows in parallel the overall aerosol and ozone relationships to NMHC and NO_x at progressive irradiation times. The relationships for aerosol and O_3 are similar at 2 hours. High concentration of NO_x show strong inhibition effects at this period, more so for ozone than for aerosol. In both cases, the crest of maximum concentrations falls along a NMHC/NO_x section near 25/1.

At 6 hours, substantial differences are apparent. The crest in the ozone surface sweeps dramatically toward lower NMHC/NO_x ratios, and lower O_3 concentrations appear where the crest was oriented at 2 hours. By 10 hours, the crest has swept to a NMHC/NO_x ratio of 8/1.

The crests in the response surfaces of aerosol concentrations each contain bends over the range of pollutant concentrations studied. At high concentrations, the crests are relatively invariant with respect to irradiation time, but, at more common concentrations, the initial NO_x concentration becomes increasingly crucial with time, as is the case with O_3. The effect of irradiation time is less pronounced than for O_3, however.

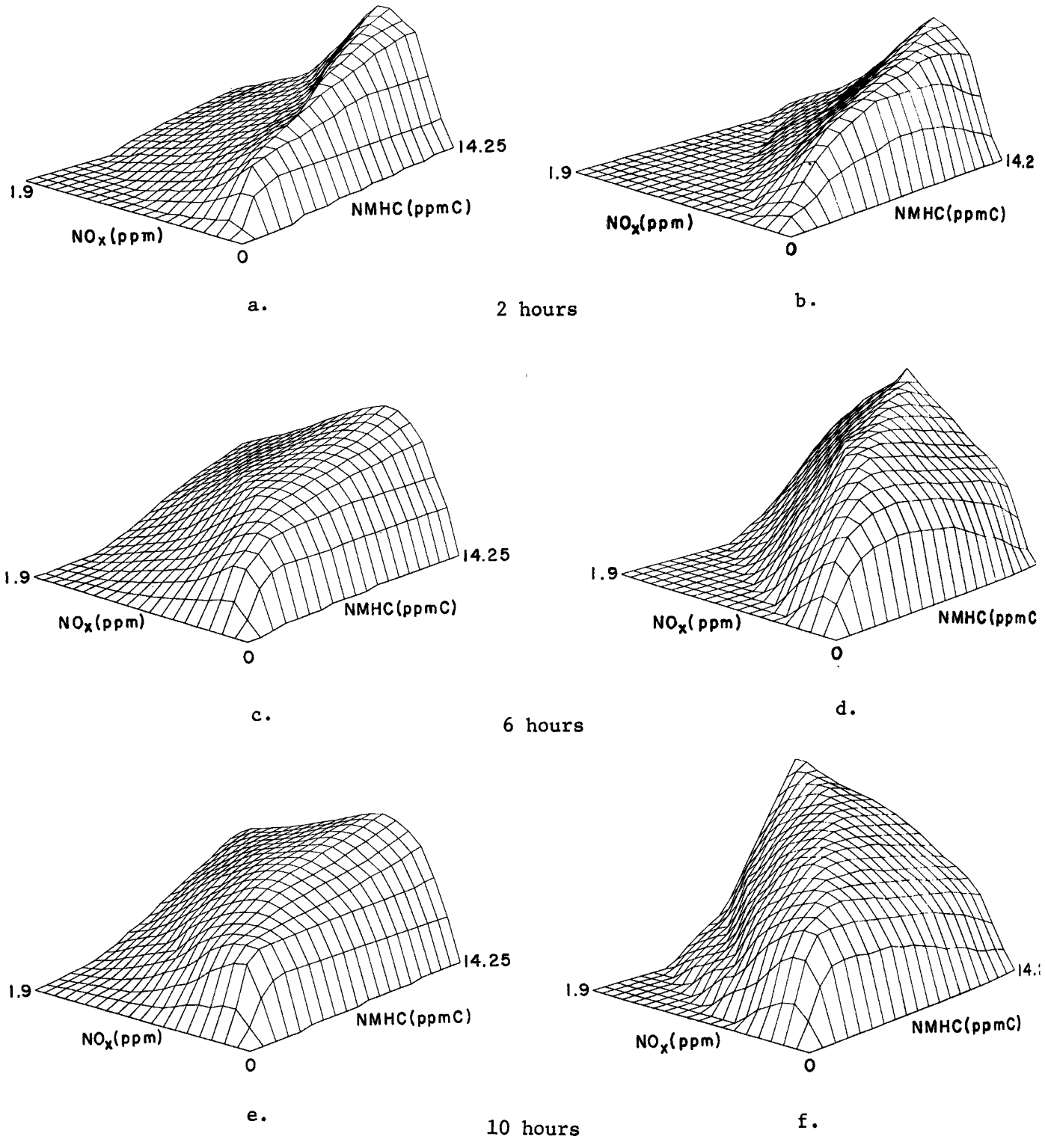

FIGURE 31. COMPARISONS OF THE CONCENTRATION DEPENDENCE OF AEROSOL (a,c,e) AND OZONE (b,d,f) VOLUME ON THE INITIAL CONCENTRATIONS OF NMHC AND NO_x AT IRRADIATION TIMES OF 2, 6, AND 10 HOURS

The crest of peak aerosol concentration changes from a NMHC/NO_x ratio of 15/1 at 2 hours to 13/1 and 10/1 at 6 hours and 10 hours, respectively.

Smog profiles show that aerosol formation often precedes ozone formation and that later in the irradiations the rate of aerosol formation often diminishes markedly while that for O_3 remains appreciable. For these reasons, the maximum aerosol concentration at 2 hours is 93 percent of the maximum at 10 hours, while for ozone the 2-hour maximum is only 65 percent of the 10 hour maximum concentration.

Additional comparisons of the precursor relationships are made by inspecting models at constant NMHC/NO_x ratios. Figure 32a-f shows the relationships at a 10/1 ratio, and Figure 33a-f shows them at a 5/1 ratio. At 2 hours and at 10/1 ratio, both the aerosol and O_3 relationships are nearly constant over a wide range of initial pollutant (NMHC and NO_x) concentrations, except at the relatively low concentrations. At 6 hours and 10 hours (NMHC/NO_x of 10/1), the initial pollutant concentration is somewhat more influential on the aerosol and ozone levels and to similar degrees.

Looking at the data at 5/1 NMHC/NO_x ratios one sees that little O_3 has formed compared to aerosol at 2 hours. Aside from the inverse relationship between O_3 concentrations and the initial pollutant levels (NO_x range > 0.4 ppm) at the 2-hour irradiation period, both aerosol and O_3 are essentially insensitive to the initial pollutant concentrations until relatively low pollutant concentrations are attained. Thus at 5/1 ratios little improvement in either aerosol or O_3 concentrations is realized until NMHC and NO_x concentrations are < 2 ppmC and 0.4 ppm, respectively, and this condition holds over a wide range of irradiation periods.

There are many ways of looking at precursor-control strategies, and we will not attempt to discuss the ramifications of all possible maneuvers. An approach considered by many as both practical and prudent is one based on unilateral control of NMHC after achieving some reasonably safe level of NO_x. For mean yearly NO_x concentrations of 0.05 ppm, hourly-average maximum concentrations of 0.35 ppm are often equated, and we will adopt this NO_x concentration for purposes of assessing the effect of unilaterial

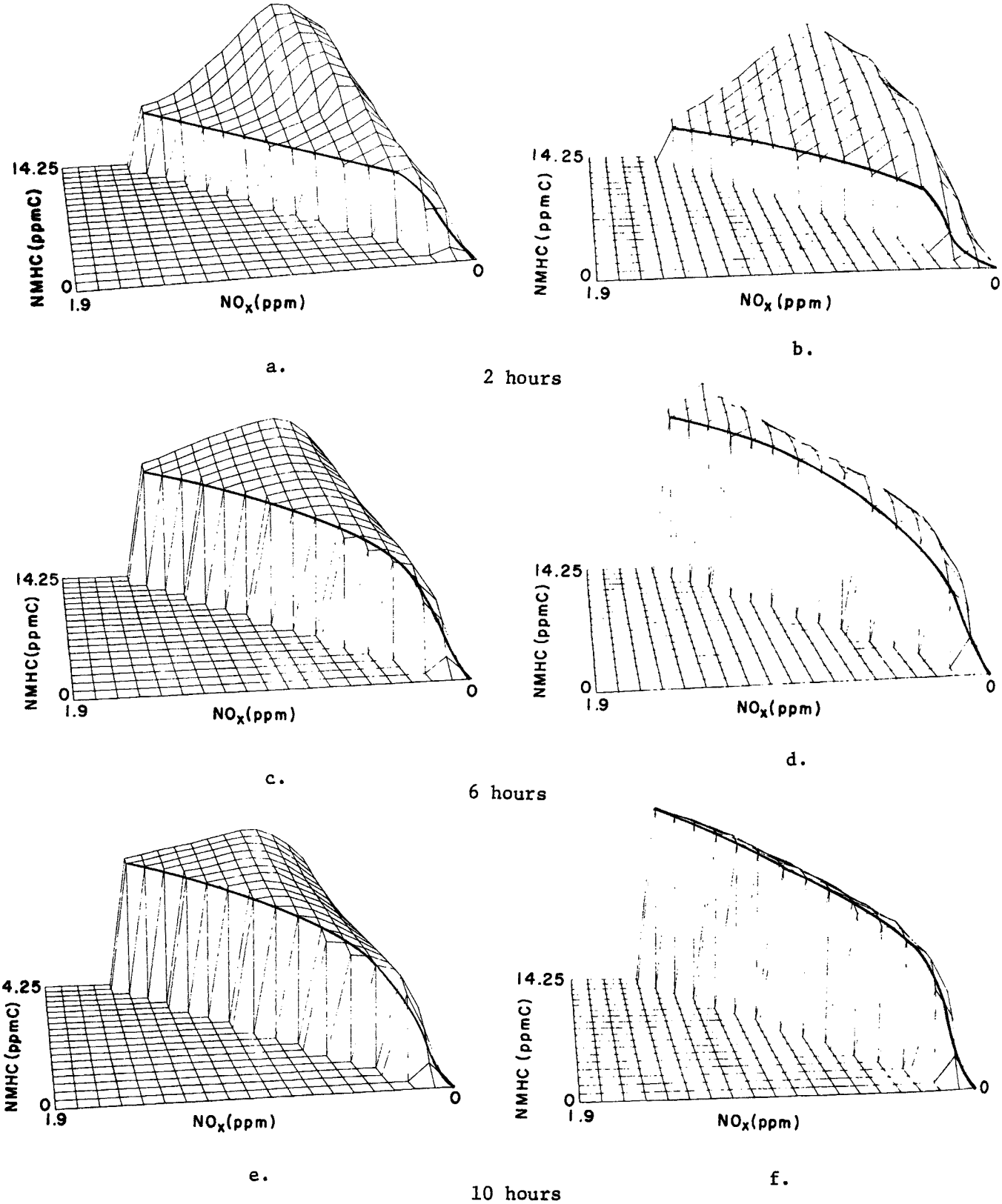

FIGURE 32. COMPARISONS OF THE CONCENTRATION DEPENDENCE OF AEROSOL (a,c,e) AND OZONE (b,d,f) VOLUME ON THE INITIAL CONCENTRATIONS OF POLLUTANTS AT A CONSTANT NMHC/NO_x RATIO OF 10/1 AND IRRADIATION TIMES OF 2, 6, AND 10 HOURS

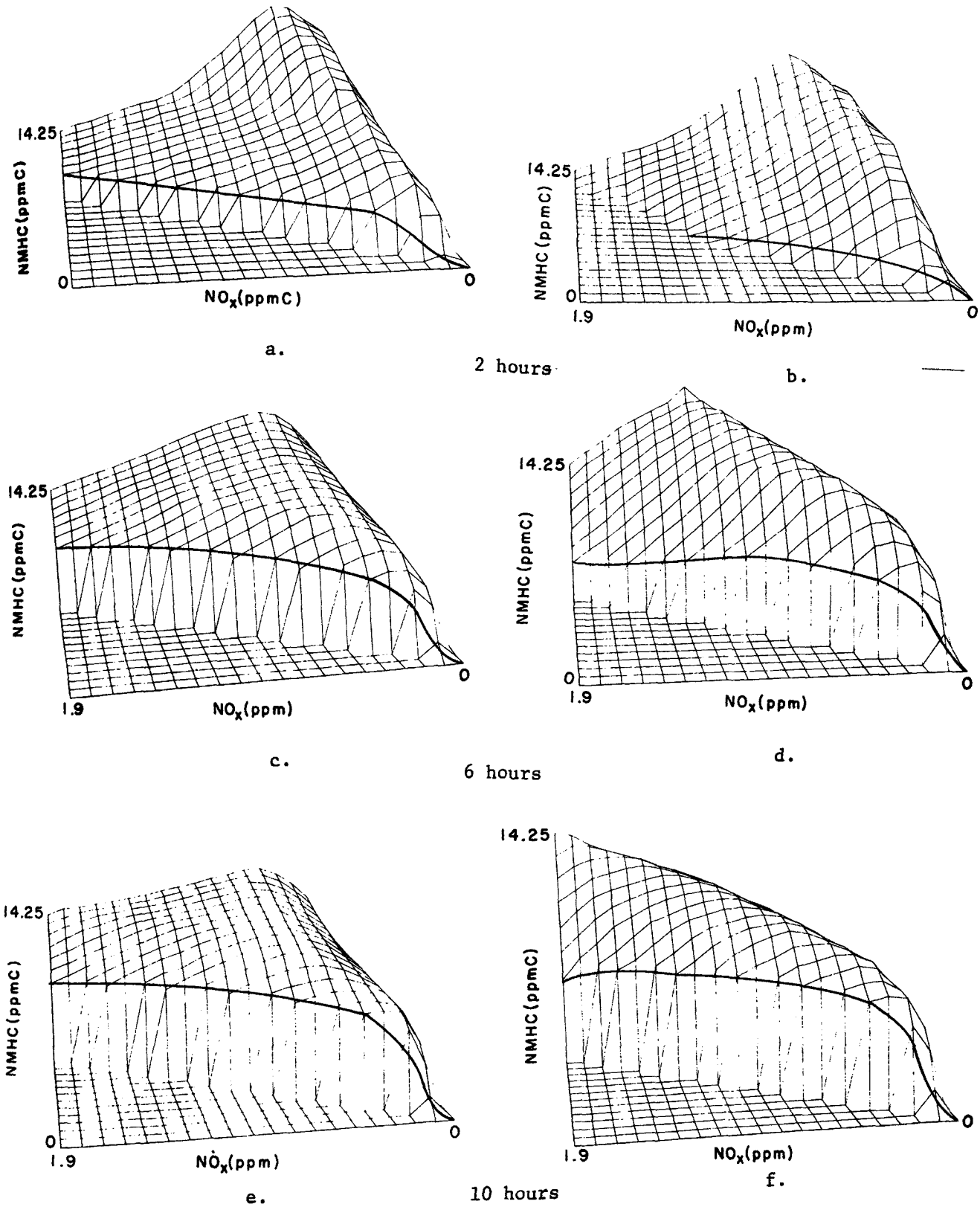

FIGURE 33. COMPARISONS OF THE CONCENTRATION DEPENDENCE OF AEROSOL (a,c,e) AND OZONE (b,d,f) VOLUME ON THE INITIAL CONCENTRATIONS OF POLLUTANTS AT A CONSTANT NMHC/NO_x RATIO OF 5/1 AND IRRADIATION TIMES OF 2, 6, AND 10 HOURS

NMHC control on both aerosol and O_3 concentrations. To further limit the discussion, only the data corresponding to 6-hour irradiations is selected. (Presumably the models presented will permit the reader to make analyses of additional control strategies, if desired). It should also be pointed out that the smog-chamber models approximate worst-case conditions with respect to both the initial pollutant concentrations and the smog manifestations.

We begin the analysis by recording O_3 data corresponding to 0.35 ppm NO_x and 3.5 ppmC NMHC; i.e., at a 10/1 NMHC/NO_x ratio. At this point the $[O_3] \geq 0.5$ ppm. If NMHC is reduced 50 percent ([NMHC] = 1.75 ppmC and NMHC/NO_x = 5/1) the model predicts a 50 percent reduction in O_3 (0.25 ppm). A 70 percent reduction in NMHC (NMHC/NO_x = 3/1) results in a 70 percent reduction in O_3 (0.15 ppm), and an 80 percent reduction in NMHC (NMHC/NO_x = 2/1) results in an 84 percent reduction in O_3 which meets the 0.08 ppm standard.

With the above control scheme applied, a 50 percent reduction in NMHC (NMHC/NO_x = 5/1 at 0.35 ppm NO_x) results in only a 28 percent reduction in aerosol concentration. Further reduction to 70 percent (NMHC = 1.05 ppmC) results in a 57 percent decrease in aerosol, and an 80 percent control of NMHC (NMHC = 0.7 ppmC) reduces the aerosol concentration 71 percent.

In conclusion, it is satisfying to find that control strategies designed to limit the photochemical formation of O_3 are mutually beneficial in limiting the formation of aerosols. Unfortunately, the model predicts that the degree of benefit for aerosols will be less than that for O_3.

REFERENCES

1. Miller, D.F., Schwartz, W.E., Gemma, J.L., and Levy, A., "Haze Formation: Its Nature and Origin-1975", EPA-650/3-75-010, NERC, Research Triangle Park, N.C. (1975).

2. Hidy, G.M., et al., "Characterization of Aerosols in Los Angeles", Report on the ACHEX Study, Volumes I-IV, prepared for the California Air Resources Board (1975).

3. Hamming, W.J. and Dickinson, J.E., *J. Air Poll. Control Assoc.*, 16, 317 (1966).

4. Brunelle, M.F., Dickinson, J.E., and Hamming, W.J., "Effectiveness of Organic Solvents in Photochemical Smog Formation", Air Poll. Control Office, Los Angeles County (1966).

5. Romanovsky, J.C., Ingels, R.M., and Gordon, R.J., *J. Air Poll. Control Assoc.*, 17, 454 (1967).

6. Heuss, J.M. and Glasson, W.A., *Environ. Sci. and Technol.*, 2, 1109 (1968).

7. Altshuller, A.P., Kopczynski, S.C., Wilson, D., Lonneman, W.A., and Sutterfield, F.D., *J. Air Poll. Control Assoc.*, 19, 791 (1969).

8. Dimitriades, B., "On the Function of Hydrocarbons and Nitrogen Oxides in Photochemical Smog Formation", U.S. Bur. Mines Rep. Invest. 7433 (1970).

9. Wilson, K.W. and Doyle, G.J., "Final Report on Investigation of Reactivities of Organic Solvents", Contract No. CPA 22-69-125, (September, 1970).

10. Levy, A., Miller, S.E., and Scofield, F., "The Photochemical Smog Reactivity of Solvents", Second Int. Clean Air Congress, Academic Press, New York, 1970, p. 305.

11. Altshuller, A.P. and Bufalini, J.J., *Environ. Sci. and Technol.*, 5, 39 (1971).

12. Glasson, W.A. and Tuesday, C.S., *Environ. Sci. and Technol.*, 5, 151, (1971).

13. Laity, J.L., Burstain, I.G., and Appel, B.R., "Photochemical Smog and Atmospheric Reactions of Solvents", Adv. in Chemistry Series 124, Washington, D.C., 1973, p. 95.

14. Dimitriades, B. and Wesson T.C., "Reactivity of Exhaust Aldehydes", U.S. Bur. Mines Rept. Invest. 7527, 1971.

15. Dimitriades, B., *Environ. Sci. and Technol.*, 6, 253 (1972).

16. Kopczynski, S.L., Altshuller, A.P., and Sutterfield, F.D., *Environ. Sci. and Technol.*, 8, 909 (1974).

17. Kopczynski, S.L., Kuntz, R.L., and Bufalini, J.J., *Environ. Sci. and Technol.*, 9, 648 (1975).

18. Prager, M.J., Stephens, E.R., and Scott, W.E., "Aerosol Formation from Gaseous Air Pollutants", *Ind. and Eng. Chem.*, 52, 521 (1960).

19. Renzetti, N.A. and Doyle, G.J., "Photochemical Aerosol Formation in Sulfur Dioxide-Hydrocarbon Systems", *Int. J. Air Poll.*, 2, 327 (1960).

20. Stevenson, H.J.R., Sanderson, D.E., and Altshuller, A.P., *Int. J. Air Wat. Poll.*, 9, 367 (1965).

21. Goetz, A. and Pueschel, R., *J. Air Poll. Control Assoc.*, 15, 90 (1965).

22. Goetz, A. and Pueschel, R., *Atmos. Environ.*, 1, 287 (1967).

23. Orr, C., Jr., Hard, F.K., and Corbett, W.J., *J. Colloid Sci.*, 13, 472 (1968).

24. Wilson, W.E., Merryman, E.L., Levy, A., and Taliaferro, H.R., "Aerosol Formation in Photochemical Smog - I. The Effect of Stirring", *J. Air Poll. Control Assoc.*, 21, 128 (1971).

25. Groblicki, P.J. and Nebel, G.J., "The Photochemical Formation of Aerosols in Urban Atmospheres", in Chemical Reactions in Urban Atmospheres, (C.S. Tuesday, Ed.) Elsevier, N.Y. (1971).

26. Wilson, W.E., "Aerosol Formation in Photochemical Smog - II. The Role of Sulfur Dioxide", presented at the 161st National ACS Meeting, Los Angeles, Calif., (1971).

27. Wilson, W.E., Miller, D.F., and Levy, A., "A Study of SO_2 in Photochemical Smog - III". Battelle-Columbus Final Report (third year) to the American Petroleum Institute, Committee for Air and Water Conservation (Project 5-11), 1971.

28. Stephens, E.R. and Price, M.A., *J. Colloid and Interface Sci.*, 39, 272 (1972).

29. Wilson, W.E., Miller, D.F., and Levy, A., *J. Air Poll. Control Assoc.*, 23, 949 (1973).

30. Miller, D.F. and Levy, A., "Environmental Chamber Studies of Atmospheric Aerosols", EPA-650/4-74-009, NERC, Research Triangle Park, N.C. (1973).

31. Smith, J.P. and Urone, P., *Environ. Sci. and Technol.*, 8, 742 (1974).

32. Kocmond, W.C., Kittelson, D.B., Yang, J.Y., and Demerjian, K.L., "Determination of the Formation Mechanisms and Composition of Photochemical Aerosols", Calspan Corp., Report No. NA-5365-M-1, Buffalo, New York (1973).

33. O'Brien, R.J., Holmes, J.R., and Bockian, A.H., *Environ. Sci. and Technol.*, 9, 568 (1975).

34. Doyle, G.J. and Renzetti, N.A., *J. Air Poll. Control Assoc.*, 8, 23 (1958).

35. Shuck, E.A., Ford, H.W., and Stephens, E.R., "Air Pollution Effects of Irradiated Automobile Exhaust as Related to Fuel Composition", Air Pollution Foundation Report 26, Oct., 1958).

36. Hamming, W.J., Mader, P.P., Nicksic, S.W., Romanovsky, J.C., and Wayne, L.G., "Gasoline Composition and the Control of Smog", Los Angeles County Air Pollution Control District Report, Sept., 1961.

37. Ripperton, L.A. and Jeffries, H.E., and White, O., "Formation of Aerosols by Reactions of Ozone with Selected Hydrocarbons", paper presented at the 161st National ACS Meeting, Los Angeles, Calif. (1971).

38. Schwartz, W.E., Jones, P.W., Riggle, C.J., and Miller, D.F., "Chemical Characterization of Model Aerosols", EPA-650/3-74-011, NERC, Research Triangle Park, N.C. (1974).

39. Miller, D.F. and Levy, A., "Exhaust Hydrocarbon Relationships with Photochemical Aerosol Formation", Paper No. 75-16.3 presented at the 68th Annual Meeting of the Air Poll. Control Assoc., Boston, Mass. (1975).

40. Smith, J.H. and Wilson, K.W., "Motor Fuel Composition and Photochemistry", Stanford Research Institute Final Report to the American Petroleum Institute (1971).

41. Vardi, J., "Selected Fuel Factors and the Formation of Automotive Photochemical Serosols and Oxidants", presented at the 66th Annual Meeting of the Air Poll. Control Assoc., Paper No. 73-71 (June, 1973).

42. Kerker, M., The Scattering of Light and Other Electromagnetic Radiation, Academic Press, New York, 1969.

43. Liu, B.Y.H. and Pui, D.Y.H., *J. Colloid and Interface Sci.*, 47, 155 (1974).

44. Whitby, K.T. and Clark, W.E., *Tellus*, 18, 573 (1966).

45. Liu, B.Y.H., Whitby, K.T., and Pui, D.Y.H., *J. Air Poll. Control Assoc.*, 24, 1067 (1974).

46. Liu, B.Y.H. and Pui, D.Y.H., *J. of Aerosol Sci.*, 6, 249 (1975).

47. Kocmond, W.C., Kittelson, D.B., Yang, J.Y., and Demerjian, K.L., "Study of Aerosol Formation in Photochemical Air Pollution", EPA-650/3-75-007, NERC, Research Triangle Park, N.C. (1975).

48. Jefferies, H., Fox, D., and Kamens, R., "Outdoor Smog Chambers" presented at the EPA Smog Chamber Conference, Research Triangle Park, N.C. (1974).

49. Kopczynski, S.L., Lonneman, W.A., Sutterfield, D.F., and Darley, P.E., *Environ. Sci. Technol.*, 6, 342 (1972).

50. Miller, D.F. and Levy, A., "Aerosol Formation in Photochemical Smog. The Effect of Humidity and Small Particles", Proceedings of the Third International Clean Air Congress, Verein Deutscher Ingenieure, Dusseldorf, Germany (1973).

51. Demerjian, K.L., Kerr, J.A., and Calvert, J.G., "The Mechanism of Photochemical Smog Formation", in Adv. Environ. Sci. Technol., (J.N. Pitts and R.L. Metcalf, Eds.) John Wiley and Sons, New York (1974) pp. 1-262.

52. Miller, D.F., "A Smog Chamber Study of the Rate of Conversion of SO_2 as a Function of Reactant Concentrations", Annual Progress Report from Battelle-Columbus to the EPA, in preparation (1976).

53. Wayne, L.G. and Yost, D.M., *J. Chem. Phys.*, 19, 41 (1951).

54. Graham, R.F. and Tyler, B.J., *J. Chem. Soc. Faraday I*, 68, 683 (1972).

55. Calvert, J.G., Private communication (1975).

56. Doyle, G.J., Lloyd, A.C., Darnall, K.R., Winer, A.M., and Pitts, J.N., *Environ. Sci. Technol.*, 9, 237 (1975).

57. Stephens, E.R., "Hydrocarbons in Polluted Air", Summary Report to the Coordinating Research Council (Project CAPA-5-68), Statewide Air Pollution Research Center at Riverside, Calif. (1973).

58. Tuesday, C.S., Chemical Reactions in the Upper and Lower Atmosphere, Interscience, New York, New York (1961).

59. Pitts, J.N., Jr., Vernon J.M., and Wan, J.K.S., *Intern. J. Air and Water Poll.*, 9, 595-600 (1965).

60. Gordon, R.J., Pilot Study of Ultraviolet Radiation in Los Angeles, J.S. Nader (Ed.), National Air Pollution Control Administration, Durham, North Carolina (1965).

61. Hodgeson, J.A., Baumgardner, R.E., Martin, B.E., and Rehme, K.A., *Anal. Chem.*, 43, 1123 (July,1971).

62. Willeke, K. and Whitby, K.T., *J. Air Poll. Control Assoc.*, 25, 529 (1975).

63. Altshuller, A.P., Cohen, I.R., and Purcell, T.C., *Can. J. Chem.*, 44, 2973 (1966).

64. Spicer, C.W., "The Fate of Nitrogen Oxides in the Atmosphere", Battelle-Columbus Report to the Coordinating Research Council (CAPA-9-71) and the EPA, September, 1974.

65. Paskind, J. and Kinosian, J.R., "Hydrocarbon, Oxides of Nitrogen and Oxidant Pollutant Relationships in the Atmosphere Over California Cities", paper presented at the 67th Annual Meeting of the Air Poll. Control Assoc., Denver, Colo. (1974).

66. Spicer, C.W., Gemma, J.L., Joseph, D.W., Sticksel, P.R., and Ward, G.F., "The Transport of Oxidant Beyond Urban Areas", Battelle-Columbus Report to EPA, draft submitted May, 1975.

67. Hecht, T.A., "Smog Simulation Models and Their Use in Evaluating Air Quality Control Strategies", paper presented at the Scientific Seminar on Automotive Pollutants, EPA-600/9-75-003, Washington, D.C.

68. Hamming, W., Chass, R., Dickinson, J., and MacBeth, W., "Motor Vehicle Control and Air Quality. The Path to Clean Air for Los Angeles", presented at the 66th Annual Meeting of the Air Pollution Control Assoc., Chicago, Ill. (1973).

69. Souten, D.R., Hopper, C.J., and Mueller, R.L., "A Critical Review of the Los Angeles County APCD Method for Simulating Atmospheric Oxidant Based on Smog Chamber Irradiation Experiments", paper presented at the 68th Annual Meeting of the Air Poll. Control Assoc., Boston, Mass. (1975).

70. Kinosian, J.R., "Ambient Air Quality Trends in the South Coast Air Basin", paper presented at the Scientific Seminar on Automotive Pollutants, EPA-600/9-75-003, Washington, D.C. (1975).

APPENDIX A

SMOG PROFILES

The profiles were drawn from the original data and are not corrected for dilution or analytical errors. The initial NMHC values indicated at the top of each profile are nonmethane readings from a total hydrocarbon analyzer. The more precise concentrations determined by gas chromatography are presented in Table 6 of the text.

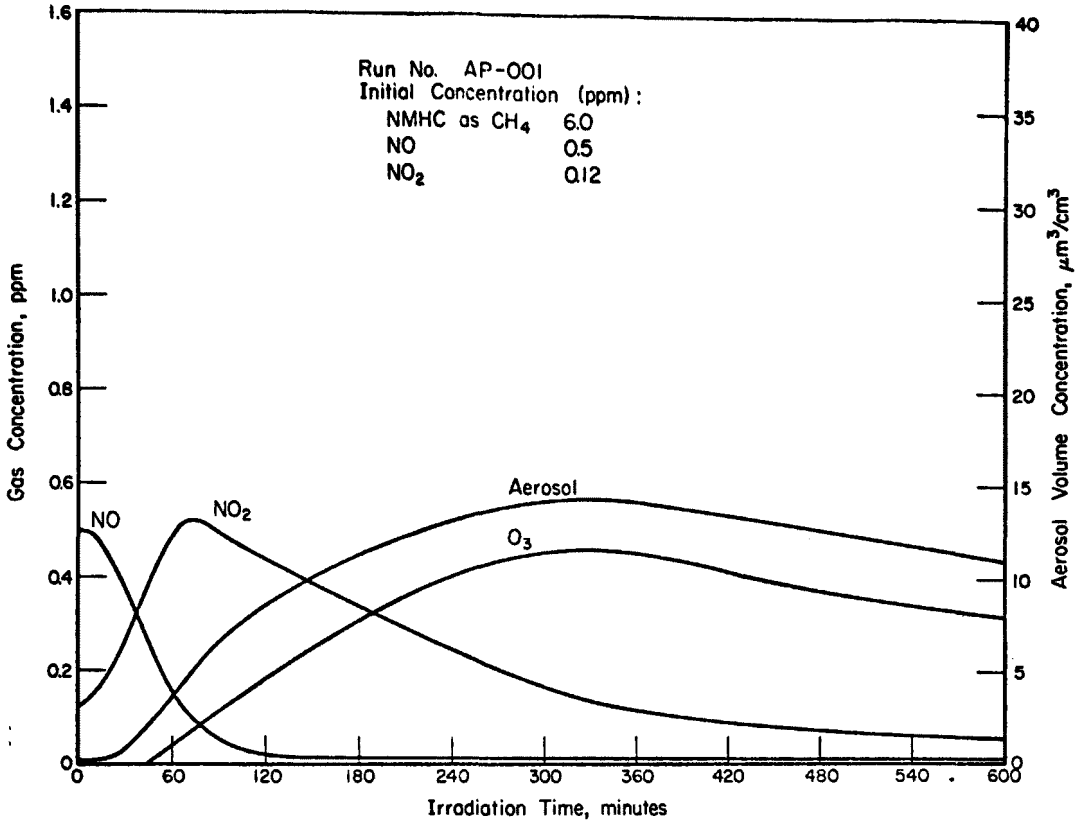
Run No. AP-001
Initial Concentration (ppm):
NMHC as CH_4 6.0
NO 0.5
NO_2 0.12
Aerosol
O_3
NO
NO_2
Gas Concentration, ppm
Aerosol Volume Concentration, $\mu m^3/cm^3$
Irradiation Time, minutes

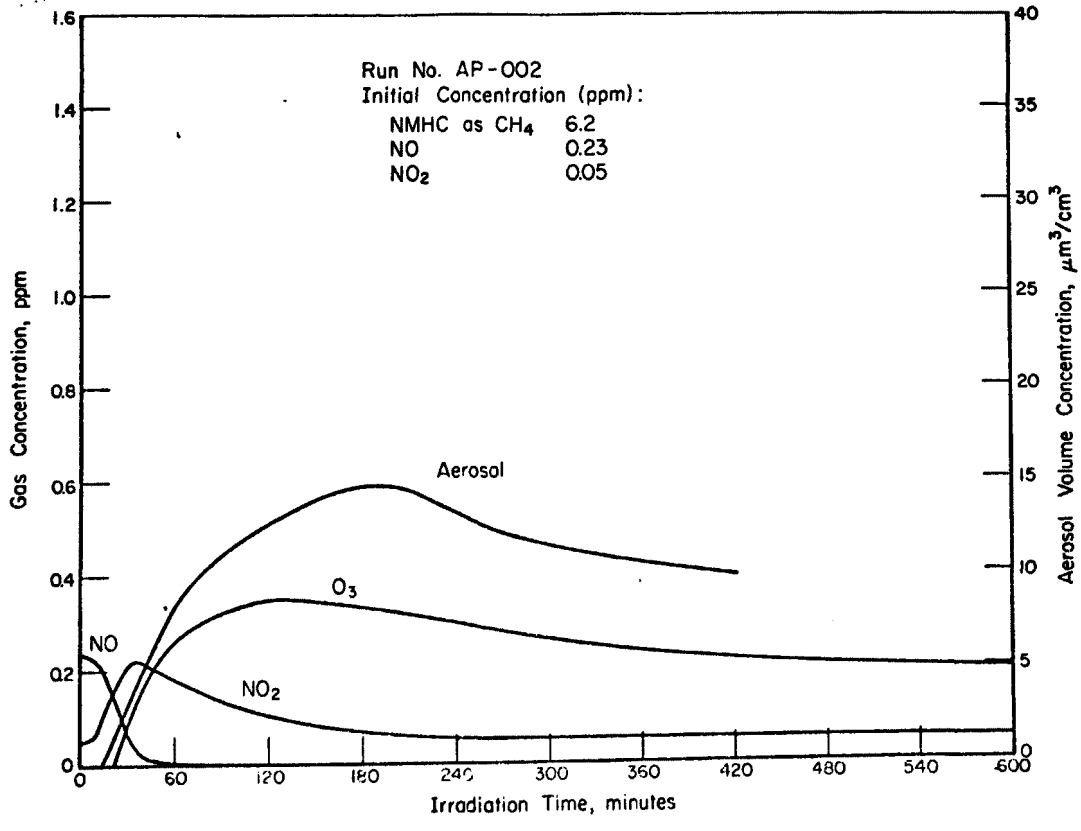
Run No. AP-002
Initial Concentration (ppm):
NMHC as CH_4 6.2
NO 0.23
NO_2 0.05
Aerosol
O_3
NO
NO_2
Gas Concentration, ppm
Aerosol Volume Concentration, $\mu m^3/cm^3$
Irradiation Time, minutes

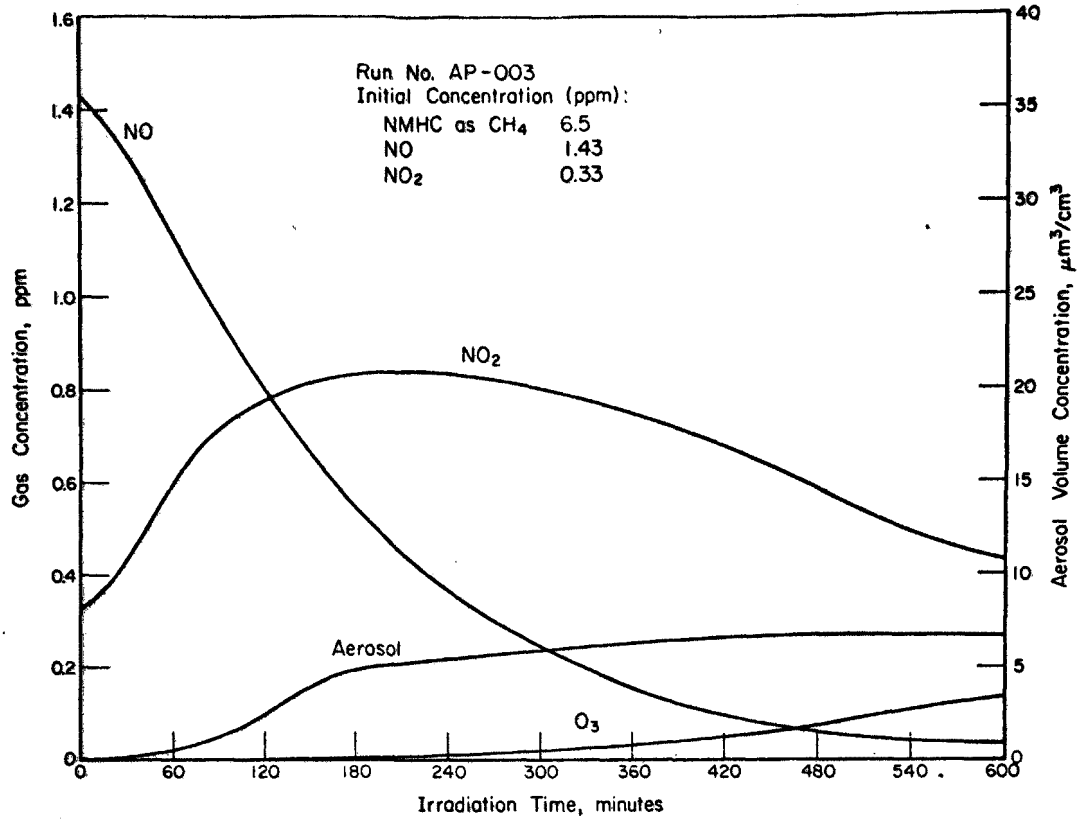
Run No. AP-003
Initial Concentration (ppm):
NMHC as CH4 6.5
NO 1.43
NO2 0.33
NO
NO2
Aerosol
O3
Gas Concentration, ppm
Aerosol Volume Concentration, μm3/cm3
Irradiation Time, minutes

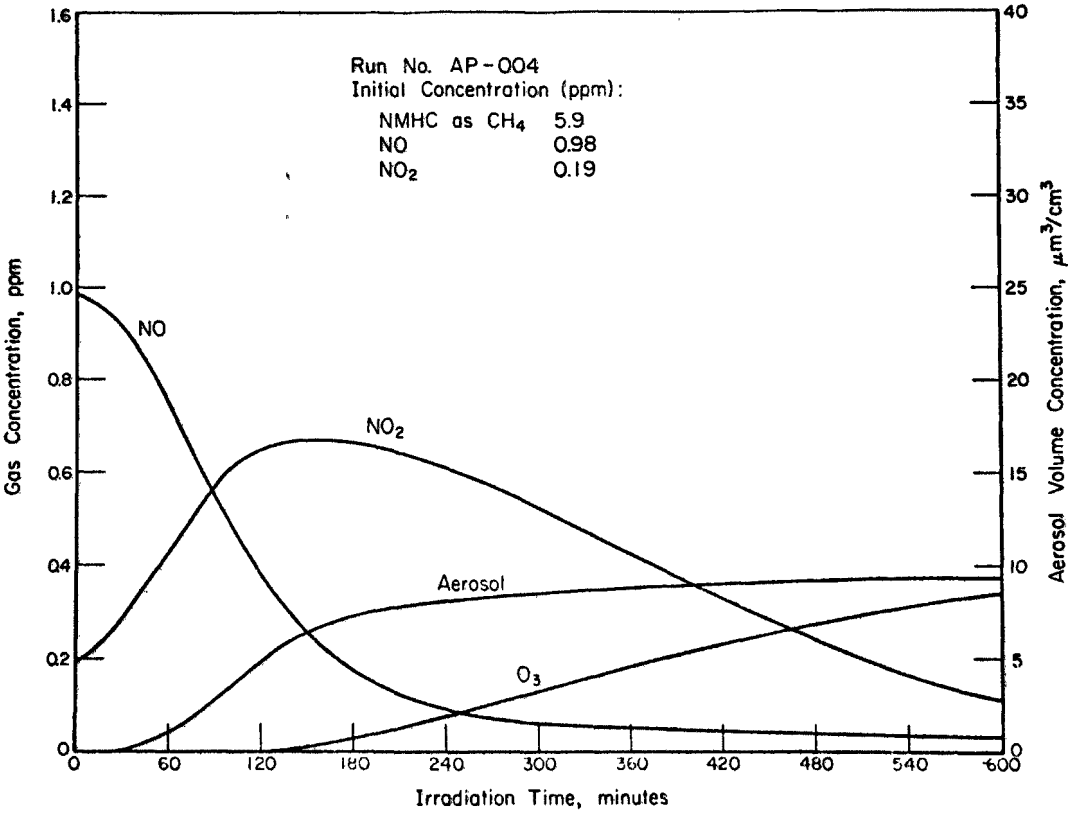
Run No. AP-004
Initial Concentration (ppm):
NMHC as CH4 5.9
NO 0.98
NO2 0.19
NO
NO2
Aerosol
O3
Gas Concentration, ppm
Aerosol Volume Concentration, μm3/cm3
Irradiation Time, minutes

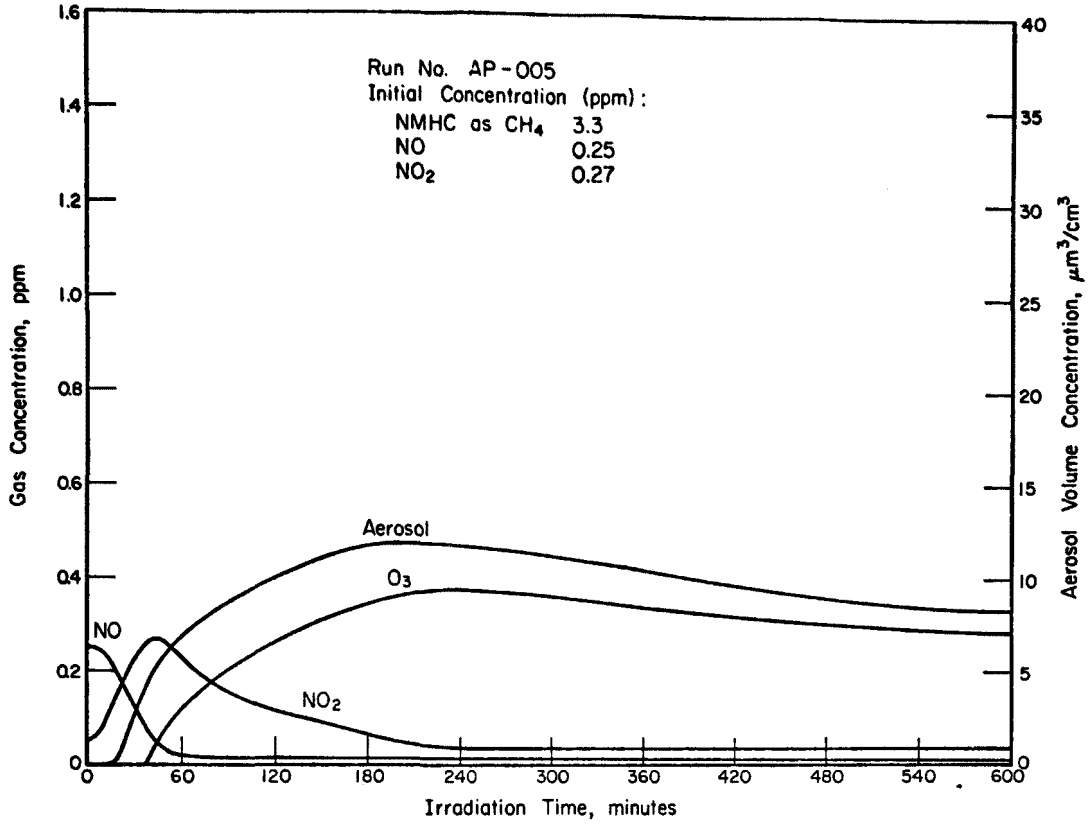
Run No. AP-005
Initial Concentration (ppm):
NMHC as CH4 3.3
NO 0.25
NO2 0.27
Aerosol
O3
NO
NO2
Gas Concentration, ppm
Aerosol Volume Concentration, μm3/cm3
Irradiation Time, minutes

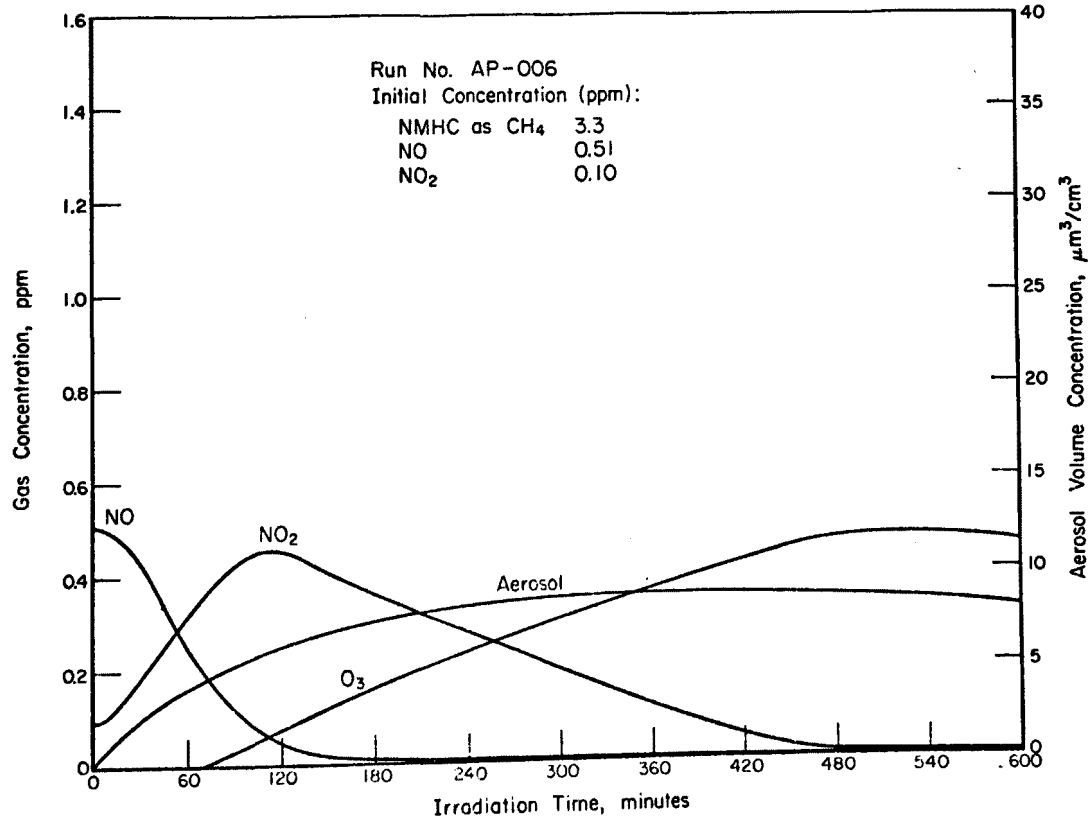
Run No. AP-006
Initial Concentration (ppm):
NMHC as CH4 3.3
NO 0.51
NO2 0.10
NO
NO2
Aerosol
O3
Gas Concentration, ppm
Aerosol Volume Concentration, μm3/cm3
Irradiation Time, minutes

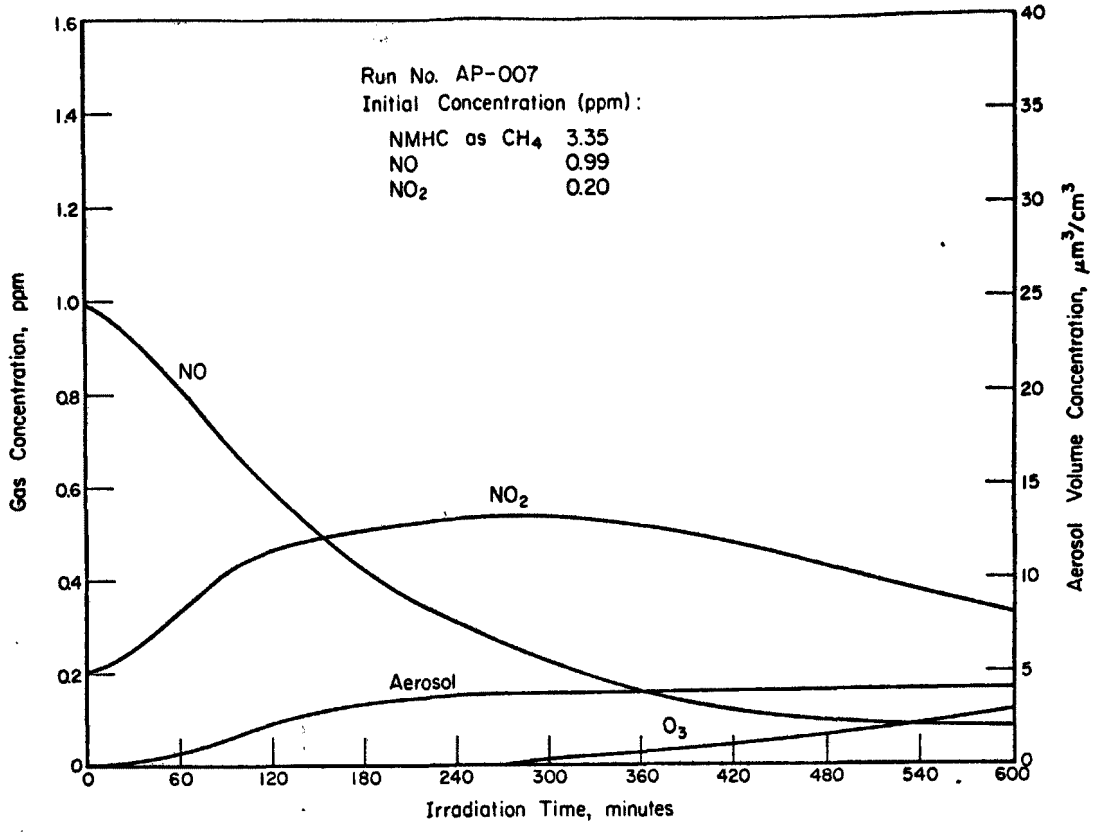
Run No. AP-007
Initial Concentration (ppm):
NMHC as CH_4 3.35
NO 0.99
NO_2 0.20
NO
NO_2
Aerosol
O_3
Gas Concentration, ppm
Aerosol Volume Concentration, $\mu m^3/cm^3$
Irradiation Time, minutes
0
60
120
180
240
300
360
420
480
540
600
0.2
0.4
0.6
0.8
1.0
1.2
1.4
1.6
5
10
15
20
25
30
35
40

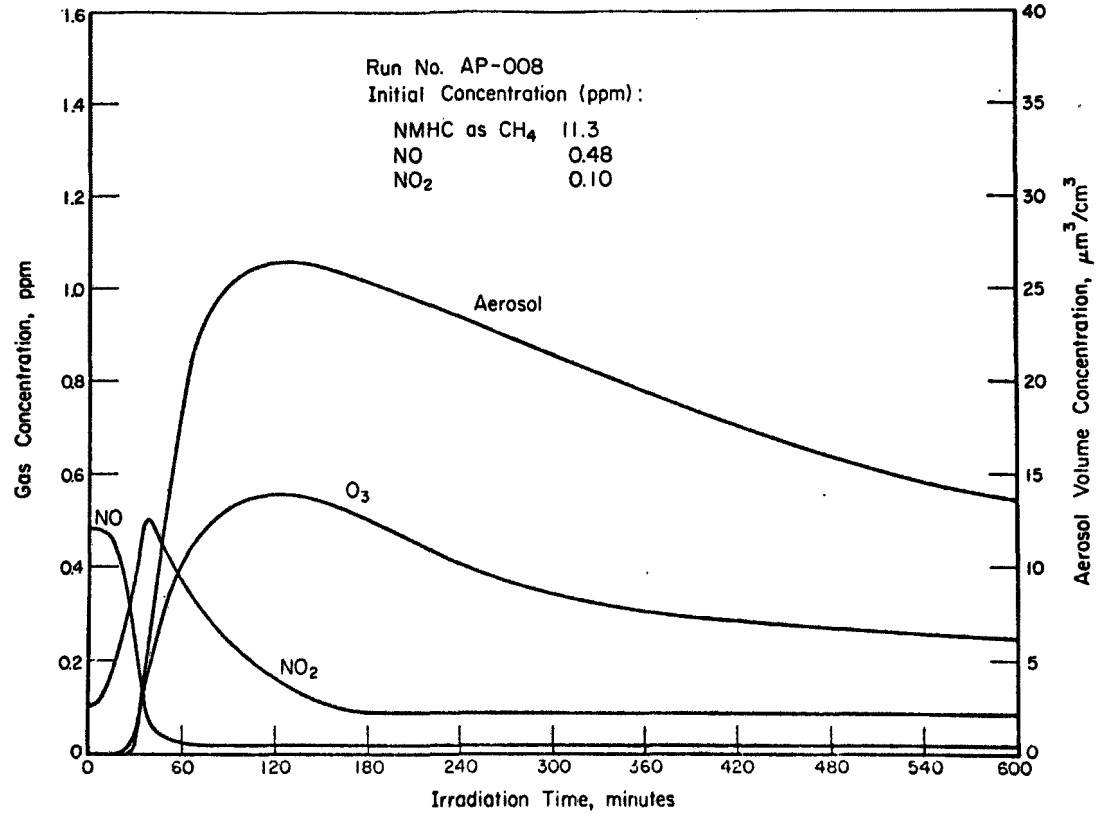
Run No. AP-008
Initial Concentration (ppm):
NMHC as CH_4 11.3
NO 0.48
NO_2 0.10
Aerosol
O_3
NO
NO_2
Gas Concentration, ppm
Aerosol Volume Concentration, $\mu m^3/cm^3$
Irradiation Time, minutes
0
60
120
180
240
300
360
420
480
540
600
0.2
0.4
0.6
0.8
1.0
1.2
1.4
1.6
5
10
15
20
25
30
35
40

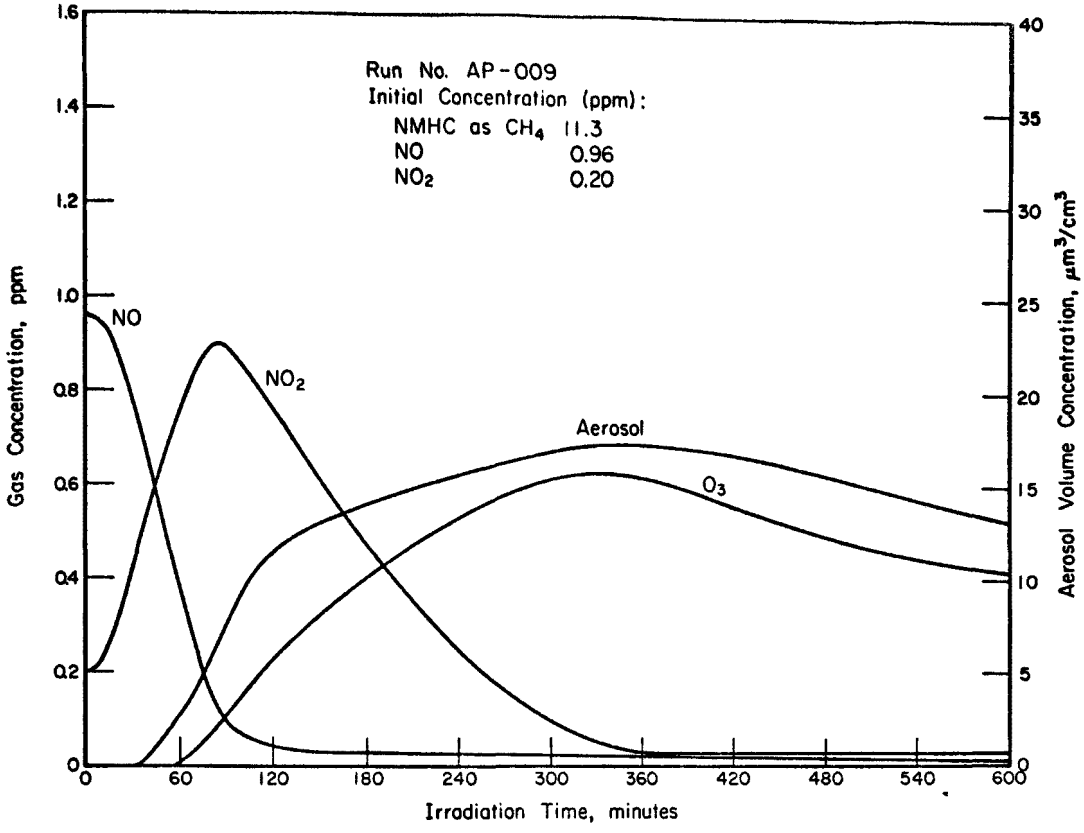
Run No. AP-009
Initial Concentration (ppm):
NMHC as CH4 11.3
NO 0.96
NO2 0.20
NO
NO2
Aerosol
O3
Gas Concentration, ppm
Aerosol Volume Concentration, μm3/cm3
Irradiation Time, minutes
0
60
120
180
240
300
360
420
480
540
600
0.2
0.4
0.6
0.8
1.0
1.2
1.4
1.6
5
10
15
20
25
30
35
40

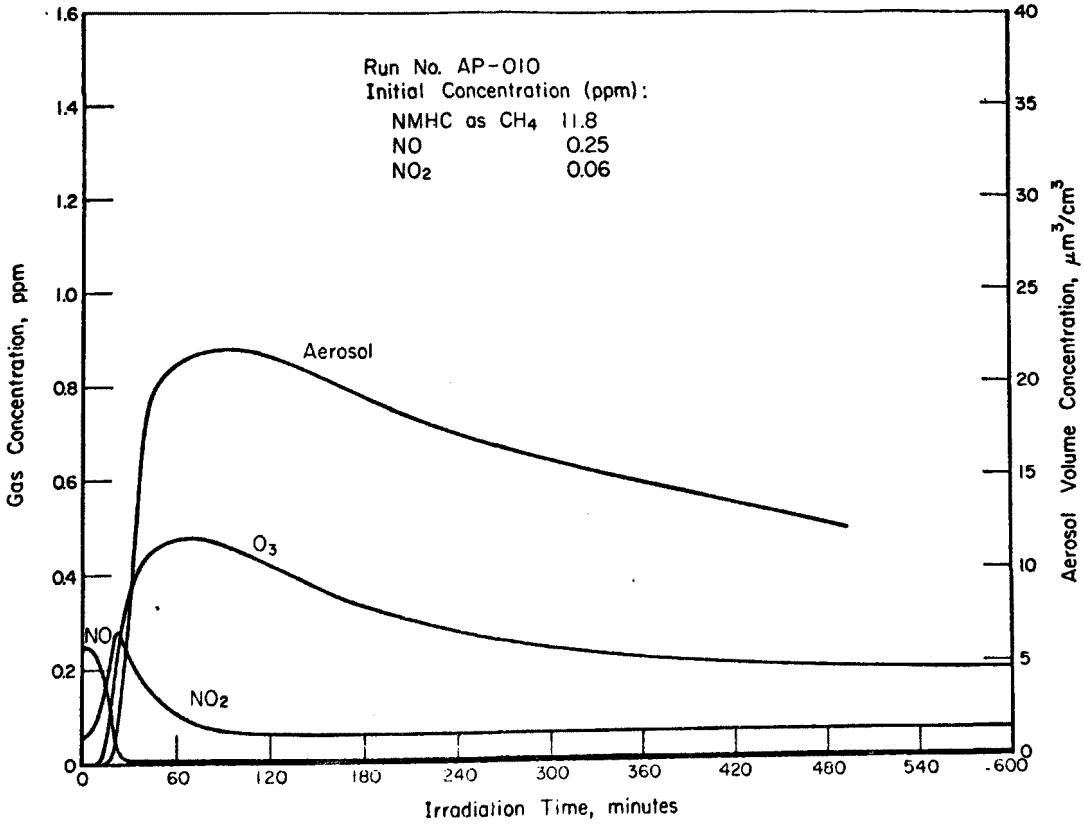
Run No. AP-010
Initial Concentration (ppm):
NMHC as CH4 11.8
NO 0.25
NO2 0.06
Aerosol
O3
NO
NO2
Gas Concentration, ppm
Aerosol Volume Concentration, μm3/cm3
Irradiation Time, minutes
0
60
120
180
240
300
360
420
480
540
600
0.2
0.4
0.6
0.8
1.0
1.2
1.4
1.6
5
10
15
20
25
30
35
40

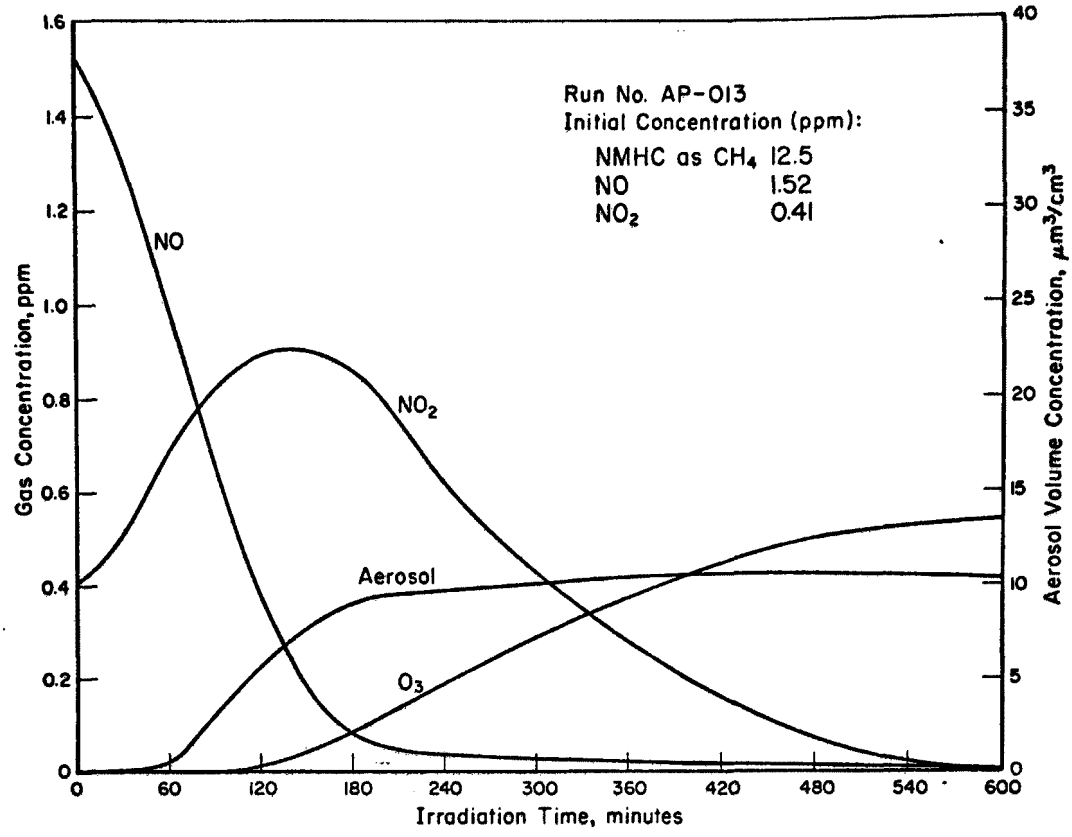
Run No. AP-013
Initial Concentration (ppm):
NMHC as CH_4 12.5
NO 1.52
NO_2 0.41
NO
NO_2
Aerosol
O_3
Gas Concentration, ppm
Aerosol Volume Concentration, $\mu m^3/cm^3$
Irradiation Time, minutes
0
60
120
180
240
300
360
420
480
540
600
0.2
0.4
0.6
0.8
1.0
1.2
1.4
1.6
5
10
15
20
25
30
35
40

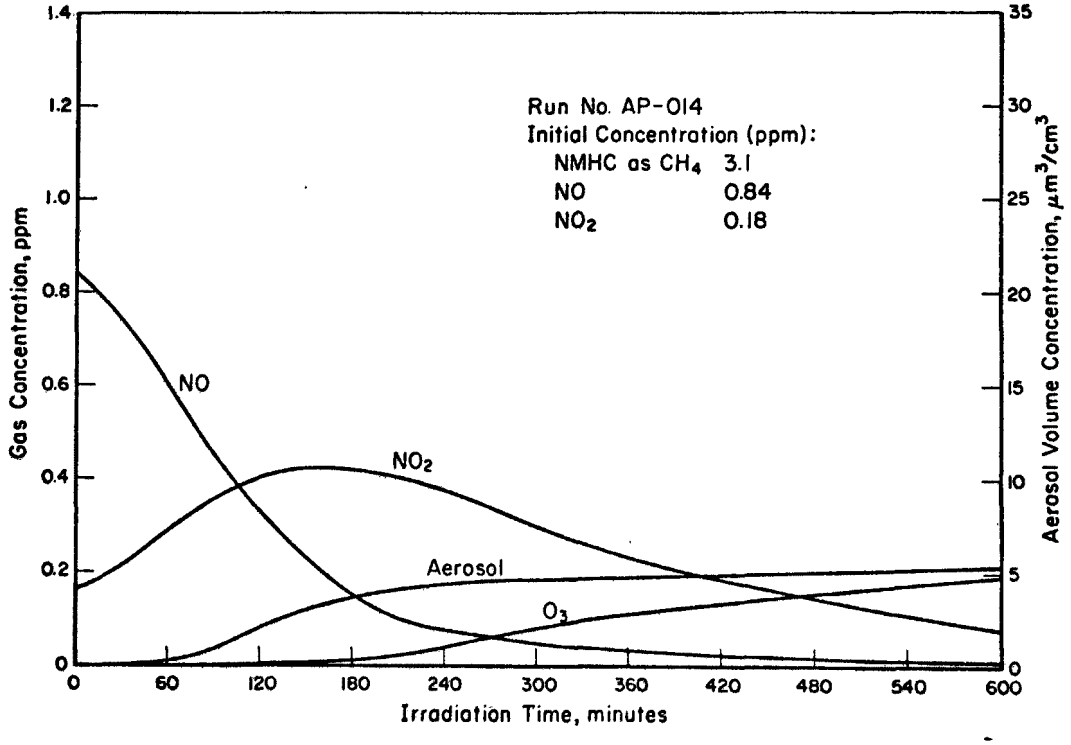
Run No. AP-014
Initial Concentration (ppm):
NMHC as CH_4 3.1
NO 0.84
NO_2 0.18
NO
NO_2
Aerosol
O_3
Gas Concentration, ppm
Aerosol Volume Concentration, $\mu m^3/cm^3$
Irradiation Time, minutes
0
60
120
180
240
300
360
420
480
540
600
0.2
0.4
0.6
0.8
1.0
1.2
1.4
5
10
15
20
25
30
35

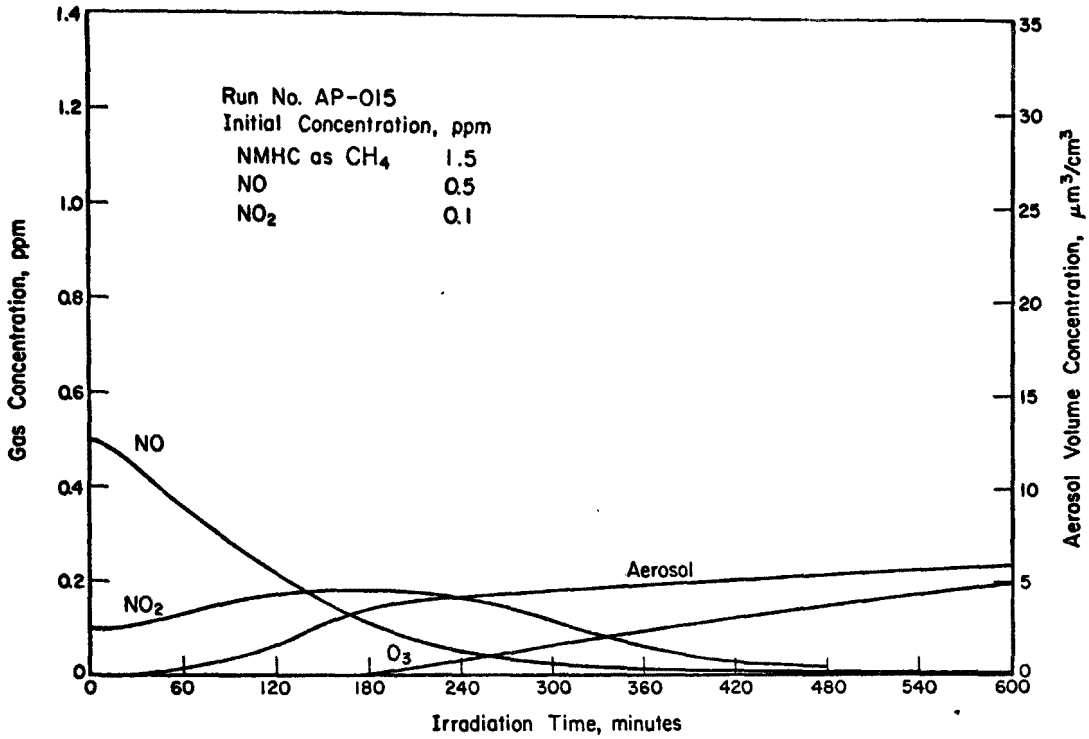
Run No. AP-015
Initial Concentration, ppm
NMHC as CH_4 1.5
NO 0.5
NO_2 0.1
NO
NO_2
O_3
Aerosol
Gas Concentration, ppm
Aerosol Volume Concentration, $\mu m^3/cm^3$
Irradiation Time, minutes

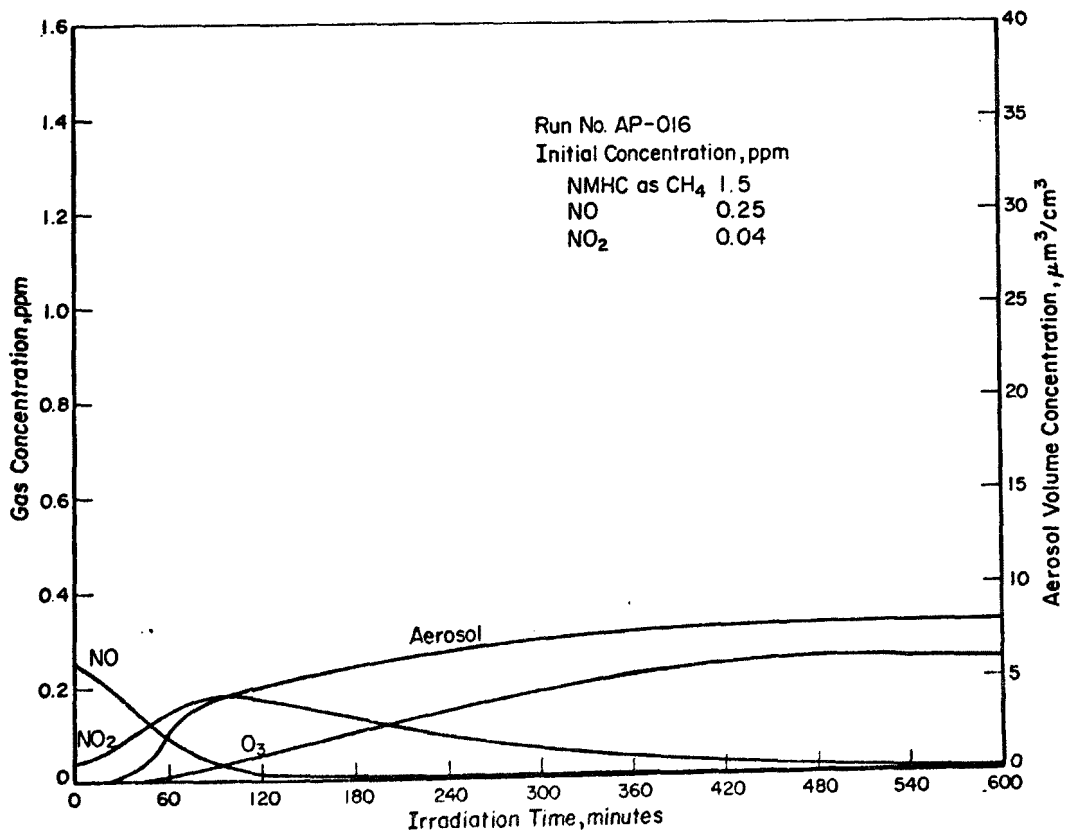
Run No. AP-016
Initial Concentration, ppm
NMHC as CH_4 1.5
NO 0.25
NO_2 0.04
NO
NO_2
O_3
Aerosol
Gas Concentration, ppm
Aerosol Volume Concentration, $\mu m^3/cm^3$
Irradiation Time, minutes

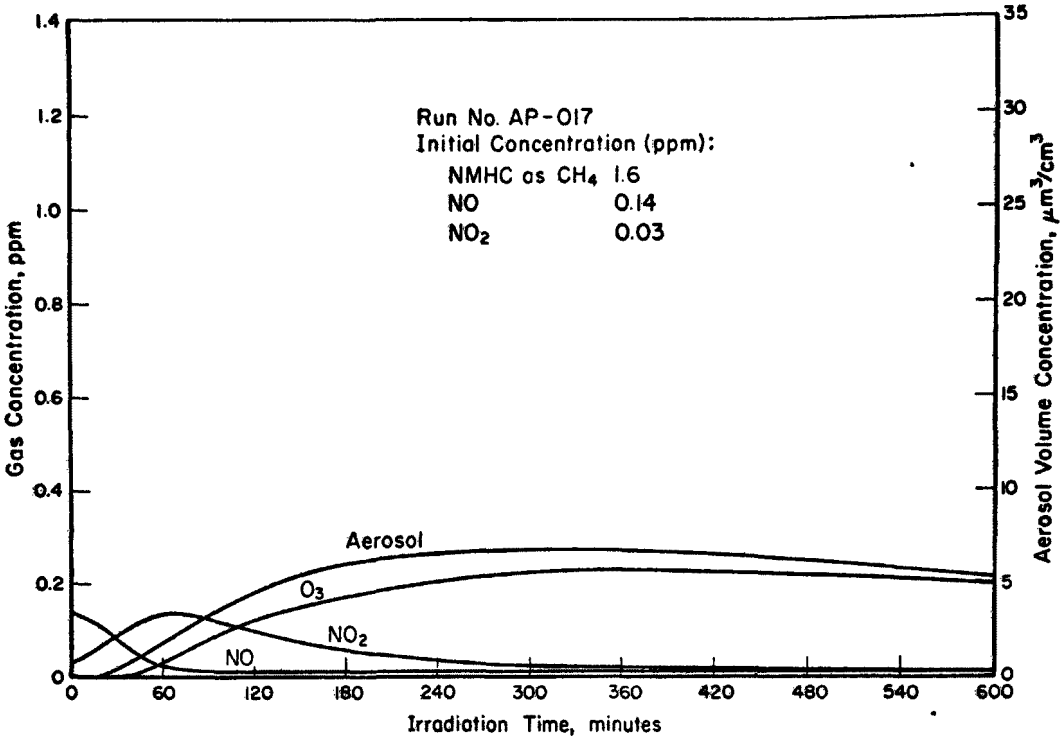
Run No. AP-017
Initial Concentration (ppm):
NMHC as CH_4 1.6
NO 0.14
NO_2 0.03
Aerosol
O_3
NO_2
NO
Gas Concentration, ppm
Aerosol Volume Concentration, $\mu m^3/cm^3$
Irradiation Time, minutes
0
60
120
180
240
300
360
420
480
540
600
0.2
0.4
0.6
0.8
1.0
1.2
1.4
5
10
15
20
25
30
35

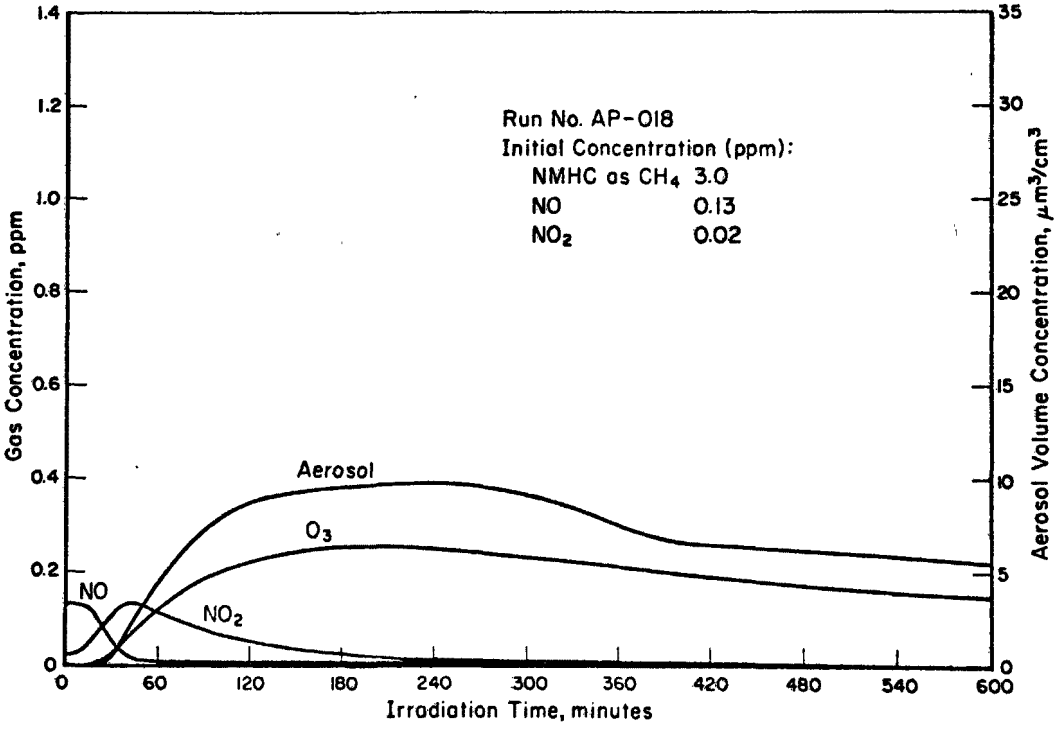
Run No. AP-018
Initial Concentration (ppm):
NMHC as CH_4 3.0
NO 0.13
NO_2 0.02
Aerosol
O_3
NO
NO_2
Gas Concentration, ppm
Aerosol Volume Concentration, $\mu m^3/cm^3$
Irradiation Time, minutes
0
60
120
180
240
300
360
420
480
540
600
0.2
0.4
0.6
0.8
1.0
1.2
1.4
5
10
15
20
25
30
35

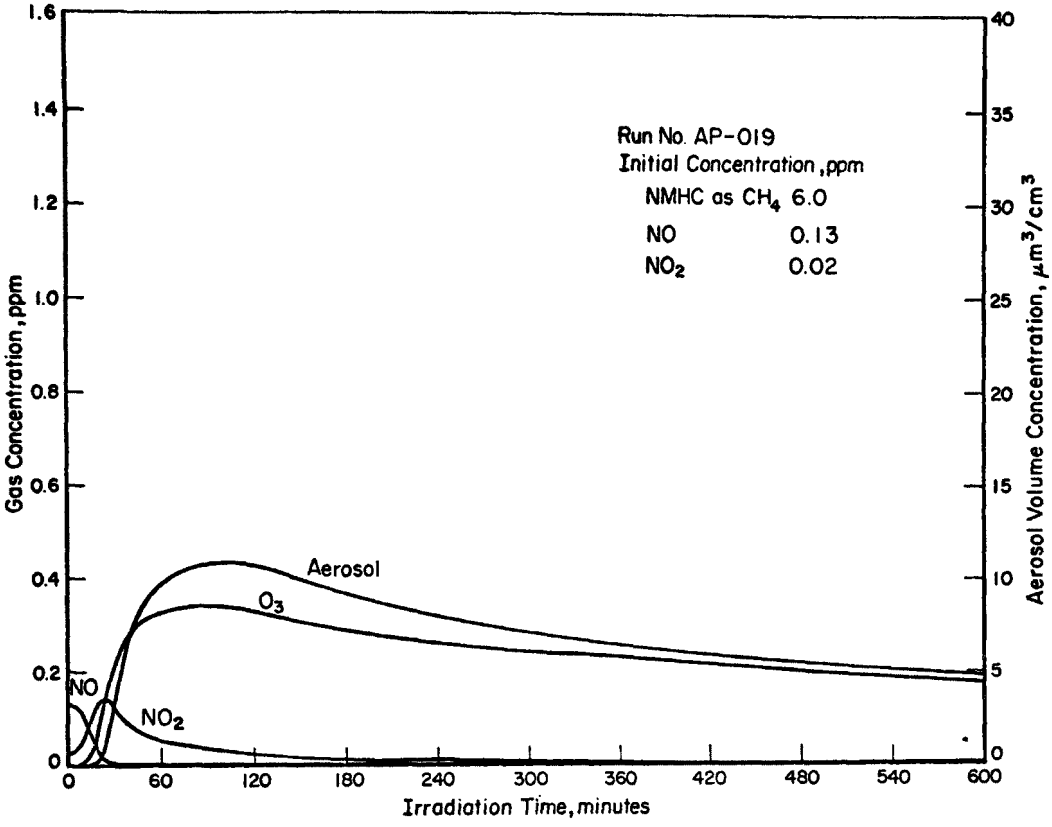
Run No. AP-019
Initial Concentration, ppm
NMHC as CH_4 6.0
NO 0.13
NO_2 0.02
Aerosol
O_3
NO
NO_2
Gas Concentration, ppm
Aerosol Volume Concentration, $\mu m^3/cm^3$
Irradiation Time, minutes
0
0.2
0.4
0.6
0.8
1.0
1.2
1.4
1.6
0
5
10
15
20
25
30
35
40
0
60
120
180
240
300
360
420
480
540
600

APPENDIX B

SUMMARY OF HYDROCARBON DATA DETERMINED BY GAS CHROMATOGRAPHY

The computer-generated summaries are designed to show the consumption of hydrocarbons after correcting for the chamber dilution rate. Each successive asterisk represents the hourly cumulative consumption (by percent) of the respective hydrocarbon. The first asterisk opposite a hydrocarbon corresponds to the initial concentration, and the second asterisk represents the percent loss of that hydrocarbon after the first hour of irradiation; the third asterisk is the cumulative loss (by percent) after the second hour, etc. Where less than 11 asterisks are present, either the hydrocarbon concentration became undetectably small or the rate of decay became indistinguishable from the dilution rate.

HYDROCARBON SUMMARY FOR RUN AP-001 11-19-74 CORRECTED FOR DILUTION

SUCCESSIVE ASTERISKS REPRESENT CUMULATIVE PERCENT CONSUMPTION PER HOUR OF IRRADIATION

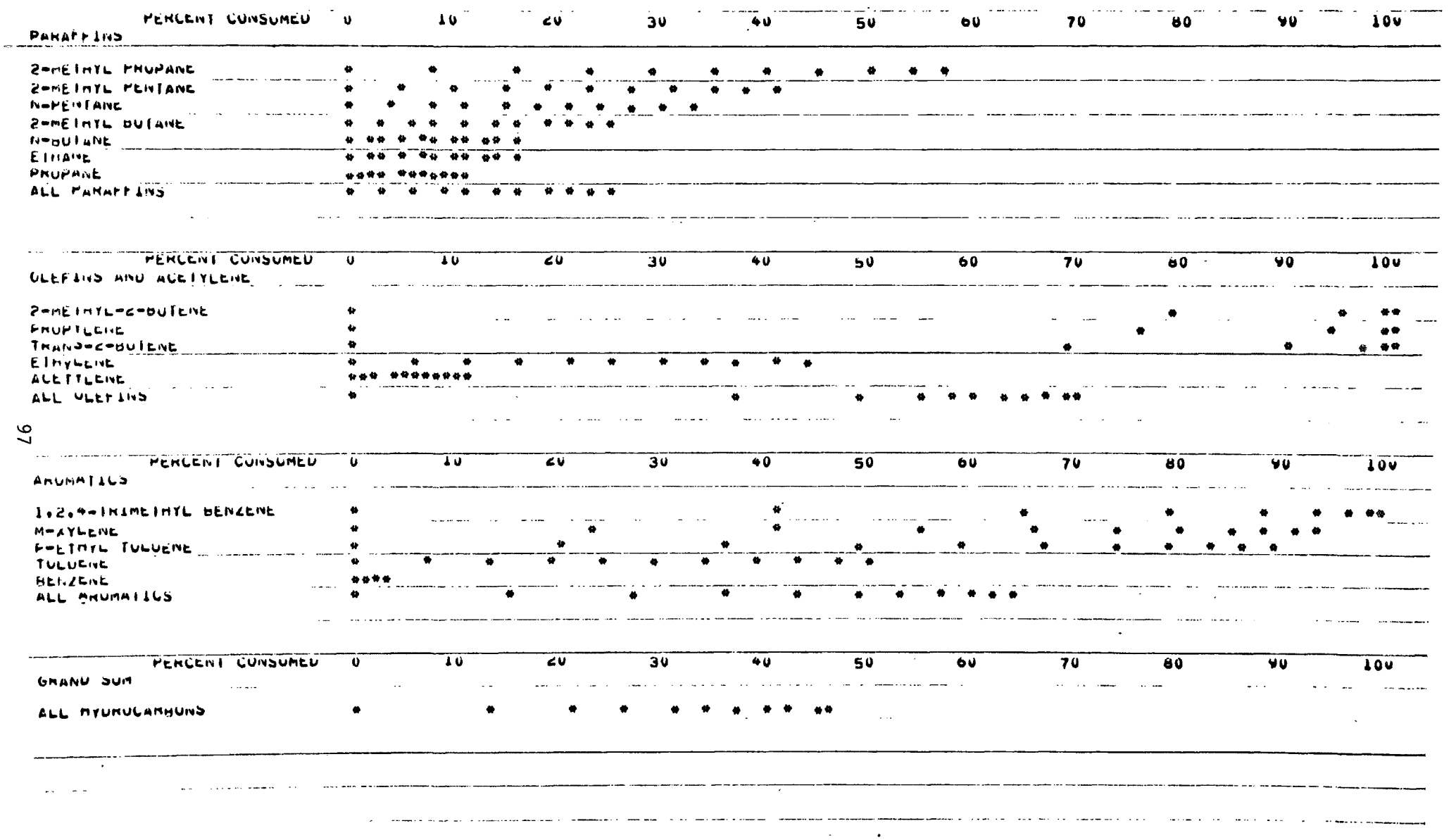

HYDROCARBON SUMMARY FOR RUN AP-002 11-20-74 CORRECTED FOR DILUTION

SUCCESSIVE ASTERISKS REPRESENT CUMULATIVE PERCENT CONSUMPTION PER HOUR OF IRRADIATION

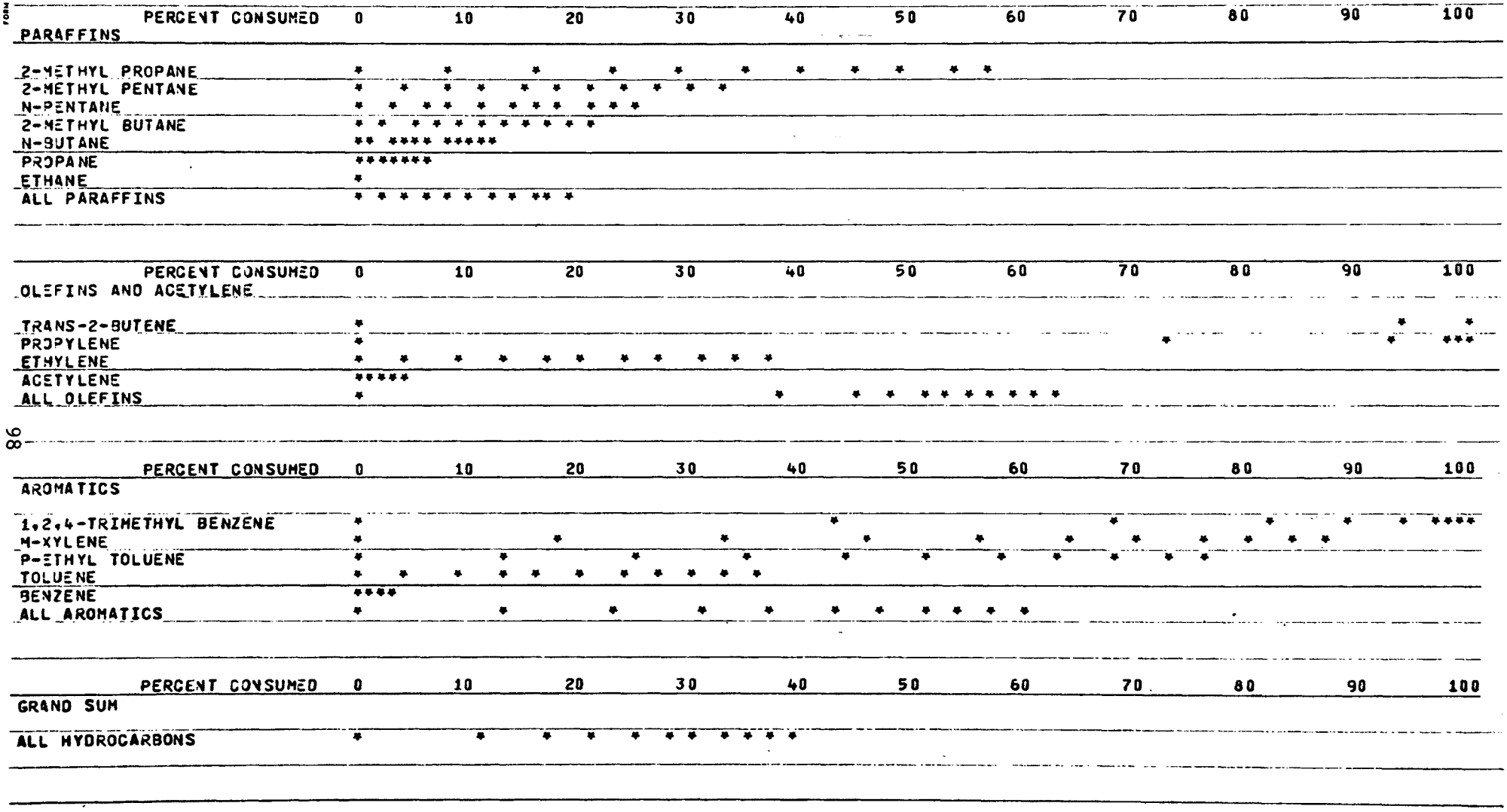

HYDROCARBON SUMMARY FOR RUN AP-003 11-21-74 CORRECTED FOR DILUTION

SUCCESSIVE ASTERISKS REPRESENT CUMULATIVE PERCENT CONSUMPTION PER HOUR OF IRRADIATION

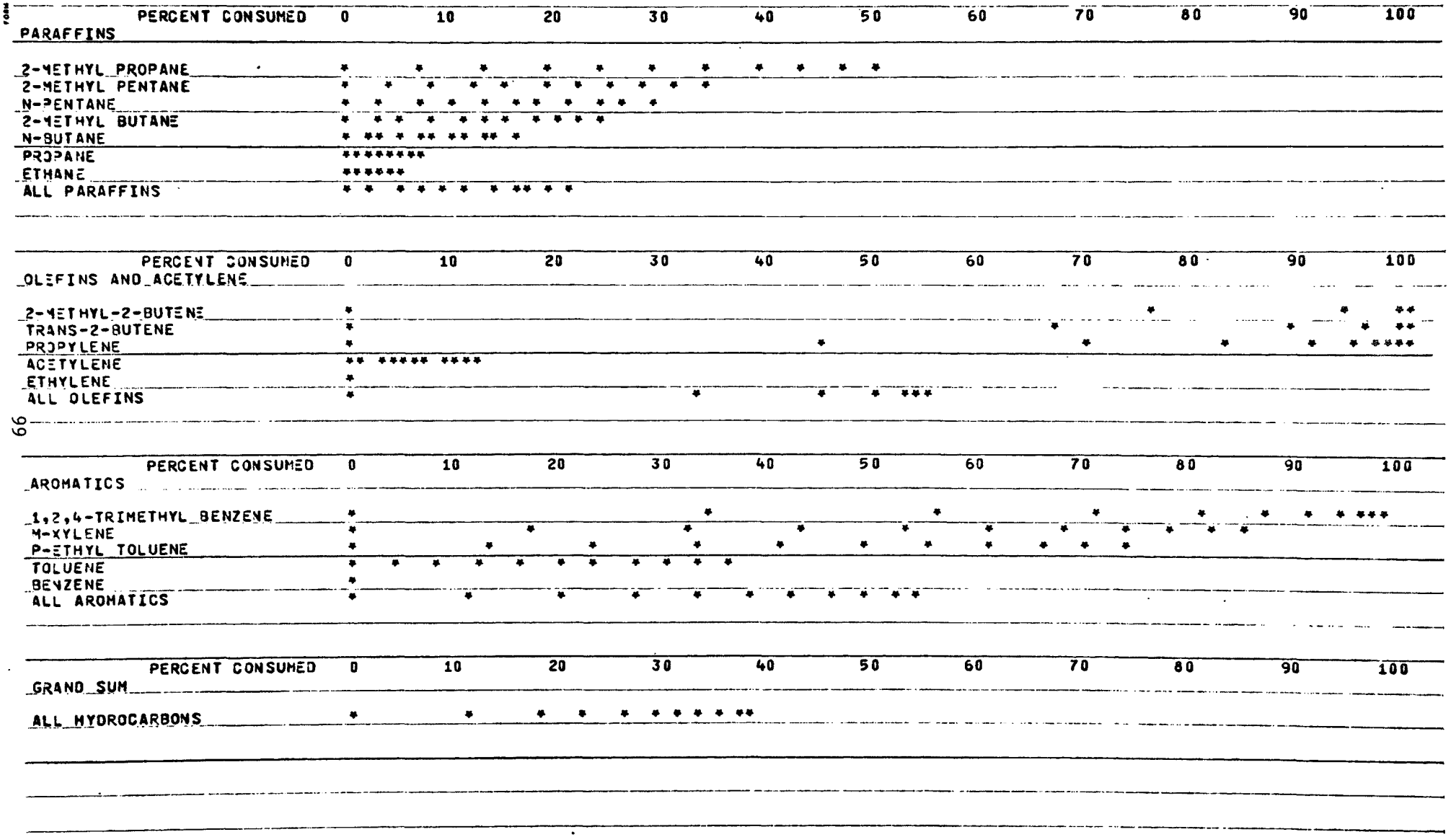

HYDROCARBON SUMMARY FOR RUN AP-004 11-25-74 CORRECTED FOR DILUTION

SUCCESSIVE ASTERISKS REPRESENT CUMULATIVE PERCENT CONSUMPTION PER HOUR OF IRRADIATION

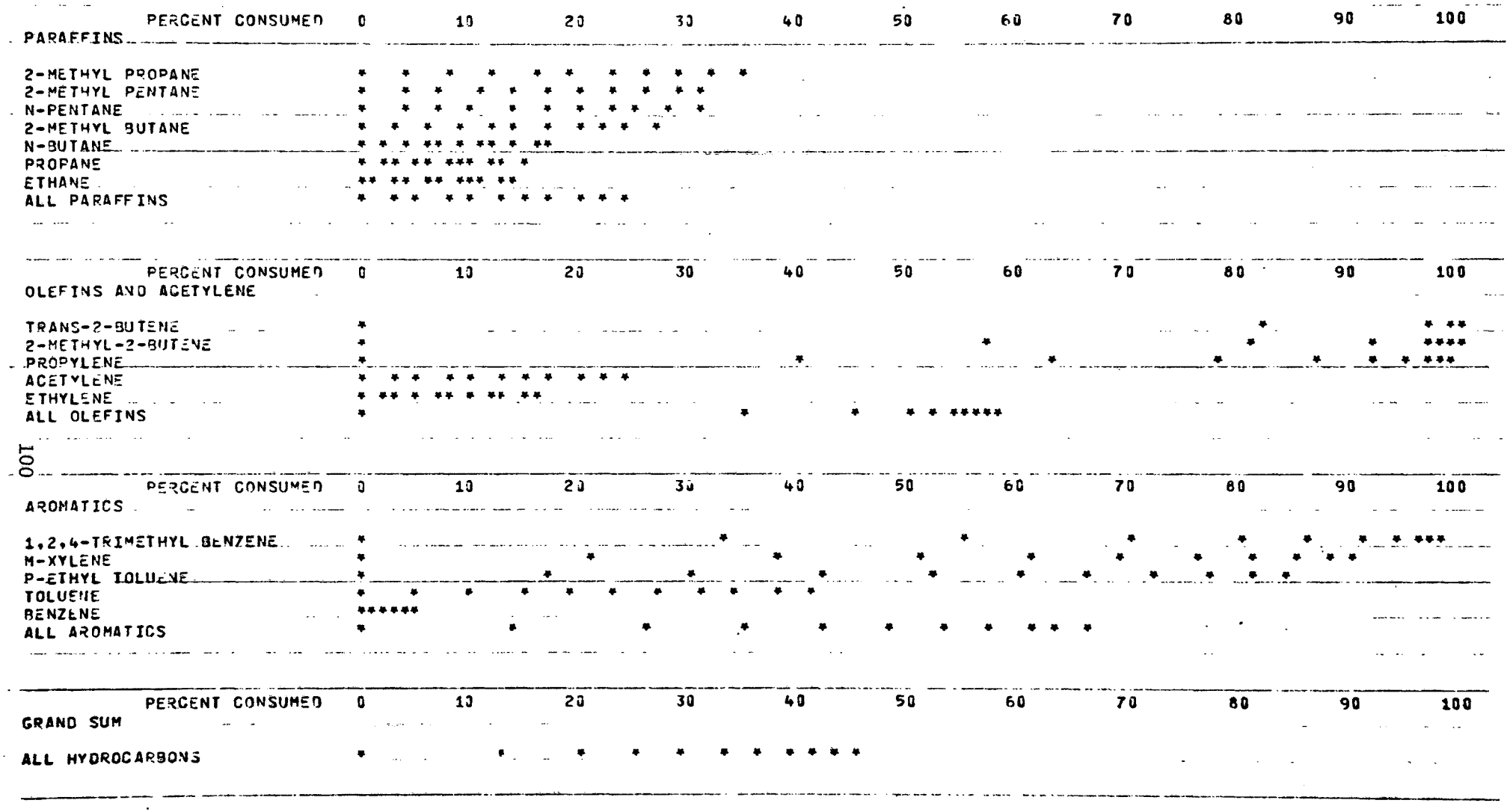

HYDROCARBON SUMMARY FOR RUN AP-005 11-26-74 CORRECTED FOR DILUTION

SUCCESSIVE ASTERISKS REPRESENT CUMULATIVE PERCENT CONSUMPTION PER HOUR OF IRRADIATION

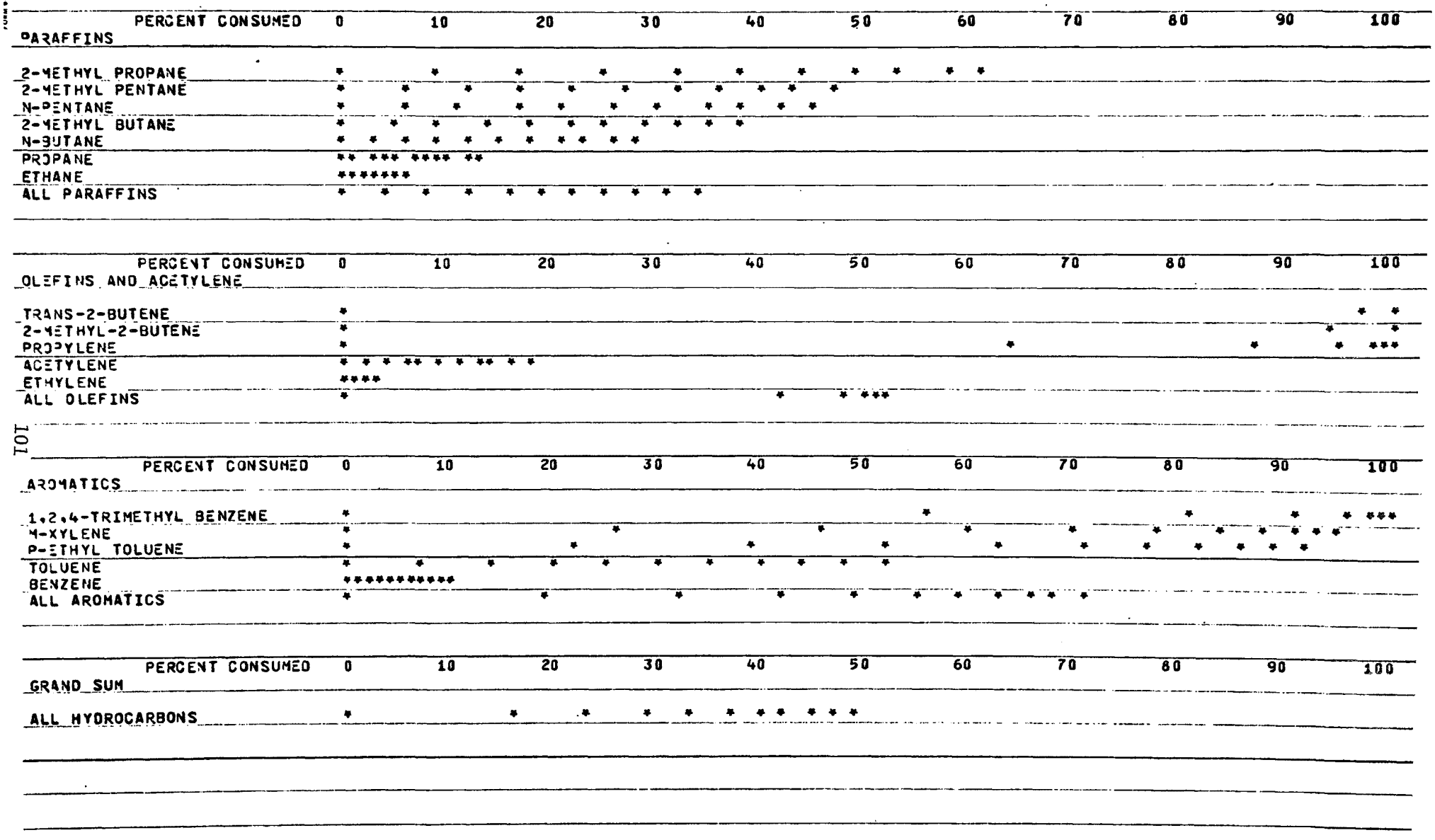

HYDROCARBON SUMMARY FOR RUN AP-006 11-27-74 CORRECTED FOR DILUTION

SUCCESSIVE ASTERISKS REPRESENT CUMULATIVE PERCENT CONSUMPTION PER HOUR OF IRRADIATION

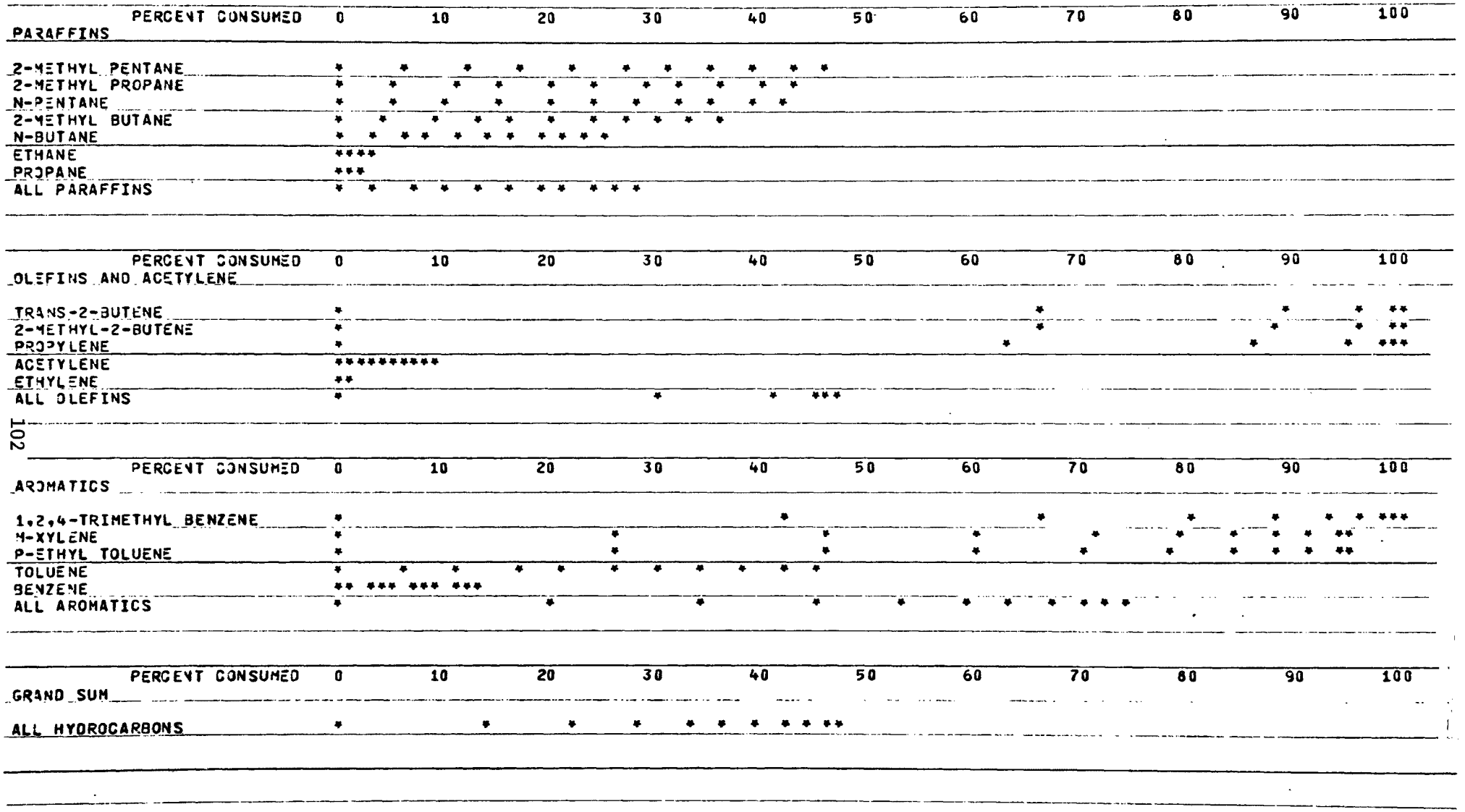

HYDROCARBON SUMMARY FOR RUN AP-007 12-02-74 CORRECTED FOR DILUTION

SUCCESSIVE ASTERISKS REPRESENT CUMULATIVE PERCENT CONSUMPTION PER HOUR OF IRRADIATION

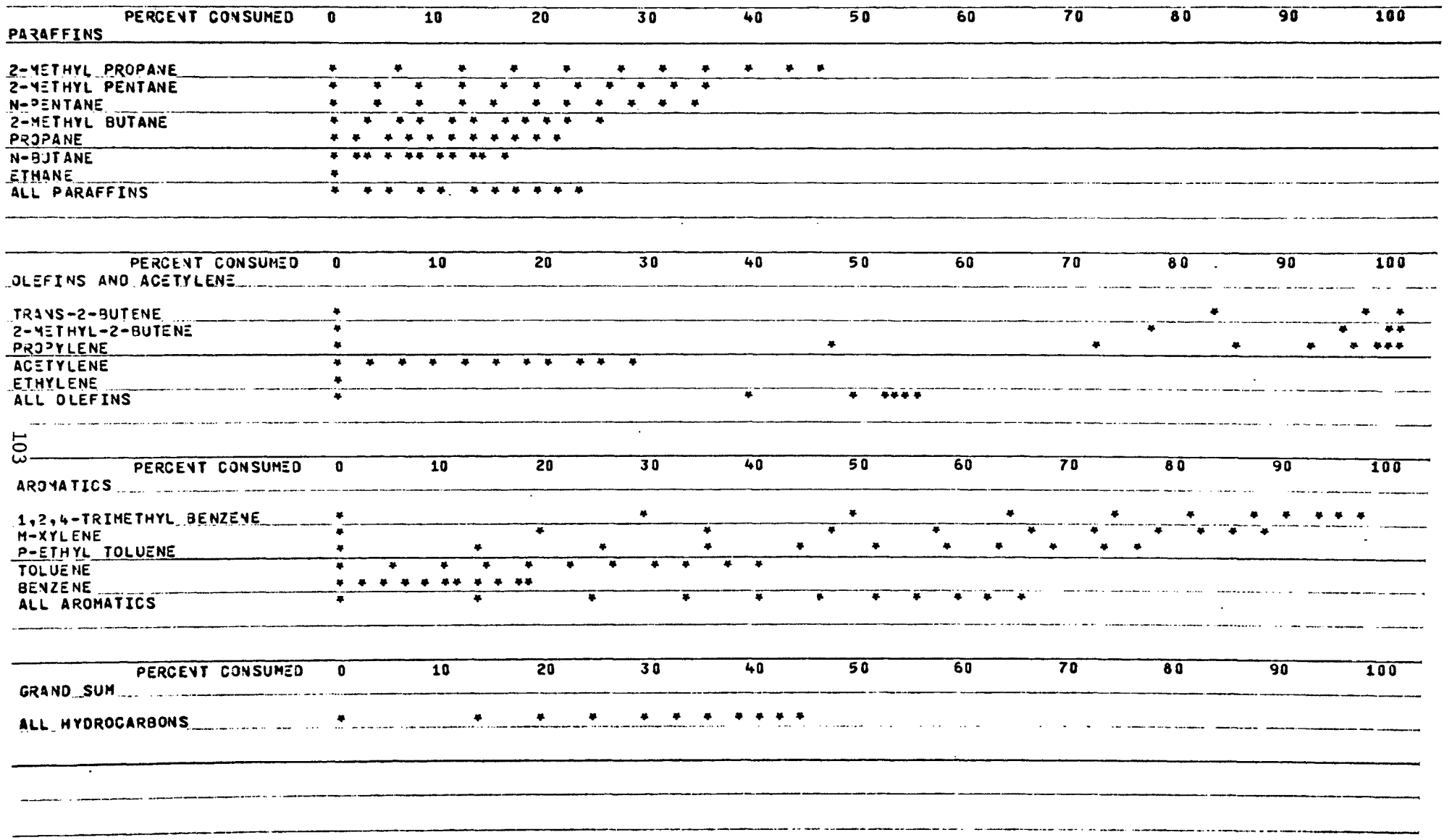

HYDROCARBON SUMMARY FOR RUN AP-008 12-03-74 CORRECTED FOR DILUTION

SUCCESSIVE ASTERISKS REPRESENT CUMULATIVE PERCENT CONSUMPTION PER HOUR OF IRRADIATION

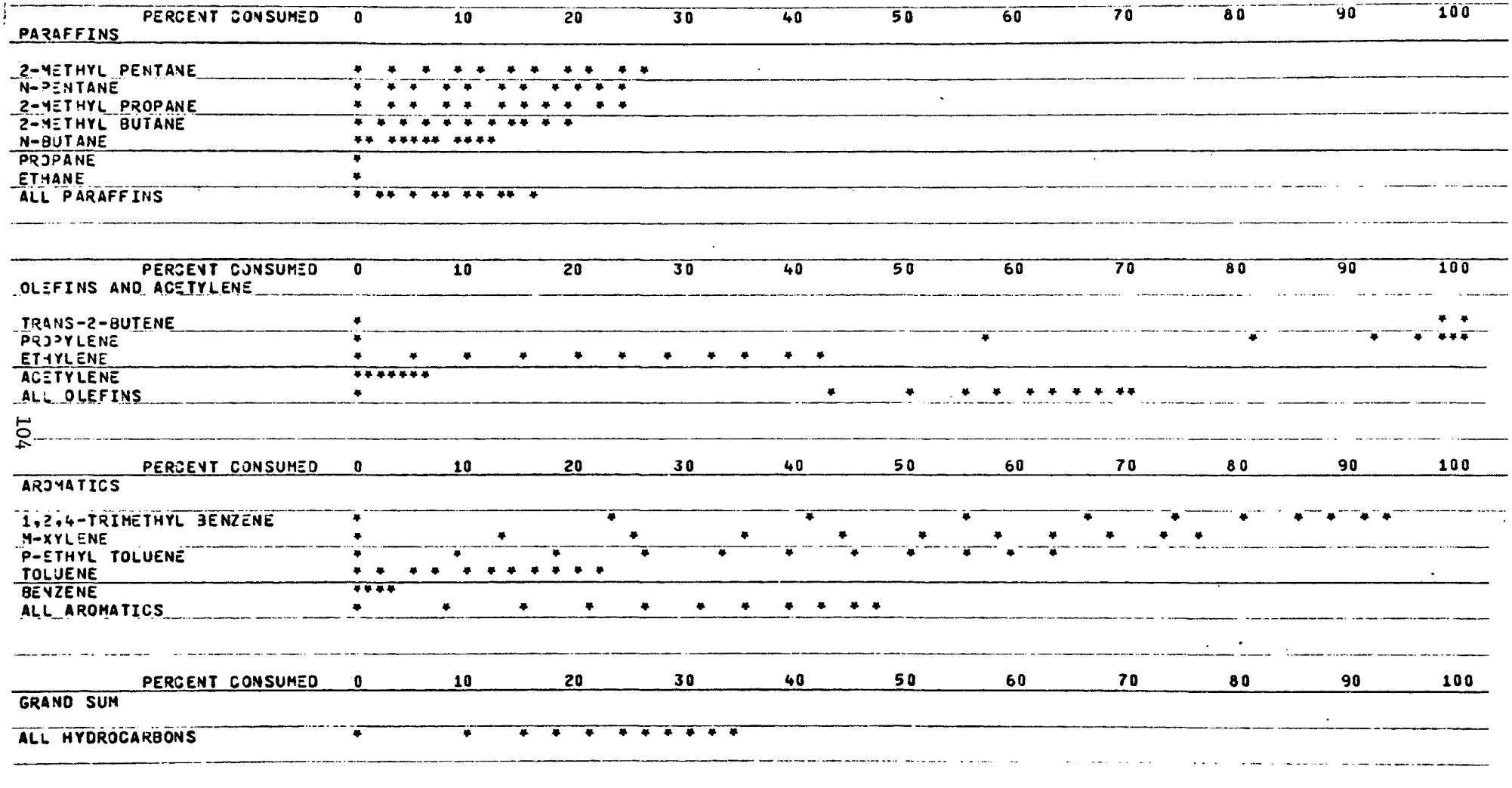

HYDROCARBON SUMMARY FOR RUN AP-009 12-04-74 CORRECTED FOR DILUTION

SUCCESSIVE ASTERISKS REPRESENT CUMULATIVE PERCENT CONSUMPTION PER HOUR OF IRRADIATION

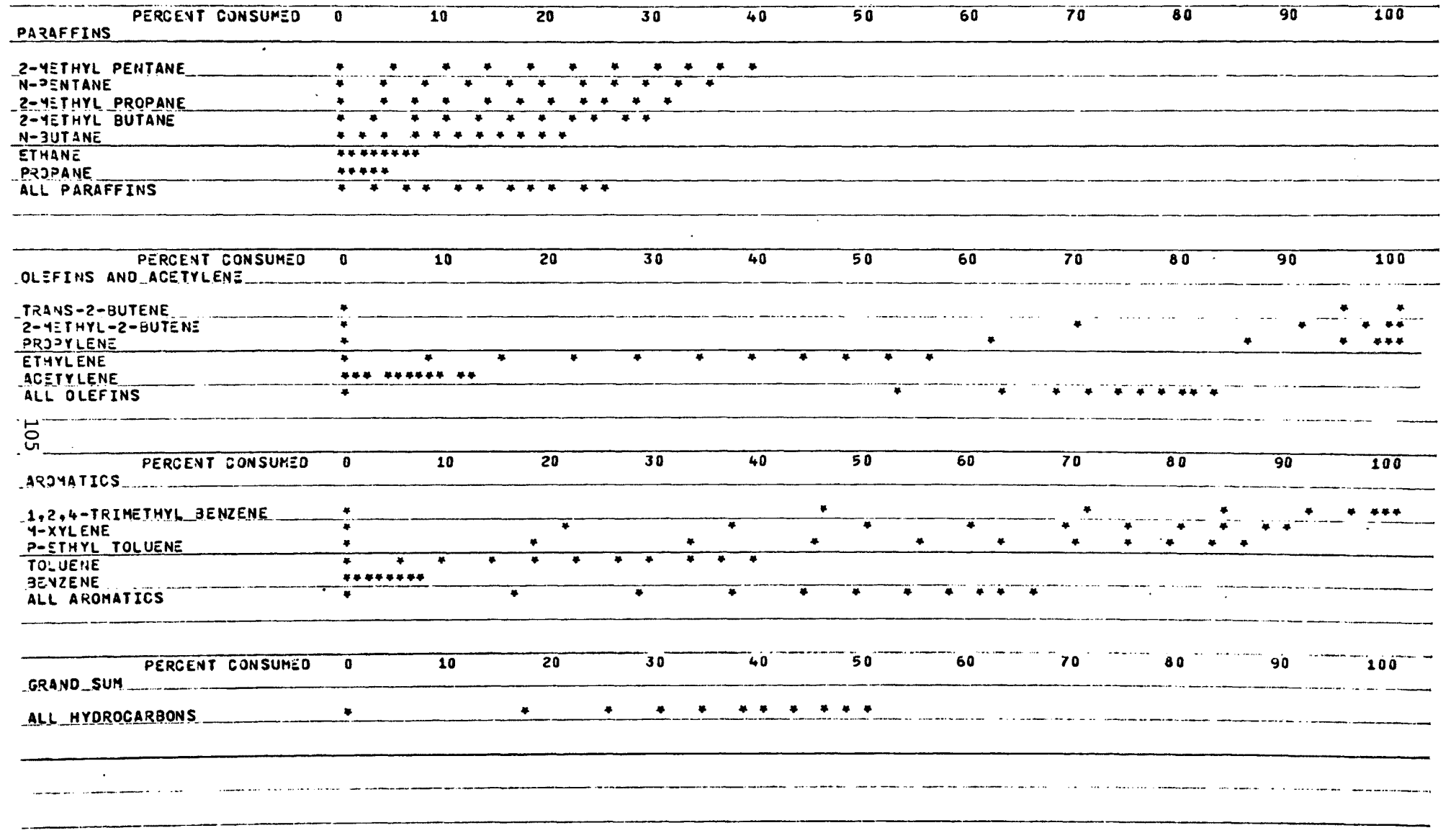

HYDROCARBON SUMMARY FOR RUN AP-010 12-05-74 CORRECTED FOR DILUTION

SUCCESSIVE ASTERISKS REPRESENT CUMULATIVE PERCENT CONSUMPTION PER HOUR OF IRRADIATION

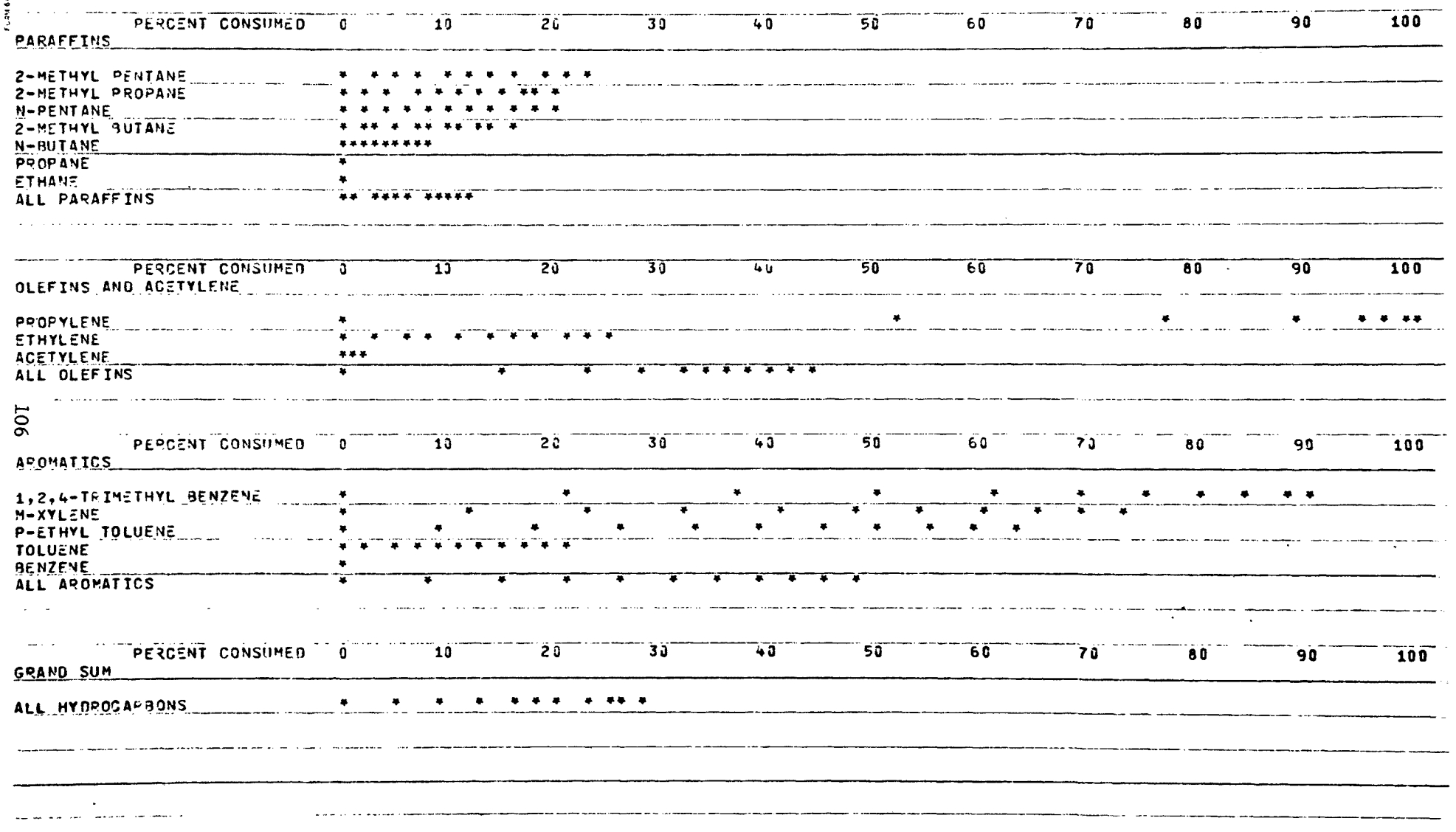

HYDROCARBON SUMMARY FOR RUN AP-013 3-18-75 CORRECTED FOR DILUTION

SUCCESSIVE ASTERISKS REPRESENT CUMULATIVE PERCENT CONSUMPTION PER HOUR OF IRRADIATION

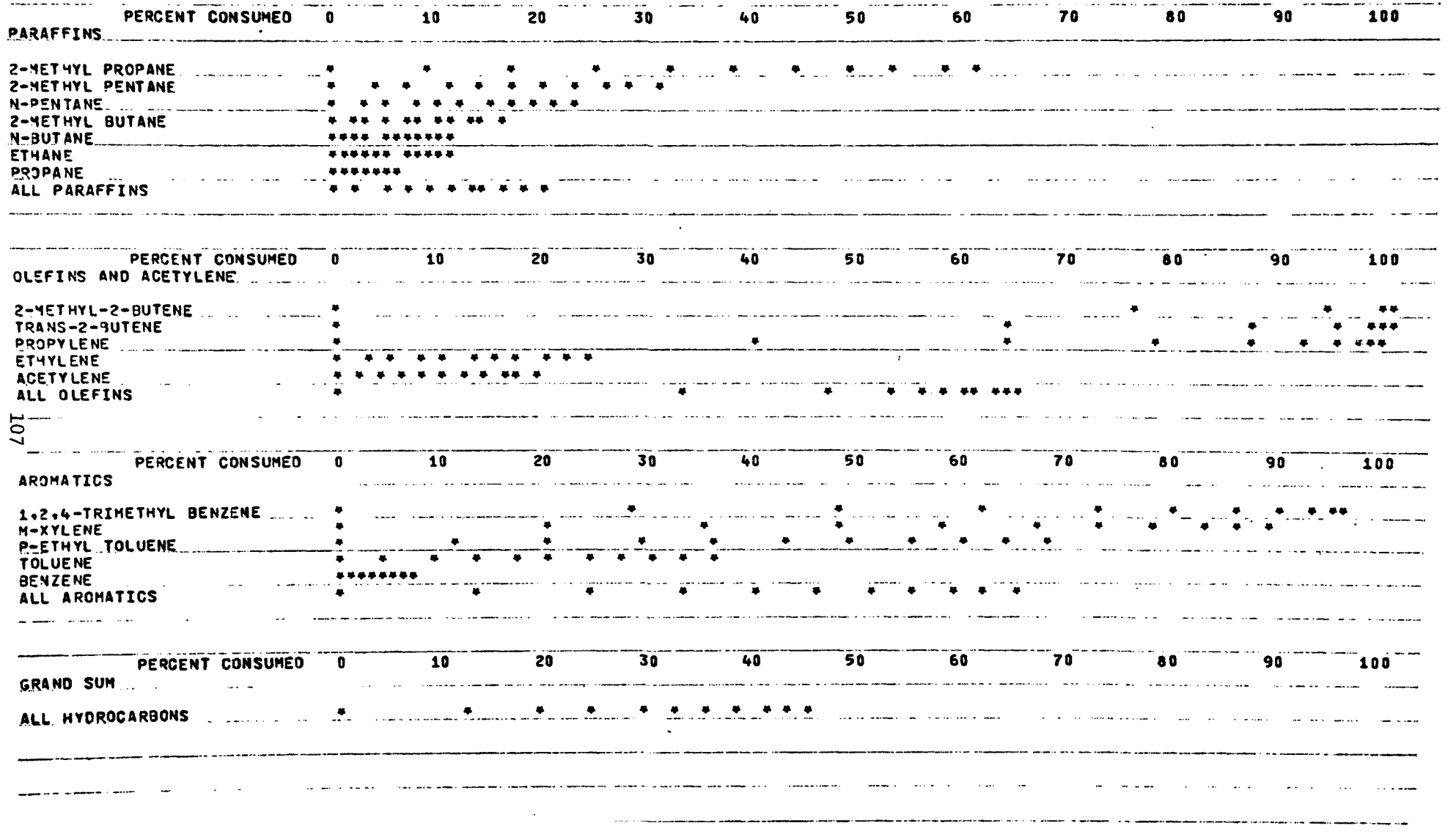

HYDROCARBON SUMMARY FOR RUN AP-014 3-20-75 CORRECTED FOR DILUTION

SUCCESSIVE ASTERISKS REPRESENT CUMULATIVE PERCENT CONSUMPTION PER HOUR OF IRRADIATION

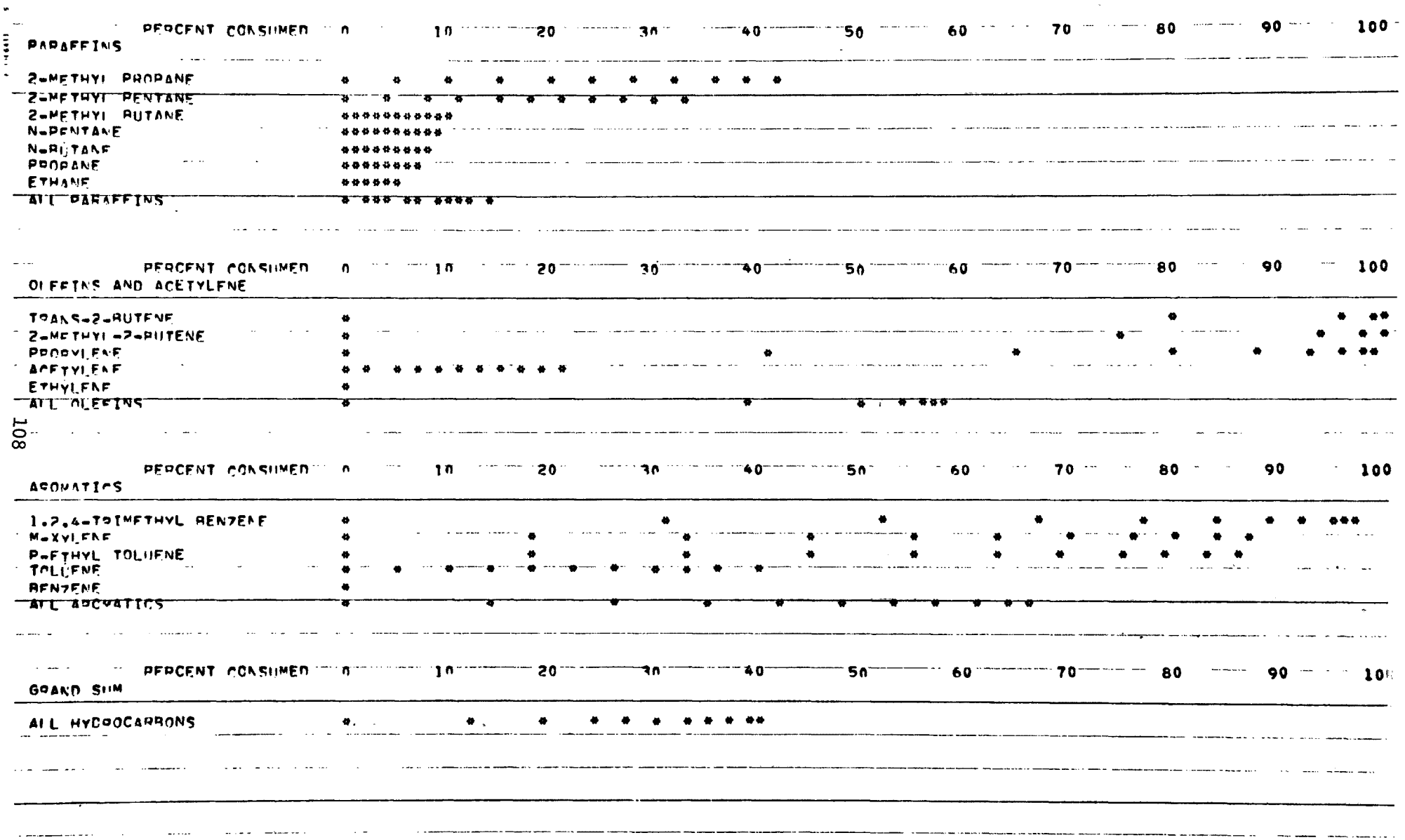

HYDROCARBON SUMMARY FOR RUN AP-0115 3-25-75 CORRECTED FOR DILUTION

SUCCESSIVE ASTERISKS REPRESENT CUMULATIVE PERCENT CONSUMPTION PER HOUR OF IRRADIATION

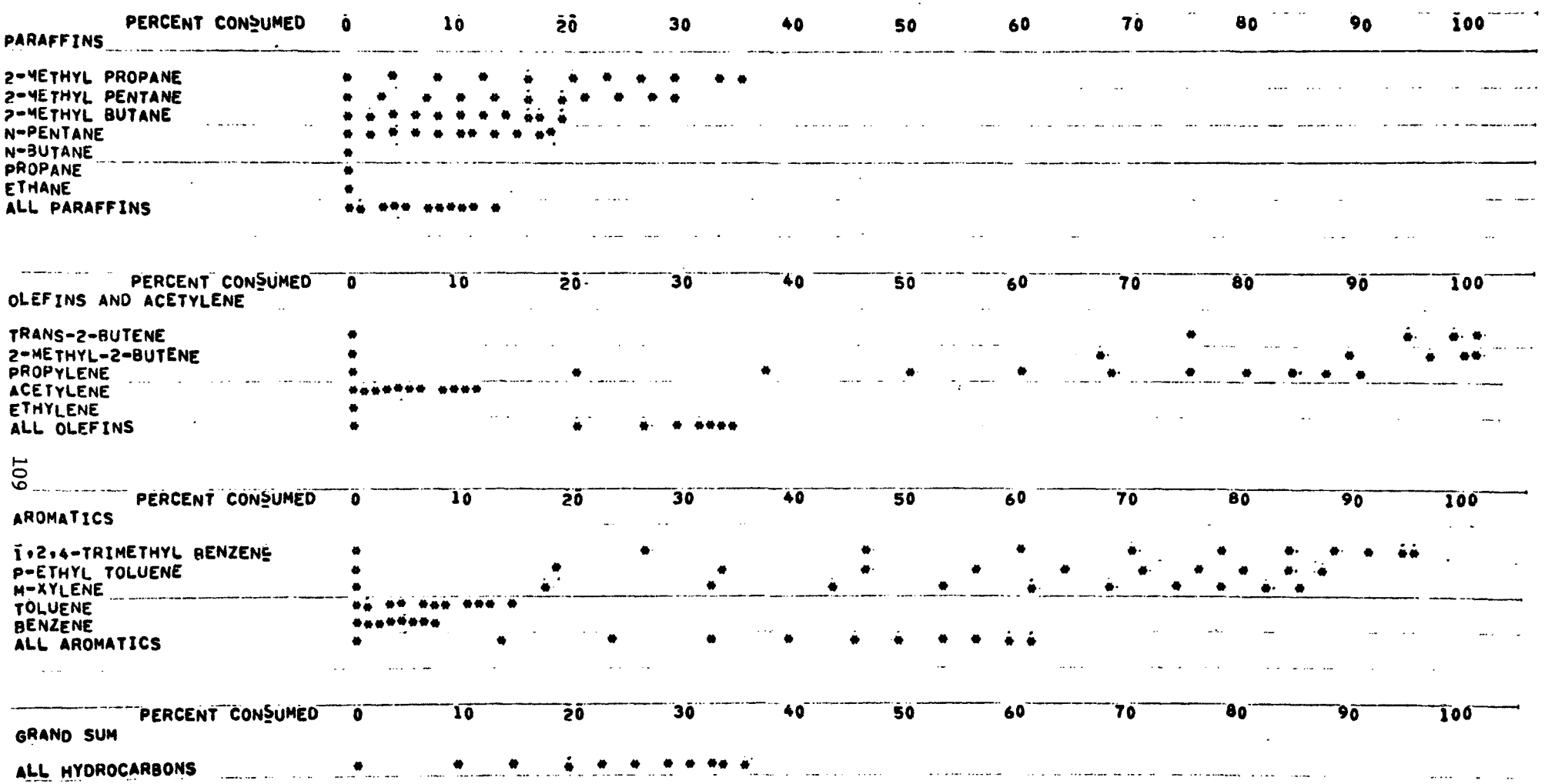

HYDROCARBON SUMMARY FOR RUN AP-016 3-26-75 CORRECTED FOR DILUTION

SUCCESSIVE ASTERISKS REPRESENT CUMULATIVE PERCENT CONSUMPTION PER HOUR OF IRRADIATION

PERCENT CONSUMED	0	10	20	30	40	50	60	70	80	90	100
PARAFFINS											
2-METHYL PROPANE	*										
2-METHYL PENTANE	*										
N-PENTANE	*										
2-METHYL BUTANE	*										
N-BUTANE	*										
PROPANE	*										
ETHANE	*										
ALL PARAFFINS	*										
PERCENT CONSUMED	0	10	20	30	40	50	60	70	80	90	100
OLEFINS AND ACETYLENE											
TRANS-2-BUTENE	*										
2-METHYL-2-BUTENE	*										
PROPYLENE	*										
ACETYLENE	*										
ETHYLENE	*										
ALL OLEFINS	*										
PERCENT CONSUMED	0	10	20	30	40	50	60	70	80	90	100
AROMATICS											
1,2,4-TRIMETHYL BENZENE	*										
P-ETHYL TOLUENE	*										
M-XYLENE	*										
TOLUENE	*										
BENZENE	*										
ALL AROMATICS	*										
PERCENT CONSUMED	0	10	20	30	40	50	60	70	80	90	100
GRAND SUM											
ALL HYDROCARBONS	*										

HYDROCARBON SUMMARY FOR RUN AP-017 3-27-75 CORRECTED FOR DILUTION

SUCCESSIVE ASTERISKS REPRESENT CUMULATIVE PERCENT CONSUMPTION PER HOUR OF IRRADIATION

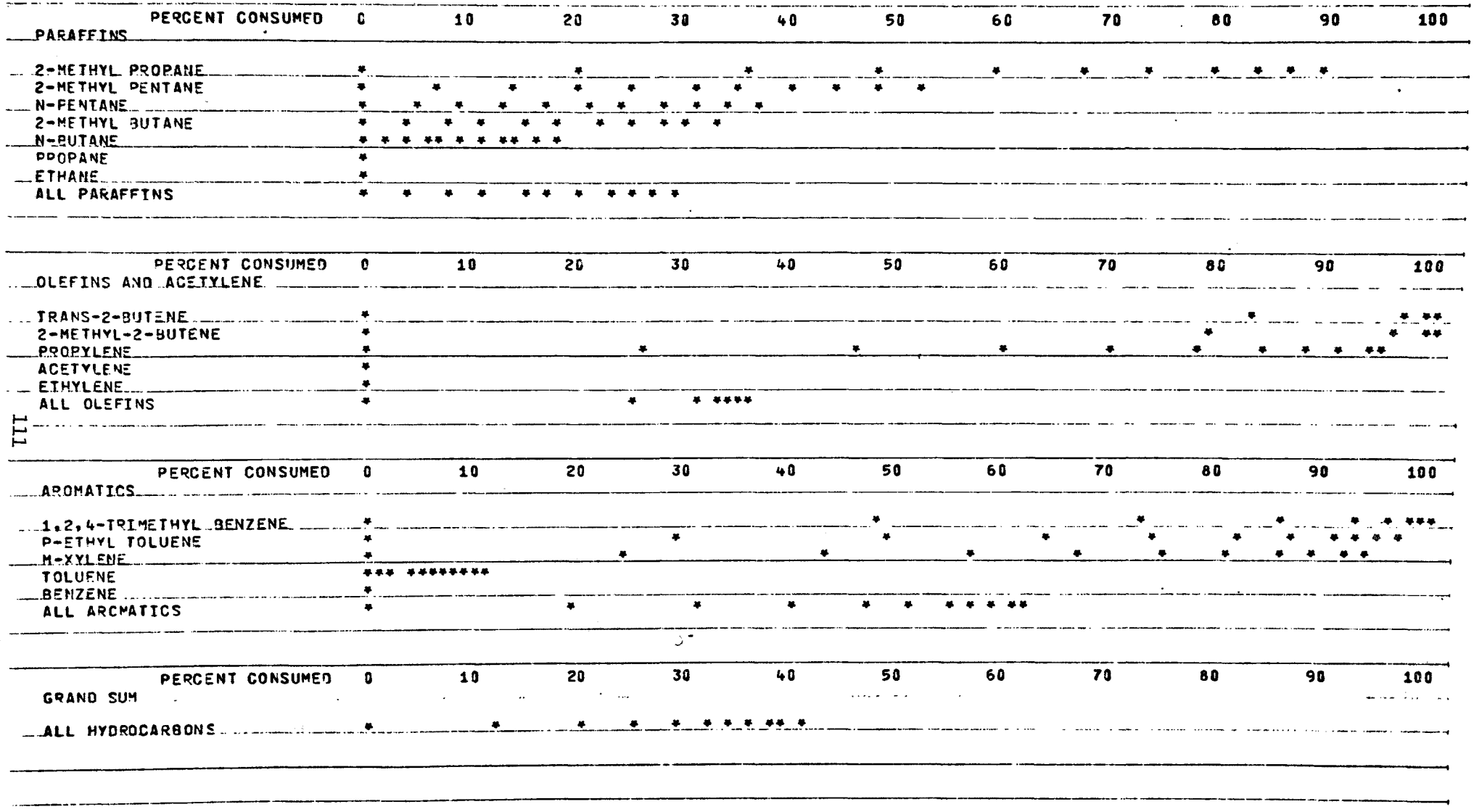

HYDROCARBON SUMMARY FOR RUN AP-018 4-01-75 CORRECTED FOR DILUTION

SUCCESSIVE ASTERISKS REPRESENT CUMULATIVE PERCENT CONSUMPTION PER HOUR OF IRRADIATION

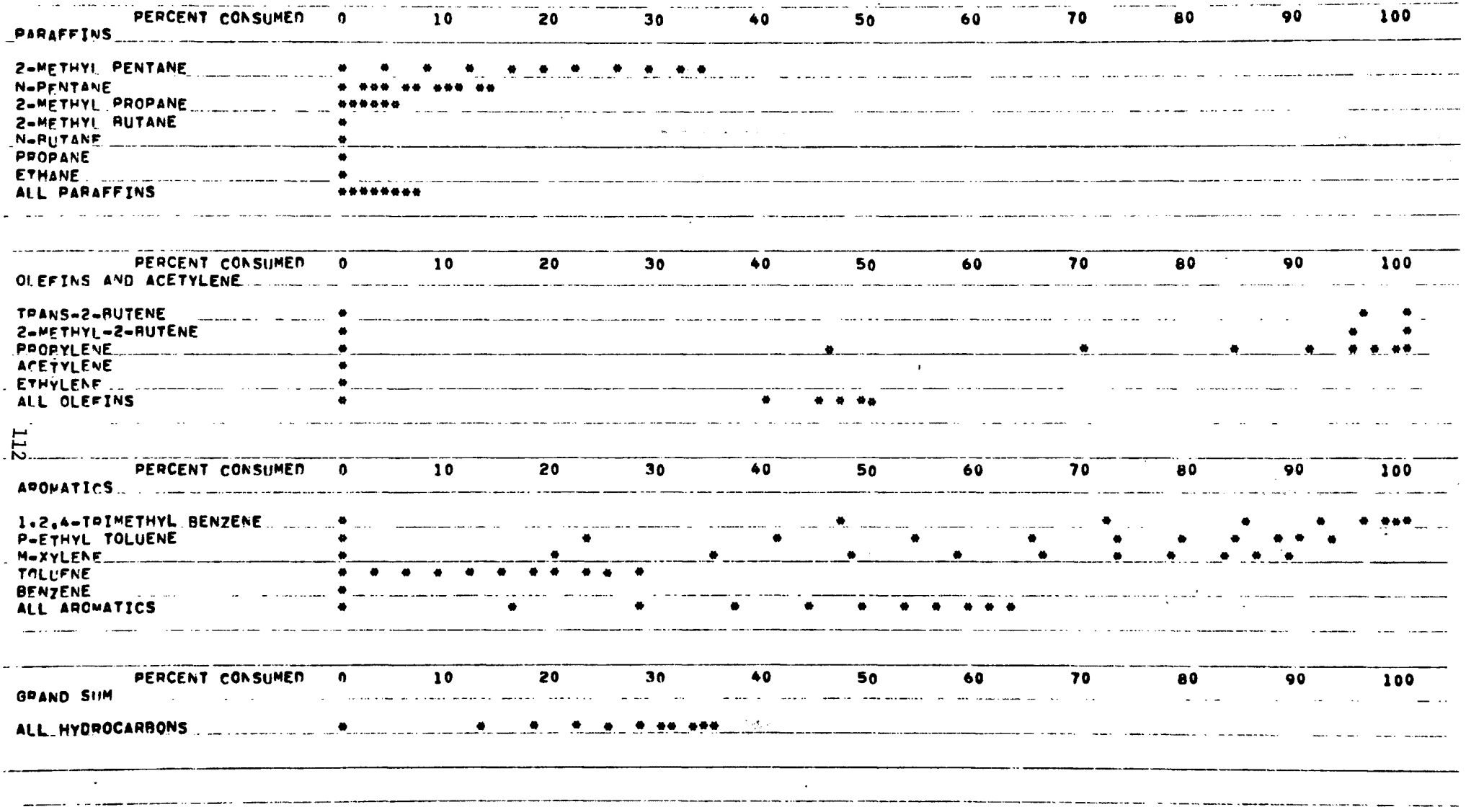

HYDROCARBON SUMMARY FOR RUN AP-019 4-02-75 CORRECTED FOR DILUTION

SUCCESSIVE ASTERISKS REPRESENT CUMULATIVE PERCENT CONSUMPTION PER HOUR OF IRRADIATION

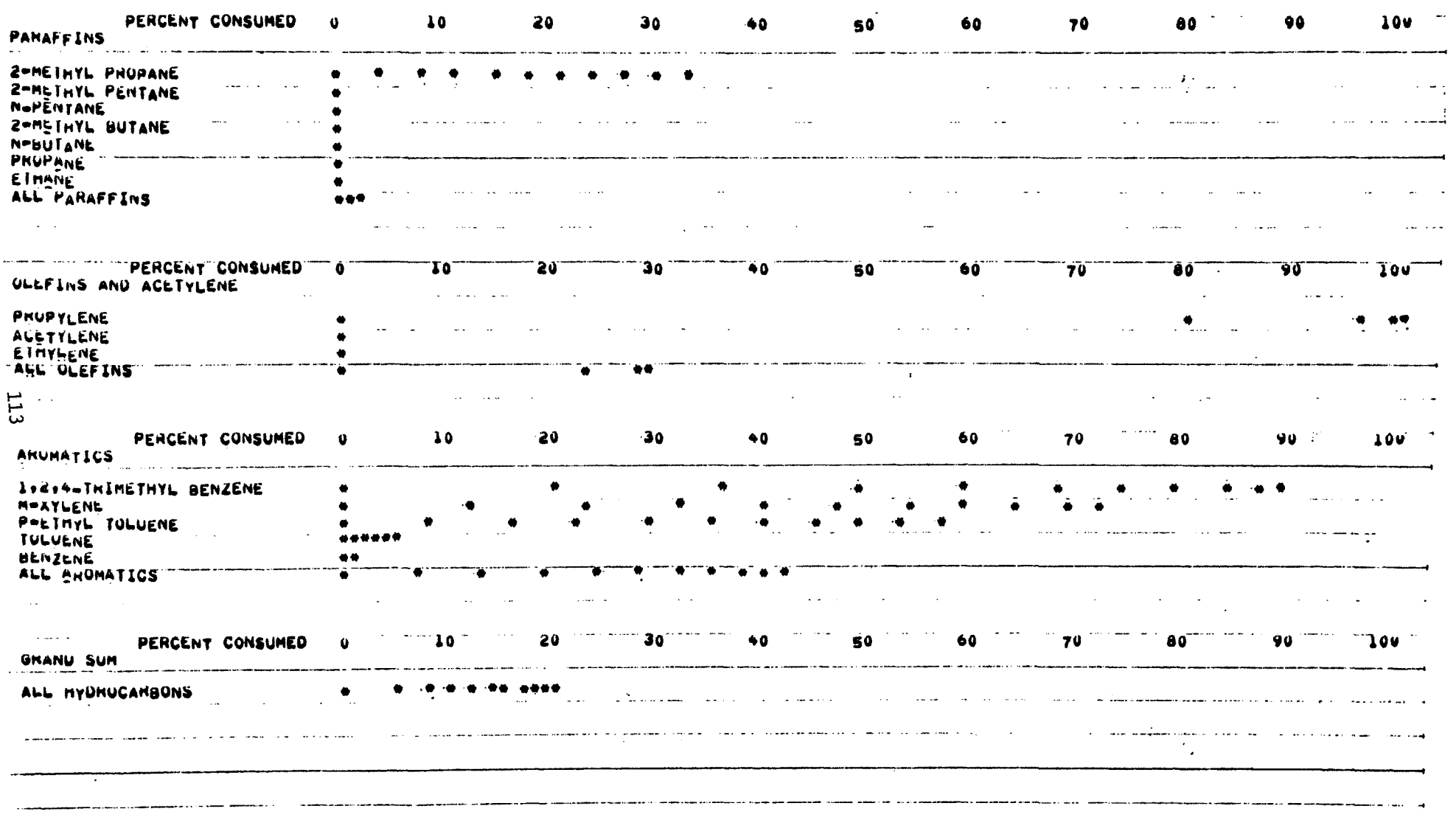

TECHNICAL REPORT DATA
(Please read Instructions on the reverse before completing)

1. REPORT NO.	2.	3. RECIPIENT'S ACCESSION NO.
EPA-600/3-76-080		

4. TITLE AND SUBTITLE
SMOG CHAMBER STUDIES ON PHOTOCHEMICAL AEROSOL-PRECURSOR RELATIONSHIPS

5. REPORT DATE
July 1976

6. PERFORMING ORGANIZATION CODE

7. AUTHOR(S)
David F. Miller and Darrell W. Joseph

8. PERFORMING ORGANIZATION REPORT NO.

9. PERFORMING ORGANIZATION NAME AND ADDRESS
Battelle Columbus Laboratories
505 King Avenue
Columbus, Ohio 43201

10. PROGRAM ELEMENT NO.
1AA008

11. CONTRACT/GRANT NO.
68-02-1718

12. SPONSORING AGENCY NAME AND ADDRESS
Environmental Sciences Research Laboratory
Office of Research and Development
U.S. Environmental Protection Agency
Research Triangle Park, NC 27711

13. TYPE OF REPORT AND PERIOD COVERED
Final 6/74-8/75

14. SPONSORING AGENCY CODE
EPA-ORD

15. SUPPLEMENTARY NOTES

16. ABSTRACT

An experimental program was conducted in which controlled atmospheres containing water vapor, CO, NO_x (NO + NO_2), and a constant distribution of 17 hydrocarbons (NMHC) were irradiated in a smog chamber. Reaction profiles were developed for NO oxidation, hydrocarbon oxidation, ozone formation, and aerosol formation over 10-hour irradiation periods. Comparison of smog chamber results with data on hydrocarbon oxidation rates observed in the Los Angeles area and with worst-case ozone episodes in that area, suggest that the models (precursor relationships) developed (in this study) for photochemical aerosol formation are highly relevant to smog problems in polluted atmospheres.

17. KEY WORDS AND DOCUMENT ANALYSIS

a. DESCRIPTORS	b. IDENTIFIERS/OPEN ENDED TERMS	c. COSATI Field/Group
*Air pollution Carbon monoxide *Nitrogen oxides *Hydrocarbons Ozone *Aerosols *Test Chambers *Photochemical reactions		13B 07B 07C 07D 14B

18. DISTRIBUTION STATEMENT	19. SECURITY CLASS *(This Report)*	21. NO. OF PAGES
RELEASE TO PUBLIC	UNCLASSIFIED	123
	20. SECURITY CLASS *(This page)*	22. PRICE
	UNCLASSIFIED	

EPA Form 2220-1 (9-73)